

Aus dem Adolf-Butenandt-Institut  
der Ludwig-Maximilians-Universität München  
Lehrstuhl Molekularbiologie  
Vorstand: Prof. Dr. rer. nat. Peter B. Becker

**Comprehensive analysis of MOF ubiquitylation,  
a Histone Acetyltransferase involved in  
*Drosophila melanogaster* Dosage Compensation**

Dissertation  
Zum Erwerb des Doktorgrades der Naturwissenschaften  
An der Medizinischen Fakultät der  
Ludwig-Maximilians-Universität München

vorgelegt von  
Sarah Schunter  
aus Stuttgart  
2016

**Gedruckt mit Genehmigung der Medizinischen Fakultät  
der Ludwig-Maximilians-Universität München**

Betreuer: Prof. Dr. rer. nat. Peter B. Becker

Zweitgutachter: PD Dr. rer. nat. Steffen Dietzel

Dekan: Prof. Dr. med. dent. Reinhard Hickel

Tag der mündlichen Prüfung: 21.02.2017

## Eidesstattliche Versicherung

Schunter, Sarah

Ich erkläre hiermit an Eides statt,  
dass ich die vorliegende Dissertation mit dem Thema

**“Comprehensive analysis of MOF ubiquitylation,  
a Histone Acetyltransferase involved in  
*Drosophila melanogaster* Dosage Compensation”**

selbständig verfasst, mich außer der angegebenen keiner weiteren Hilfsmittel bedient und alle Erkenntnisse, die aus dem Schrifttum ganz oder annähernd übernommen sind, als solche kenntlich gemacht und nach ihrer Herkunft unter Bezeichnung der Fundstelle einzeln nachgewiesen habe.

Ich erkläre des Weiteren, dass die hier vorgelegte Dissertation nicht in gleicher oder in ähnlicher Form bei einer anderen Stelle zur Erlangung eines akademischen Grades eingereicht wurde.

---

Ort, Datum

---

Unterschrift Doktorandin/Doktorand



# Table of Contents

<b>SUMMARY</b>	<b>1</b>
<b>ZUSAMMENFASSUNG</b>	<b>3</b>
<b>1 INTRODUCTION</b>	<b>5</b>
<b>1.1 Chromatin</b>	<b>6</b>
1.1.1 Chromatin structure and organization	6
1.1.2 Histone modifications	9
1.1.3 Histone acetyltransferases	11
1.1.4 Histone chaperones	13
<b>1.2 Dosage Compensation</b>	<b>15</b>
1.2.1 The Dosage Compensation Complex of <i>Drosophila melanogaster</i>	16
1.2.2 Targeting and assembly of the MSL-DCC to the male X chromosome	17
1.2.3 Mechanism of <i>Drosophila</i> dosage compensation	19
1.2.4 Properties and functions of MSL2	20
1.2.5 Properties and functions of MOF	20
<b>1.3 Ubiquitylation</b>	<b>22</b>
1.3.1 The mechanism of ubiquitin attachment onto substrate protein	22
1.3.2 Diversity of ubiquitylation	23
1.3.3 Biological consequences of ubiquitylation	23
<b>1.4 Objective</b>	<b>25</b>
<b>2 MATERIALS &amp; METHODS</b>	<b>27</b>
<b>2.1 Materials</b>	<b>28</b>
2.1.1 Chemicals	28
2.1.2 Enzymes, Kits and Markers	29
2.1.3 Consumables	29
2.1.4 Antibodies	30
2.1.5 Oligonucleotides	32
2.1.6 Plasmids	33
2.1.7 Insect cell lines and bacterial strains	35
2.1.7.1 <i>E.coli</i> strains	35

2.1.7.2 Insect cell lines	35
2.1.7.3 Stable <i>Drosophila melanogaster</i> cell lines	36
2.1.8 Technical devices	37
2.1.9 Software	38
<b>2.2 Standard buffers and solutions</b>	<b>39</b>
<b>2.3 Molecular biology methods</b>	<b>41</b>
2.3.1 General molecular biology methods	41
2.3.2 Cloning of FLAG-tagged expression constructs	41
2.3.2.1 Generation of MOF deletion mutants	41
2.3.2.2 Generation of N-terminal MOF mutants	41
2.3.2.3 Generation of C-terminal MOF mutants	41
2.3.3 Cloning of GFP-tagged expression constructs	42
2.3.4 Cloning of FLAG-tagged constructs to pUAST-attB	42
<b>2.4 Cell biological methods</b>	<b>43</b>
2.4.1 Maintenance of <i>D. melanogaster</i> and <i>S. frugiperda</i> cell lines	43
2.4.2 Cryopreservation and thawing of <i>Drosophila</i> cells	43
2.4.3 Generation of stable SL2 and Kc cell lines	43
2.4.4 Whole cell extracts from SL2 and Kc cells	44
2.4.5 RNA interference in SL2 and Kc cells	44
2.4.6 Immunofluorescence on SL2 cells	45
2.4.7 Immunoprecipitation experiments	45
2.4.7.1 Immunoprecipitation of transgenic MOF-GFP from stable cell lines	45
2.4.7.2 Immunoprecipitation of transgenic MOF-GFP for mass spectrometry	45
2.4.8 Precipitation of proteins for ubiquitylome analysis	46
<b>2.5 <i>Drosophila melanogaster</i> studies</b>	<b>47</b>
2.5.1 Generation of transgenic fly lines	47
2.5.2 Fly crosses for male viability assays	47
2.5.3 Immunostaining of polytene chromosomes	47
2.5.4 Preparation of protein extracts from salivary glands	48
<b>2.6 Biochemical methods</b>	<b>49</b>
2.6.1 SDS-polyacrylamide gel electrophoresis (SDS-PAGE)	49
2.6.2 Coomassie staining of protein gels	49
2.6.3 Western Blot	49
2.6.4 <i>In vitro</i> ubiquitylation assay	50
2.6.5 Histone acetylation assay	50

<b>2.7 Expression and purification of MSL-DCC proteins in Sf21 cells</b>	<b>51</b>
2.7.1 Generation of recombinant Baculovirus	51
2.7.2 Infection of Sf21 cells with Baculovirus	51
2.7.3 Preparation of Sf21 cell extracts	51
2.7.4 Purification of FLAG-tagged MSL-DCC proteins from Sf21 cell extracts	52
<b>3 RESULTS</b>	<b>53</b>
<b>3.1 <i>In vitro</i> characterization of MOF ubiquitylation</b>	<b>54</b>
3.1.1 MOF is ubiquitylated by MSL2 <i>in vitro</i>	54
3.1.2 <i>In vitro</i> ubiquitylation of MOF mutants by MSL2	56
3.1.3 MOF is ubiquitylated by a DCC-unrelated E3 ligase <i>in vitro</i>	58
3.1.4 Allosteric modulation of MSL2 ubiquitylation activity	60
3.1.5 Enzymatic activity of MOF derivatives	60
<b>3.2 <i>In vivo</i> characterization of MOF ubiquitylation</b>	<b>63</b>
3.2.1 MOF is ubiquitylated <i>in vivo</i>	63
3.2.2 Analysis of MSL2-dependent MOF ubiquitylation <i>in vivo</i>	67
3.2.3 Analysis of proteasome-related MOF ubiquitylation <i>in vivo</i>	68
3.2.4 Characterization of MOF mutants <i>in vivo</i> using immunofluorescence	70
3.2.4 Association of MOF mutants with the MSL-DCC	77
3.2.5 Male viability of MOF mutants	79
<b>3.3 MSL2-dependent ubiquitylation outside of the MSL-DCC</b>	<b>81</b>
3.3.1 Generation and characterization of SPT6 monoclonal antibodies	81
3.3.2 Purification of recombinant SPT6 protein	86
3.3.3 <i>In vitro</i> ubiquitylation of recombinant SPT6	87
<b>4 DISCUSSION</b>	<b>89</b>
<b>4.1 MOF ubiquitylation</b>	<b>90</b>
4.1.1 Discrepancies between MOF ubiquitylation <i>in vitro</i> and <i>in vivo</i>	90
4.1.2 MOF ubiquitylation - a male-specific role in dosage compensation?	92
4.1.3 MOF-9KC mutant exhibits male-specific lethality	95
4.1.4 Possible functions of MOF ubiquitylation	97
4.1.5 Conclusions and future perspectives on MOF ubiquitylation	99
<b>4.2. SPT6, a target for MSL2-mediated ubiquitylation?</b>	<b>101</b>
<b>4.3 The analysis of ubiquitylation- limitations and challenges</b>	<b>102</b>
<b>5 ABBREVIATIONS</b>	<b>105</b>

<b>6 REFERENCES</b>	<b>109</b>
<b>7 APPENDIX</b>	<b>121</b>
Acknowledgements	123





## SUMMARY

The process that balances the X-chromosome monosomy in male *Drosophila* flies is known as dosage compensation. Dosage compensation results in a twofold increase in transcription of X-chromosomal genes mediated by a complex known as the male-specific-lethal dosage compensation complex (MSL-DCC) that regulates gene expression at the step of transcriptional elongation. Appropriate levels of MSL-DCC and hence of the protein subunits it consists of - MSL1, MSL2, MSL3, MOF and MLE - are essential for male viability. Recently, the male-specific MSL2 protein was discovered to bear E3 ubiquitin ligase activity enabling auto-ubiquitylation as well as ubiquitylation of the other MSL-DCC subunits. Ubiquitylation most likely contributes to maintaining complex homeostasis through proteasomal degradation. However, some ubiquitin marks may also serve to modulate the molecular interactions or activity of MSL proteins. The MSL-DCC subunit MOF is a prominent substrate for MSL2. MOF is a histone acetyltransferase that catalyzes acetylation of histone H4 at lysine 16, a hallmark of the dosage-compensated male X chromosome.

The present study provides the first comprehensive analysis of MOF ubiquitylation. Results from *in vitro* ubiquitylation assays indicate that MSL2 preferentially modifies N-terminal lysine residues in MOF. However, using a mass spectrometry-based approach a different ubiquitylation pattern was observed on both endogenous MOF and tagged derivatives expressed in cell lines. To analyze the functions MOF ubiquitylation in more detail and to distinguish potential MSL2-dependent from MSL2-independent MOF ubiquitylation, mutated MOF proteins, in which relevant lysines were changed to arginines (K>R) were characterized both *in vitro* and *in vivo* using recombinant protein, stable cell lines and transgenic flies, respectively.

Most of the K>R mutations of MOF exhibited only mild effects on MSL-DCC association and male viability, suggesting that lack of ubiquitylation or any other modification of these lysines are either dispensable or otherwise buffered by the biological system. Only the mutation of 9 lysines in the C-terminal half of MOF (MOF-9KC) had an effect as expression of this mutant *in vivo* resulted in impaired X-territorial targeting, MSL-DCC association and male viability. However, these defects are most likely unrelated to ubiquitylation but rather result from impaired complex association due to lack of interaction with the scaffold protein MSL1. MSL2-dependent MOF ubiquitylation could not be detected *in vivo* in the context of abundant ubiquitylation of MOF catalyzed by other E3 ligases, both in the nucleus and cytoplasm.

Earlier work from the group had indicated that MSL2 also targets proteins outside the MSL-DCC. Of particular interest was the H3-H4 histone chaperone and elongation factor SPT6. To

## SUMMARY

---

enable future investigations of the involvement of SPT6 in dosage compensation and MSL2-dependent ubiquitylation, a toolkit consisting of recombinant SPT6 and monoclonal antibodies directed against SPT6 was established. First assays demonstrated that MSL2 extensively ubiquitylates SPT6 *in vitro*.

## ZUSAMMENFASSUNG

Männliche Vertreter der Fruchtfliege *Drosophila melanogaster* weisen durch die Anwesenheit eines einzelnen männlichen X Chromosoms eine Monosomie auf, die durch den Prozess der Dosiskompensation an das Niveau der zwei weiblichen X Chromosomen angepasst wird. Dazu wird die Genexpression X-chromosomaler Gene durch den sogenannten Dosiskompensationskomplex (MSL-DCC) selektiv in Männchen verdoppelt, ein Prozess der auf Ebene der transkriptionellen Elongation gesteuert wird.

Das korrekte Verhältnis der einzelnen Komplexproteine - MSL1, MSL2, MSL3, MOF und MLE - ist hierbei unabdingbar für die Lebensfähigkeit der männlichen Fruchtfliege. Erst kürzlich konnte nachgewiesen werden, dass MSL2 eine E3 Ubiquitin Ligase ist, welche sich selbst und andere Untereinheiten des Dosiskompensationskomplexes durch Ubiquitylierung modifiziert. In diesem Zusammenhang trägt die Ubiquitylierung durch die Vermittlung proteasomaler Abbauprozesse zur Aufrechterhaltung der korrekten Komplexhomöostase bei. Abgesehen von Degradationsprozessen, beeinflussen Ubiquitylierungen auch molekulare Interaktionen oder modulieren die Aktivität der MSL-DCC Proteine. So ist die Komplexuntereinheit MOF als prominentes Substrat für MSL2-vermittelte Ubiquitylierungen bekannt. MOF ist eine Histon Acetyltransferase, die den Transfer einer Acetylgruppe auf das Lysin 16 des Histonproteins 4 katalysiert, eine Modifikation, die das dosiskompensierte männliche X Chromosom charakterisiert.

Die vorliegende Arbeit liefert eine umfassende Untersuchung und Charakterisierung der MOF Ubiquitylierung. Ergebnisse aus *in vitro* Ubiquitylierungsreaktionen konnten zeigen, dass MSL2 vorzugsweise Lysinseitenketten im Bereich des MOF N-terminus modifiziert. Im Gegensatz dazu wurde mittels massenspektrometrischer Untersuchungen ein anderes Ubiquitylierungsmuster an endogenem bzw. transgenem MOF aus entsprechenden Zelllinien nachgewiesen. Um die Funktionen der MOF Ubiquitylierung im Detail zu untersuchen, sowie potentielle MSL2-abhängige und -unabhängige Ubiquitylierungsprozesse voneinander abzugrenzen, wurden MOF Mutanten generiert, in denen relevante Lysinreste (K) durch Argininreste (R) ausgetauscht wurden. Mittels rekombinanter Proteine, stabiler Zelllinien und transgener Fliegenstämme wurden die generierten K>R MOF Mutanten sowohl *in vitro* als auch *in vivo* charakterisiert. Dabei zeigte sich, dass die meisten der integrierten K>R MOF Mutationen lediglich geringe Effekte auf die Komplex-Assoziation und die Lebensfähigkeit männlicher Fliegen hatten. Diese Beobachtung impliziert, dass das Fehlen von Ubiquitylierung oder anderer Modifikationen an den entsprechenden Lysinresten entweder nur unwesentlichen Einfluss hat oder anderweitig durch das biologische Umfeld ausgeglichen wird. Lediglich die Mutation von insgesamt 9 Lysinresten im Bereich des MOF C-terminus

(MOF-9KC) zeichnete sich *in vivo* durch einen Verlust der X-territorialen Lokalisation, Komplexassoziation, sowie reduzierter Lebensfähigkeit männlicher Fliegen aus. Vermutlich beruhen diese Einschränkungen jedoch nicht auf dem Fehlen entsprechender Ubiquitylierungen, sondern resultieren aus der mangelnden Interaktion von MOF-9KC mit dem Gerüstprotein MSL1. Letztendlich erschwerte ubiquityliertes MOF, das vermutlich nicht durch MSL2 sondern eine Vielzahl anderer E3 Ligasen modifiziert wurde und reichlich in Nukleus und Zytoplasma vorhanden ist, den Nachweis MSL2-abhängiger MOF Ubiquitylierung *in vivo*.

Frühere Studien innerhalb der Arbeitsgruppe deuteten bereits darauf hin, dass MSL2 auch Proteine außerhalb des MSL-DCC modifiziert. Von besonderem Interesse war hierbei SPT6, ein H3-H4 Chaperon und Elongationsfaktor. Um zukünftige Untersuchungen bezüglich der Beteiligung von SPT6 im Zusammenhang mit der Dosiskompensation und MSL2-anhängiger Ubiquitylierung zu ermöglichen, wurden sowohl rekombinantes SPT6 also auch entsprechende monoklonale Antikörper generiert. Erste Untersuchungen *in vitro* ergaben, dass MSL2 in der Lage ist, SPT6 in erheblichem Maße zu ubiquitylieren.

# **1 INTRODUCTION**

### 1.1 Chromatin

Almost 60 years have passed from the discovery of DNA as the carrier of genetic information (Avery, Macleod and McCarty, 1944) to the determination of the human DNA sequence by the international human genome project (HGP) at the beginning of the 21<sup>st</sup> century. Fast it became clear that the sole information about the genome sequence provided more questions than answers. Multi-cellular organisms comprise many different cell types. Still, all of them exhibit the same genetic information stored within their nuclei. The realization of this “blue print” into cellular processes such as differential gene expression relies on a highly dynamic environment to allow for responses to endogenous and exogenous stimuli. Nature has developed highly efficient tools to ensure proper gene expression at the right time and place throughout the lifetime of an organism. Distinct molecular factors but also genome organization and chromatin play major roles when it comes to fine-tuning mechanisms and modulation of gene expression.

#### 1.1.1 Chromatin structure and organization

Eukaryotic cells store their large genomes in a highly organized manner as DNA-protein complex within their nuclei. Already at the end of the nineteenth century Flemming observed that some nuclear structures heavily absorb a basic dye, thus naming these structures “chromatin”, from the Greek word for color. It took almost another 100 years to the discovery of nucleosomes as the structural and functional unit of chromatin. The basic unit of each nucleosome is represented by the nucleosome core particle (Kornberg, 1974; Dekker and Oudet, 1975) that consists of 147 bp of superhelical, left-handed, negatively charged DNA wrapped in 1.65 turns around a positively charged histone octamer (Figure 1). Multiple protein-protein interactions between the single histones but also electrostatic and hydrogen bonds between DNA and histone proteins stabilize the nucleosome structure (Rohs, 2009; Davey, 2002). The canonical histone-octamer is composed of two H3-H4 and two H2A-H2B histone dimers (Luger, 1997; Richmond and Davey, 2003).

Two structurally and functionally distinct domains can be assigned to the small and basic histone proteins: a core and a tail. The core resembles the structured and globular domain of the histones, facing the inner part of the nucleosome unit. In contrast to the histone core, the largely unstructured and flexible C- and N-terminal tails face the surface of the nucleosome representing the accessible part of chromatin. Fifteen to 38 amino acids from the basic and unstructured N-terminal tails of the histones serve as modules for posttranslational modifications such as methylation, phosphorylation, acetylation and ubiquitylation.

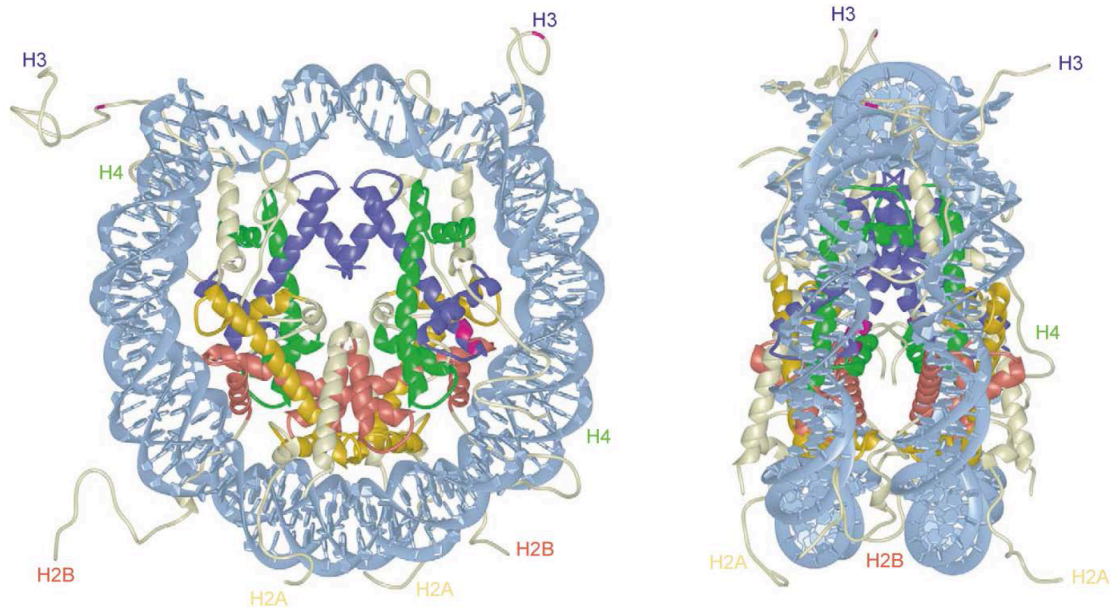


**Figure 1: Structure of the nucleosome core particle, viewed in two orientations.** First published in Luger, 1997, the scheme shows both the view down the super-helical axis (left) as well as a rotation of the nucleosome core particle rotated by 90° around the vertical axis (right). The 2.8 Å high-resolution crystal structure displays the wrapping of DNA (light blue) around the octamer of histones (blue: H3; green: H4; yellow: H2A; red: H2B) in 1.65 left-handed helical turns. Histone tails and extensions reaching out of the structure are displayed in white. [Adapted and reprinted with permission from Elsevier (Luger, 2003; Current Opinion in Genetics & Development).]

The nucleosome composition can be varied both through the incorporation of non-canonical histone variants and the attachment of posttranslational modifications to the flexible histone tails. In contrast to canonical histones that are expressed only during S-phase (Marzluff, 2002), non-canonical histones are expressed throughout the cell cycle (Loyola and Almouzni 2007). Encoded by distinct genes non-canonical histones are non-allelic isoforms of canonical histones that differ in their sequences and expression patterns. Except for histone H4, all other histones have several histone variants. In humans for example, almost 20 different histone variants have been described so far. Replacement of the canonical histones by histone variants is facilitated independently of the cell cycle by specialized replication-independent enzymes such as remodeling enzymes or chaperones. The replacement of canonical histones by histone variants can be used to label the state of chromatin or mark specialized genome regions. In line with this human H2A.Z or the *Drosophila* H2A.V, respectively were shown to be phosphorylated after DNA double strand breaks thus triggering the recruitment of DNA repair processes (Thiriet, 2005).

Electron microscopy studies have visualized nucleosomes that line up on a DNA stretch as “beads-on-a-string” (Benbow, 1992), able to generate a fiber with a diameter of 11 nm and resulting in a ~5-fold condensation of the underlying DNA. This first layer of packaging is further compacted by the association with histone H1 to the 10-80 bp linker DNA bridging two nucleosomes and allowing the formation of the 30 nm fiber (Thoma and Koller, 1977;

Adkins, 2004) that subsequently fold into higher order chromatin structures like interphase or mitotic chromosomes. To date the existence of the 30 nm fiber is a matter of constant debate and most data that demonstrate the existence of the 30 nm fiber were obtained *in vitro*. Using electron microscopy isolated nucleosome fibers were observed to form structures with a diameter of roughly 30 nm *in vitro* (Finch and Klug, 1976). Moreover, it was proposed that nucleosomal arrays and H1-chromatin form 30 nm fibers only under very specific ionic conditions *in vitro* (Maeshima, 2016). However, the evidence for the 30 nm fiber *in vivo* is rather limited as all attempts to visualize the fibers failed so far (Eltsov, 2008; Maeshima, 2010; Fussner, 2011). Currently it is assumed that there are no regular chromatin structures present *in vivo* beyond the 10 nm fiber (Joti, 2012; Nishino, 2012). In fact a recent model suggests the presence of irregularly folded nucleosome fibers that give rise to the higher order chromatin organization present in interphase nuclei (Belmont and Bruce, 1994) or mitotic chromosomes (Rattner and Lin, 1985). Furthermore, it was proposed that once the H4 tail promotes folding and oligomerization of the 10 nm fiber it can no longer engage the interaction with the acidic patch of neighboring nucleosomes in order to adopt the 30 nm fiber (Maeshima, 2016; Figure 2).

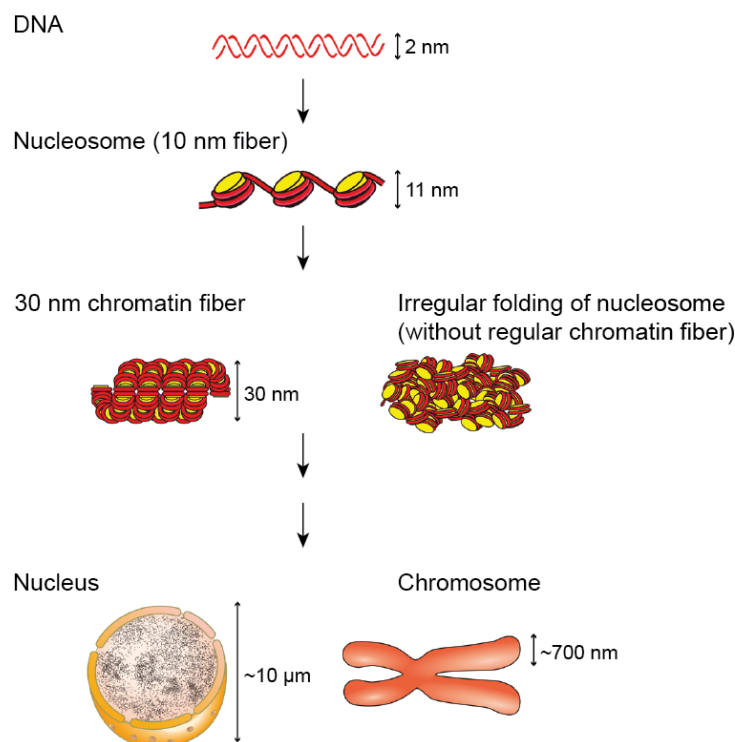


**Figure 2: Chromatin structure according to the old and new view.** A molecule of DNA with a diameter of ~2 nm is wrapped around a histone octamer forming a nucleosome fiber of ~10 nm. According to the old model the nucleosome was assumed to fold into 30 nm chromatin fibers (left) and subsequently into higher organization of interphase nuclei or mitotic chromosomes, respectively. Depicted on the right is the novel hypothesis of irregularly folded fibers [Adapted and reprinted with permission from Springer (Maeshima, 2014; Chromosoma)].

### 1.1.2 Histone modifications

Chromatin features and organization affect gene transcription in various ways as the compaction status of chromatin determines the accessibility of DNA. Two major mechanisms are crucial for alteration of chromatin structure: (1) chromatin remodeling complexes that affect the interaction between histones and DNA in an ATP-dependent manner (Längst, 2015; Jin, 2005); and (2) attachment of posttranslational modifications (PTMs) to the N-terminal histone tails, and to a lesser extent also within the C-terminal tails and globular domains of histones (Kouzarides, 2007; Jack and Hake, 2014). For example acetylation of histone H4 at lysine 16 (H4K16ac) directly affects chromatin structure as it is suggested to prevent formation of the 30 nm fiber (Robinson, 2008; Shogren-Knaak, 2006). Consequently, transcription is substantially derepressed after targeting of H4K16ac to promoters *in vitro* and *in vivo* (Akhtar and Becker, 2000). On the other hand placement of histone modifications by chromatin modifying enzymes indirectly affect chromatin structure in a way that they provide binding platforms for the recruitment of specific effector proteins that locally act on chromatin organization (Fischle, 2008).

The placement of post translational modifications to the flexible histone tails is facilitated by a multitude of highly specific histone-modifying enzymes and their recruitment to chromatin is triggered by diverse factors such as DNA-binding factors, co-activators and repressors, RNA polymerase II (RNAPII) or preceding histone modifications (Luger, 2012). PTMs of histone tails such as phosphorylation, methylation, ubiquitylation and acetylation are major regulators of chromatin structure as those histone marks affect inter-nucleosomal interactions. Hence, histone modifications are involved in regulation of DNA accessibility as well as the manipulation and expression of DNA in various cellular processes (Zentner and Henikoff, 2013).

Phosphorylation of histone tails is a highly dynamic process resulting from the addition and removal of phosphate groups by kinases and phosphatases, respectively. The transfer of a phosphate group from ATP to the hydroxyl group of an amino-acid side chain predominantly occurs on serines, threonines and tyrosines. Placement of a phosphate group onto histone tails introduces a negative charge that significantly influences chromatin structure. In contrast, the attachment of methyl groups to arginines and lysines does not alter the charge of the histone protein. Methylation of target protein is carried out by methyltransferases that catalyze the transfer of a methyl group from S-adenosylmethionine (SAM) to the  $\omega$ -guanidino group of arginine or the  $\epsilon$ -amino group of lysine, respectively (Struck, 2012). Methylation of histones adds a layer of complexity as arginines may be mono-, symmetrically or asymmetrically dimethylated, whereas lysines may be mono-, di- or tri-methylated (Torres and Fujimori, 2015). In the past methylation of histones was considered to be a rather stable and static histone

modification. However, in 2004 the first lysine demethylase was identified (Shi, 2004) thus providing a tight regulation of histone methylation by the concise action of methylases and demethylases. While phosphorylation and methylation of histones result in relatively small molecular changes on the amino-side chains, ubiquitylation on the other hand introduces a much larger covalent modification and changes histone mass to a higher extent. The attachment of the 76 aa ubiquitin polypeptide to lysines occurs in different degrees (mono-, di-, multi-, poly-ubiquitylated). However, on histones mono-ubiquitylation seems to be the most relevant modification (Bannister and Kouzarides, 2011). Histone mono-ubiquitylation is mainly found on histones H2A and H2B and is not involved in proteasomal targeting but rather affects nucleosomal dynamics (Meas and Mao, 2015).

Posttranslational modification of histones and histone acetylation in particular was first documented in the early 1960s (Phillips, 1963; Allfrey, 1964). Since then the involvement of histone acetylation in the regulation of transcription and gene expression has been studied extensively. In fact, the transfer of an acetyl group from acetyl-Coenzyme A to the  $\epsilon$ -amino group of lysines neutralizes the positive charge of lysine side chains. Consequently, the interactions between histones and nucleosomal DNA are weakened leading to increased DNA accessibility for the transcription machinery (Dion, 2005). On the other hand, histone acetylation changes binding properties of effector proteins (eg. PHD/ bromodomain proteins) which in turn regulate gene expression through the recruitment of chromatin remodelers (Bannister and Kouzarides, 2011).

### 1.1.3 Histone acetyltransferases

Chromatin-dependent processes such as transcriptional regulation, DNA repair and chromatin accessibility are tightly coupled to histone modification states. Histone acetylation was one of the first described histone modifications, yet it took several decades to unravel the biological functions of histone acetylation and histone modifications in general. The covalent acetylation of lysine residues is a highly dynamic process regulated by antagonizing histone-modifying enzymes: histone acetyltransferases (HATs) and deacetylases (HDACs; Figure 3). Both enzymes are found at sites of active transcription (Wang, 2009).

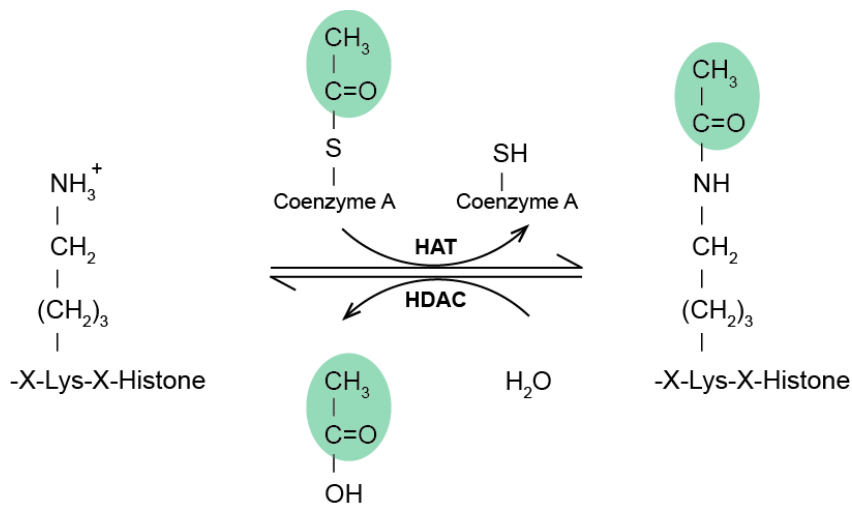


**Figure 3: Histone acetylation is maintained by the opposing activities of histone acetyltransferases (HATs) and deacetylases (HDAC).** HATs transfer the high-energy acetyl moiety from acetyl Coenzyme A (Ac-CoA) to the respective  $\epsilon$ -amino group of a respective lysine residue of the histone N-tail. HDACs catalyze the reversal reaction.

HATs have been identified in eukaryotic organisms from yeast to human and can be grouped in at least four different families based on the structural homology within their respective HAT domains (Marmorstein and Roth, 2001; Wang, 2008): p300/CBP, Rtt109, Gcn5/PCAF and MYST. While p300/CBP (named for the two human paralogs p300 and CBP) is metazoan-specific, Rtt109 (named for its initial identification as a regulator of Ty1 transposition gene product 109) is fungal-specific, Gcn5/PCAF (named for its founding member yeast Gcn5 and its human ortholog, PCAF) and MYST families have homologues from yeast to human. The MYST (named for the founding members MOZ, Ybf2/ Sas3, Sas2 and Tip60) represents the largest family of HATs (Marmorstein and Trievel, 2009) and will be discussed hereafter in more detail.

The defining feature of MYST histone acetyltransferases is the presence of the highly conserved MYST (HAT) domain that comprises the acetyl-CoA binding site (Figure 4). Furthermore, most MYST domains are characterized by the presence of a C2HC zinc finger

(Yang, 2004). In dMOF the C2HC zinc finger is crucial for both HAT activity and nucleosome binding *in vitro* (Akhtar and Becker, 2001). The lysine residue at position K274 of the human MOF protein sequence is a highly conserved autoacetylated residue, relevant for conformational changes, substrate induced binding and HAT activity on H4K16 (Yuan, 2012).

\*

hMOF	259	YQNLCLLAKLFLDHK <sup>*</sup> TL <sup>*</sup> YFDVEPFV <sup>*</sup> FYILTEVDRQGA(0)HIVGYFSKEKESPDGNNVACILTL <sup>*</sup> PPYQRRG	328
ySas2	153	FCQCLCLFTKLYLDNKSMYFKVDHYE <sup>*</sup> FYIVYETGSTKP(0)..MGFFSKDLVSYQQNNLACIL <sup>*</sup> LIFPPYQRRG	220
dMOF	590	YQLLCLMAK <sup>*</sup> LFLDHK <sup>*</sup> VLYFDMDPFL <sup>*</sup> FYILCETDKEGS(0)HIVGYFSKEKKSLENYNVACIL <sup>*</sup> LVLP <sup>*</sup> PHQRKG	659
hMOZ	589	YQNLCLLAKLFLDHK <sup>*</sup> TL <sup>*</sup> YDVEPF <sup>*</sup> LYVLTQNDVKGC(0)HLVGYFSKEKHCCQKY <sup>*</sup> NVSCIMIL <sup>*</sup> PPYQRRG	658
hTip60	312	YSQNLCLLAKCFLDHK <sup>*</sup> TL <sup>*</sup> YDTPDF <sup>*</sup> LYVMTEYDCKGF(0)HIVGYFSKEKESTEDYNVACIL <sup>*</sup> TL <sup>*</sup> PPYQRRG	381
ySas3	352	YSQNLCLLAKCFINSK <sup>*</sup> TL <sup>*</sup> YDVEPF <sup>*</sup> IFYILTEREDTEN(9)HFVGYFSKEKFSNNDYNLS <sup>*</sup> CIL <sup>*</sup> TL <sup>*</sup> PIYQRRG	430

**Figure 4: Sequence alignment of the active site residues of selected MYST protein members.** The conserved autoacetylated lysine residue is indicated with an asterisk. Sequence similarity is encoded by background color: identical aa = dark gray, similar aa = light gray, different aa = white.

MYST proteins structurally resemble each other in many ways still they are involved in the regulation of various biological processes from DNA repair and cell cycle progression to epigenetic and transcriptional control (Yuan, 2012). Some of the MYST family members share additional structural features such as chromodomains and plant homeodomain-linked (PHD) zinc fingers. Domain organization and structural features of selected MYST proteins from *S.cerevisiae*, *Drosophila* and human are depicted in Figure 5.

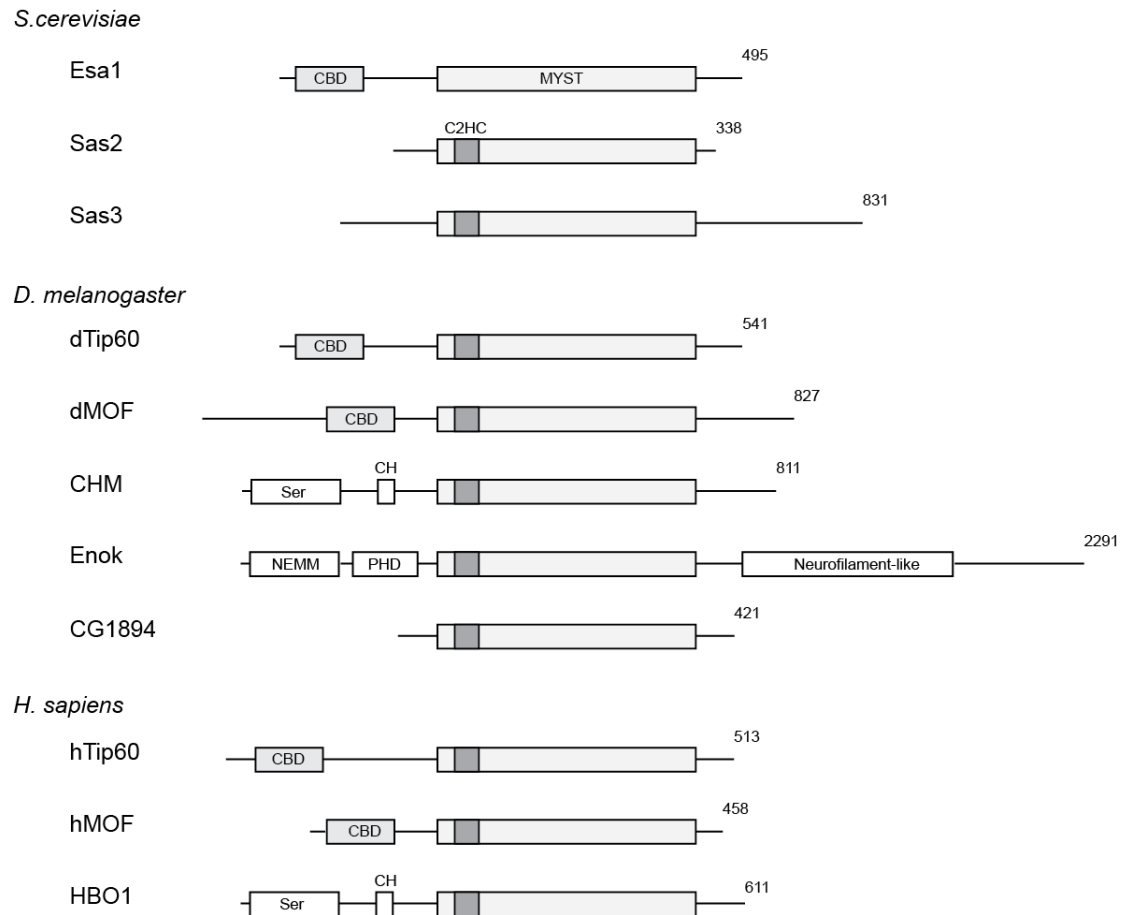


**Figure 5: Domain organization and structural features of MYST proteins.** Schematic representation of MYST proteins from *S. cerevisiae* (Esa1, essential Sas2-related acetyltransferase 1; Sas2, something about silencing 2; Sas3, something about silencing 3), *D. melanogaster* (dTip60, HIV Tat interacting 60 kDa protein; dMOF, male-absent on the first; CHM, Chameau; CG1894, uncharacterized MYST protein) and human (hTip60; hMOF; HBO1, HAT bound to ORC1, a Chameau ortholog). CBD, chromobarrel domain; Ser, serine-rich domain; CH, cysteine/histidine-rich domain; C2HC, zinc finger; NEMM, N-terminal part of Enok, MOZ or MORF; PHD, PHD zinc finger. Numbers at the end of each structure correspond to the total protein residues. Figure adapted from Yang, 2004.

#### 1.1.4 Histone chaperones

Synthesis and assembly of canonical histones mainly happens during DNA replication, whereas expression and incorporation of histone variants into chromatin also happens outside of S-phase. However, both canonical histones and histone variants are highly dependent on histone chaperones. Histone chaperones associate with histones and regulate nucleosome assembly in an ATP-dependent manner (Avvakumov, 2011; Gurard-Levin, 2014). All histone chaperones share a fundamental property: they promote the transfer of histones to naked DNA *in vitro* to reconstitute nucleosomes (De Koning, 2007). However, *in vivo* not all histone chaperones necessarily promote nucleosome assembly, instead they are involved in DNA repair and transcription (Jeronimo and Robert, 2016).

The classification into H3-H4 or H2A-H2B histone chaperones is based on the selectivity for respective histone proteins, yet it is not fully strict. This is mainly due to the fact that some histone chaperones also exhibit affinity for different histone proteins in addition (Gurard-Levin, 2014). Moreover, many histone chaperones are characterized by the presence of an acidic patch that is suggested in neutralizing the basic nature of histone proteins (Belotserkovskaya, 2003; Park and Luger, 2006). But also PTMs are capable in changing the electrostatic properties of histone chaperones thus directly affecting histone binding (Regnard, 2000).

SPT6 is an essential and highly conserved histone H3-H4 chaperone and transcription elongation factor suggested to restore nucleosomes in the wake of RNAPII transcription (Dronamraju and Strahl, 2014). In *Drosophila* the 1831 aa SPT6 was demonstrated to positively stimulate the elongation rate of RNAPII *in vivo* (Ardehali, 2009). The N-terminus of SPT6 features a highly conserved and acidic region harboring multiple negatively charged amino acids (Figure 6) essential for the binding of positively charged histone molecules and the histone chaperone activity of SPT6. A region rich in certain amino acids such as serine, threonine, and glycine characterizes the C-terminus of SPT6. There are two more interaction domains present in SPT6: first, an RNA-binding S1 domain that is essential in protein translation as it interacts with the ribosome and mRNA and second, a SH2 domain that mediates interaction with the phosphorylated CTD of RNAPII (Dronamraju and Strahl, 2014).

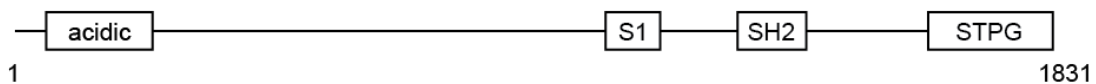


**Figure 6: Schematic representation of SPT6 domain structure.** Acidic N-terminal region (acidic, aa 6-245), RNA-binding S1 domain (S1, aa 1217-1286), phospho-tyrosine binding SH2 domain (SH2, aa 1329-1440), C-terminal domain rich in serine, threonine, proline and glycine (STPG, aa 1552-1831).

## 1.2 Dosage Compensation

Aneuploidy describes genomic deviation from the normal diploid set of chromosomes. Already one century ago aneuploidy was described to be involved in cancer, birth defects and impaired cell proliferation (Boveri, 1902). Hence, aneuploidy is not well tolerated in cells, as it unbalances the fine-tuned organization of the genome. Spontaneously arising aneuploidies have to be discriminated from “natural” monosomies occurring in sex determination. For example, sex determination via dimorphic sex chromosomes, like it is found in mammals and *Drosophila*, creates a homogametic genotype (XX) in females, whereas the male genotype is heterogametic (XY).

It is obvious that the chromosomal imbalance resulting from male and female sex chromosomes has to be balanced. To adjust levels of products resulting from X-linked gene expression heterogametic organisms have evolved different mechanisms grouped under the term “dosage compensation” (Lucchesi, 2005). In mammalian females one of the two X chromosomes is inactivated, consequently genes are only expressed from the remaining single X chromosome. While nematodes reduce transcription from both X chromosomes by half (hypotranscription), in *Drosophila* transcription from the single male X-chromosome is increased by twofold (hypertranscription). Although mammals, nematodes and flies use different strategies to realize dosage compensation, they all share chromatin-based mechanisms to regulate transcription (Figure 7).

		male	=	female/ hermaphrodite	
<i>Homo sapiens</i>		$\begin{matrix} X & Y \\ 1 & \end{matrix}$	=	$\begin{matrix} X & [x] \\ 1 & \end{matrix}$	<b>X inactivation</b>
<i>Caenorhabditis elegans</i>		$\begin{matrix} X \\ 1 \end{matrix}$	=	$\begin{matrix} x & x \\ 1/2 & + & 1/2 \end{matrix}$	<b>Hypotranscription</b>
<i>Drosophila melanogaster</i>		$\begin{matrix} X & Y \\ 2 & \end{matrix}$	=	$\begin{matrix} X & X \\ 1+1 \end{matrix}$	<b>Hypertranscription</b>

**Figure 7: Mechanisms of dosage compensation in human, nematodes and flies.** Dosage compensation in humans is characterized by the inactivation of one X chromosome in females. In *C. elegans* the monosomy of the male X chromosome is compensated by twofold reduction of X-linked gene expression (hypotranscription) in hermaphrodites. In *D. melanogaster* gene expression from the single male X-chromosome is twofold upregulated (hypertranscription). Numbers indicate the gene dose from the distinct chromosomes.

### 1.2.1 The Dosage Compensation Complex of *Drosophila melanogaster*

Balancing the monosomy of the X-chromosome in *Drosophila* males is a crucial process that equalizes X-linked gene expression between the two sexes (Gelbart and Kuroda, 2009). Here this process results in a twofold increased transcriptional output of X-chromosomal genes and is mediated by the ribonucleoprotein dosage compensation complex (MSL-DCC). The MSL-DCC consists of five proteins MSL1, MSL2, MSL3 (Male-Specific-Lethal 1, 2, 3), MLE (Maleless), MOF (Males-absent-On-the-First) and two redundant non-coding *roX* RNAs (*roX1* and *roX2*; Figure 8). In males, the MSL-DCC is specifically targeted to actively transcribed genes on the X chromosome where MOF exhibits acetylation of H4K16, a modification correlating with increased transcription (Akhtar and Becker, 2000).

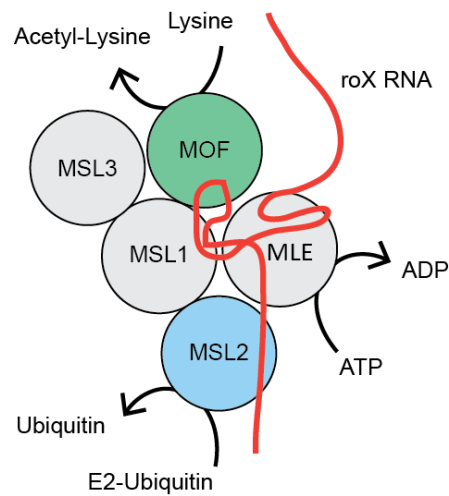


**Figure 8: Schematic representation of the *Drosophila* Dosage compensation complex.** The Dosage compensation complex is composed of five male-specific lethal (MSL) proteins and a non-coding *roX* RNA. Three enzymatic activities reside in the DCC: MSL2 is an E3 ubiquitin ligase, MLE is an ATP-dependent helicase and MOF is a histone acetyltransferase.

MSL1 functions as a scaffold protein for the complex as it exhibits binding sites for all other MSL subunits except MLE. Interaction with MSL2 is achieved via the N-terminal part of MSL1 while MSL3 and MOF binding sites are located within the C-terminus of MSL1 (Morales, 2004; Hallacli, 2012). MSL2 is an E3 ligase found to regulate complex homeostasis by ubiquitylation of the MSL proteins (Villa, 2012). MSL3 harbors a chromodomain able to bind H3K36me3 at active genes (Larschan, 2007). MLE is an ATP-dependent helicase that remodels the *roX* RNA and triggers complex assembly by ATP-dependent recruitment of MSL2 (Maenner, 2013). The histone acetyltransferase MOF is essential for acetylation of lysine 16 of histone 4 (H4K16ac) a modification that is strongly enriched on the male X-chromosome found to be implicated in the derepression of transcription (Bone, 1994; Hilfiker, 1997; Akhtar and Becker, 2000). The *roX* RNAs are essential for X-chromosomal targeting and are present in two different forms in *Drosophila*. *roX1* and *roX2* support the

assembly of the MSL-DCC, yet they differ greatly in size and sequence similarity (Franke and Baker, 1999). *roX1* is expressed early during embryonic development of both sexes, whereas *roX2* expression is expressed later exclusively in males (Meller, 2003).

Both the MSL-DCC proteins and *roX* RNAs are essential for male but not for female viability (Belote, 1980). All DCC-subunits, except MSL2 are expressed in females as well. Yet, it is still controversial which impact the DCC proteins have in female flies. Assembly of a functional DCC on the X chromosome is restricted to male flies as female flies express the splicing regulator SXL (sex lethal) an RNA binding protein that negatively regulates translation of MSL2 (Bashaw and Baker, 1997). For this purpose *msl2* transcripts contain multiple SXL-binding sites both in the 5' and 3' untranslated regions of *msl2* mRNA (Kelley, 1995). Depletion of SXL is lethal to female flies due to activation of dosage compensation and MSL2 expression. Experiments confirmed that ectopically expressed MSL2 in females is sufficient to assemble the DCC on both female X chromosomes. On the other hand ectopic expression of SXL in males will result in loss of dosage compensation, consequently these males die.

### **1.2.2 Targeting and assembly of the MSL-DCC to the male X chromosome**

Immunostainings of polytene chromosomes highlight that in the absence of MOF, MLE or MSL3 targeting of a subcomplex composed of MSL1 and MSL2 is restricted to a subset of binding sites, while painting of the entire chromosome is only achieved once the full complex is assembled (Straub and Becker, 2007; Figure 9).

Indeed, the initial targeting of MSL1 and MSL2 to the male X chromosome is achieved via recognition of a subset of distinct sites known as high-affinity sites (HAS) or chromatin entry sites (CES) by the MSL2 CXC domain. HAS are distributed along the X chromosome in intervals of ~50 kb and were postulated to function as nucleation sites that allow access of the MSL-DCC to the X chromosome. Already in the past, recognition of HAS was shown to be a highly sequence-dependent step as most of the HAS share a 21 bp GA-rich motif (MSL recognition element, MRE). Inserted on autosomes this motif was found to attract the MSL-DCC and mutations of the MRE in turn abolished MSL-DCC recruitment to these sites (Alekseyenko, 2008). While the identification of a specific DNA sequence is crucial in understanding the targeting mechanisms the identification the MRE alone is not sufficient to explain the X specificity for the MSL-DCC on the male X chromosome. On the one hand the MRE is less than twofold enriched on the X chromosome, on the other hand there is also a large subset of non-used sites matching the MRE consensus motif (Lucchesi and Kuroda, 2015). Hence, additional features like chromatin context were proposed to be involved in MRE recognition (Alekseyenko, 2012). Recent evidence supports this hypothesis,

highlighting that the initial recognition of high affinity sites is both dependent on DNA-shape of the underlying motif and a highly specialized motif called PionX (Villa, 2016). Interestingly, the X chromosome harbors regions unable to recruit the MSL-DCC, yet those regions are occupied by the complex if targeting elements are close by (Nusinow, 2005). This observation suggests a “two-step” model for MSL-DCC recruitment to the male X chromosome: after the initial targeting of an MSL1-MSL2 core complex to HAS this complex provides a platform that invite MSL3, MOF, MLE and the *roX* RNAs for a full complex assembly on the male X chromosome. In a second step the fully assembled MSL-DCC spreads from high affinity sites in *cis* to active genes marked by trimethylation of H3K36. It was proposed that the recruitment of the complex from HAS to sites of active transcription is carried out by MSL3, as it was shown that MSL3 is able to bind H3K36me3 *in vitro* (Larschan, 2007). Unlike other transcriptional regulators the MSL-DCC does not bind to promoters. Instead, the DCC associates with the transcribed middle and 3’ regions of active genes (Straub, 2013). Finally, MOF catalyzes the site-specific acetylation of H4K16 (H4K16ac) on active gene bodies to increase transcriptional output from the single male X chromosome in a twofold range.

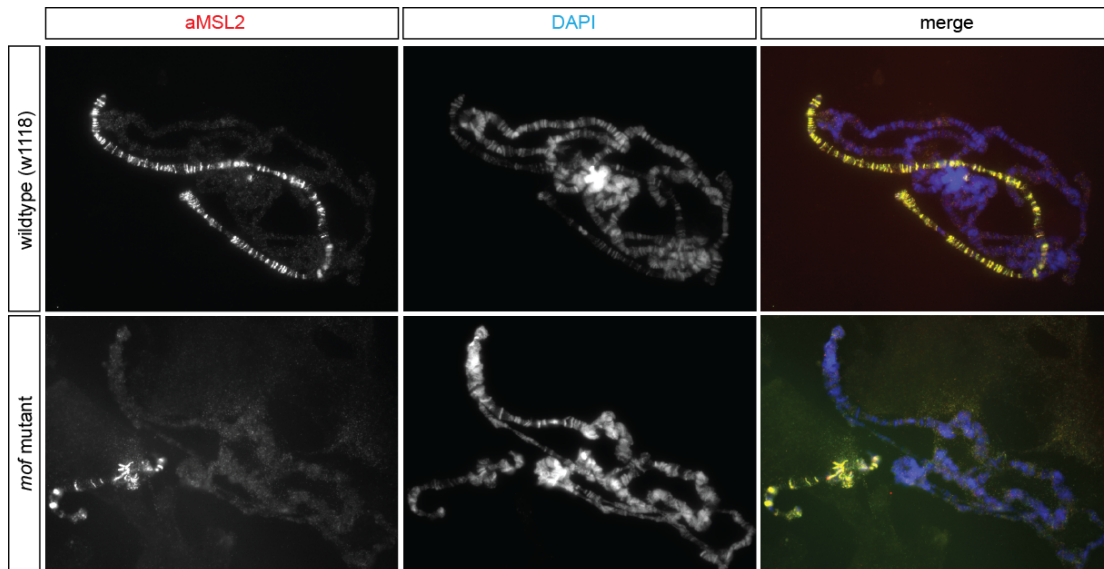


**Figure 9: The MSL-DCC specifically targets the male X chromosome.** Polytene chromosomes from *Drosophila melanogaster* larvae stained with MSL2 antibodies visualize the X-specific targeting of the MSL-DCC to the male X chromosome. In a *mof* mutant background only a subset of binding sites is occupied by MSL2. DNA is counterstained with DAPI.

### 1.2.3 Mechanism of *Drosophila* dosage compensation

Recent evidence indicates that dosage compensation is regulated posttranscriptionally (Graindorge, 2011). In theory, gene expression can be regulated at different steps during transcription initiation, release of RNAPII from pausing or elongation, respectively. A study from 2012 suggested that dosage compensation is mediated through increased transcription initiation (Conrad and Akhtar, 2012). The authors report nearly twofold enrichment in RNAPII occupancy at promoters and slight enhancement of RNAPII release into gene bodies. Interpretation of this observation suggests that dosage compensation mainly operates in the absence of productive elongation however, transition into elongation might be facilitated. Another model for the coordinate regulation of X-linked genes in *Drosophila* males favors enhanced transcriptional elongation. Indeed, several lines of evidence suggest that the enhanced expression of X-linked genes is mediated during transcriptional elongation (Larschan, 2011; Prabhakaran and Kelley, 2012; Ferrari, 2013). The regulation of transcription elongation through alterations in chromatin structure, such as trimethylation of lysine 36 of histone H3 (H3K36me3), acetylation of H4K16 or presence of other elongation factors was found to be a highly regulated process (Saunders, 2006; Sims, 2004). According to an *in vitro* model H4K16 acetylated regions on the male X-chromosome lead to diminished inter-nucleosomal interactions that facilitate nucleosome eviction and RNAPII progression *in vivo* (Straub and Becker, 2007). Reduced steric hindrance on X-linked gene bodies resulting from H4K16ac was suggested to be involved in the release of RNAPII from pausing into elongation (“jump start”). Indeed, this suggestion was further supported by the increase of elongating RNAPII marked by phosphorylation at serine-2 (Ser2P) over X-linked gene bodies (Regnard, 2011). As H4K16ac levels increase RNAPII density on X-linked gene bodies is gained (“gain”). Taken together, this “jump start and gain model” explains the coordinated expression of X-linked genes through an acetylated chromatin template that facilitates transcription elongation (Ferrari, 2013).

In the human system MSL2 was shown to be directly involved in the facilitation of transcription elongation through its E3 ubiquitin ligase activity. MSL2-mediated ubiquitylation of H2B (H2Bub) in turn facilitates the methylation of H3K4 and H3K79 (Wu, 2011). Both H2Bub and H3K79 methylation represent histone marks important for transcription elongation (Minsky, 2008).

### 1.2.4 Properties and functions of MSL2

The male specific MSL2 protein features several characteristic domains: RING, CXC and Pro-Bas domain (Figure 10). The conserved N-terminal RING domain is essential for dosage compensation and enables self-ubiquitylation as well as ubiquitylation of the other MSL proteins (Villa, 2012). Moreover, the RING finger mediates the interaction with MSL1 (Coppes, 1998). Both CXC and proline/basic-residue rich domains (Pro-Bas) are implicated in the identification of DNA elements on the X chromosome. MSL2 is implicated in the binding of HAS, as lack or mutation of the CXC domain results in diminished targeting of MSL2 to distinct reporter regions as well as disturbed MSL-DCC localization on the X-territories (Fauth, 2010). The structural basis of CXC binding to DNA was resolved and highlighted that a single arginine is involved in the readout of a dinucleotide sequence from the minor groove (Zheng, 2014). Moreover, the DNA binding capacity of the Pro-Bas and CXC DNA-binding surfaces was only recently refined in more detail demonstrating that the non-conserved Pro-Bas domain is implicated in general DNA binding, whereas the CXC region selectively recognizes the X chromosome using the PionX motif (Villa, 2016).

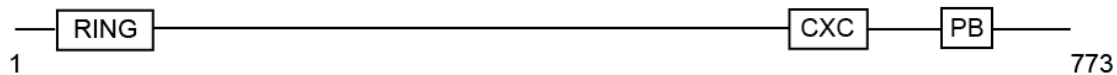


**Figure 10: Schematic representation of MSL2 domain structure.** RING domain (really interesting new gene, aa 41-85), cysteine-rich region (CXC, aa 525-561), proline-rich Pro-Bas region (PB, aa 685-713).

### 1.2.5 Properties and functions of MOF

The histone acetyltransferase MOF is one of the best-characterized proteins of the MSL-DCC (Figure 11). Two well-characterized and highly conserved domains are present in the MOF protein: chromo-barrel domain (CBD) and histone acetyltransferase domain (HAT). Unlike other chromodomains that target methylated lysine residues, the MOF chromobarrel domain (CBD) lacks a structural feature that abolishes methyl-lysine binding (Nielsen, 2005). Instead the MOF CBD is implicated in binding of nucleic acids (RNA and DNA) both *in vitro* and *in vivo* (Akhtar and Becker, 2000; Nielsen, 2005). Based on the structural homology within its HAT domain MOF belongs to the family of MYST HATs, defined by the presence of the highly conserved MYST (HAT) domain that comprises the acetyl-CoA binding site (Marmorstein and Trievel, 2009). Most MYST domains are characterized by the presence of a C2HC zinc finger (Yang, 2004). In *Drosophila* MOF the C2HC zinc finger is crucial for both HAT activity and nucleosome binding *in vitro* (Akhtar and Becker, 2001). Absent in the human ortholog, *Drosophila* MOF exhibits a large and unstructured N-terminus of roughly

350 aa with a highly acidic character (pI ~3.88). For a long time no specific function was assigned to the MOF N-terminus, however recently it was described to fulfill sex-specific functions essential for male viability (Conrad, 2012).

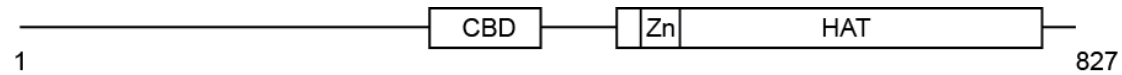


**Figure 11: Schematic representation of MOF domain structure.** Chromo-like chromobarrel domain (CBD, aa 370-476), histone acetyltransferase (HAT, aa 538-824), C2HC zinc finger (Zn, aa 575-592).

As MOF is targeted to ectopic sites exhibited H4K16 acetylation activity leads to derepression of transcription. Hence, MOF was proposed to be involved in the activation of X-linked genes (Akhtar and Becker, 2001). However, the function of MOF exceeds sole histone acetylation activity. For example MOF exhibits autoacetylation activity on K605, which resides in the highly conserved region of the C2HC zinc finger domain (Kadlec, 2011). Point mutants of K605 or disruption of the zinc finger leads to lack of MOF enzyme activity, suggesting a critical involvement of K605ac for MOF substrate specificity and HAT activity. Furthermore, MOF is able to acetylate MSL3 at K116, a modification that affects the interaction between MSL3 and RNA and ultimately leads to the fine-tuning of dosage compensation (Buscaino, 2003). Alternatively, MOF also participates in a complex consisting of NSL1, NSL2, NSL3, MCRS2, MBD-R2, and WDS. This complex was termed the NSL (non-specific lethal) complex since disruption of respective genes is lethal in both sexes (Mendjan, 2006). The evolutionarily conserved NSL complex acts as a major transcriptional regulator for housekeeping genes in *Drosophila* (Feller et al. 2012). ChIP-Chip experiments from adult flies revealed that in females MOF colocalizes with MBD-R2 at the 5' end of most actively transcribed genes. Whereas in the context of the MSL-DCC MOF is enriched together with MSL1 on the coding regions of actively transcribed X chromosomal genes. Induction of dosage compensation in female flies through ectopic reconstitution of the MSL-DCC results in redistribution of MOF from the autosomes to the X chromosome suggesting that MOF distributes between the MSL-DCC and the NSL complex (Prestel, 2010).

### 1.3 Ubiquitylation

Ubiquitin is a highly conserved, 76-residue regulatory protein that is found ubiquitously in eukaryotes. It was first described due to its involvement in protein turnover and degradation via the proteasome (Ciechanover, 1980; Hershko, 1980). However, today it is clear that the attachment of ubiquitin onto substrate protein not only serves a proteolytic signal, but also acts as a key mechanism in the regulation of diverse cellular mechanisms such as DNA repair, signal transduction, modulation of chromatin structure and intracellular trafficking.

#### 1.3.1 The mechanism of ubiquitin attachment onto substrate protein

The posttranslational attachment of ubiquitin onto substrate protein relies on a cascade of three sequential enzymatic reactions: ubiquitin-activating enzyme E1, ubiquitin-conjugating enzyme E2 and ubiquitin protein ligase E3 (Hershko and Ciechanover, 1992). In the first step of the ubiquitylation cascade, ubiquitin is activated by adenylation via E1 on its C-terminal glycine residue. An ATP-dependent two-step reaction generates a high-energy E1-thiol-ester-ubiquitin intermediate. The activated ubiquitin is subsequently transferred to a specific cysteine residue in the active site of E2. The family of E3 ubiquitin ligases carries out the final transfer of ubiquitin from E2 to the substrate. E3 ligases are crucial for substrate recognition and can be divided into two groups distinct in structure and sequence of their catalytic modules: HECT (homology to the E6AP carboxyl terminus) and RING (really interesting new gene) proteins. HECT domain containing E3 ligases catalyze reactions in which the enzyme form intermediate thioesters with ubiquitin at their active site cysteine residue before the ubiquitin moiety is finally transferred to the substrate. In contrast, RING finger containing E3 ligases act as scaffolds binding both E2 and the substrate to ensure proximity for efficient and direct transfer of the activated ubiquitin from E2 to the substrate (Özkan, 2005).

Most organisms exhibit one or two E1 enzymes with promiscuous specificities capable of transferring the activated ubiquitin moiety to almost any E2 enzyme. In contrast, the class of E2 and E3 enzymes is more diverse reflecting the specificity of substrate selection for ubiquitin conjugation. Two E1 enzymes (Pelzer et al., 2007; Groettrup, 2008), 37 E2 enzymes (Markson, 2009; Michelle, 2009) and >600 E3 ligases are encoded in the human genome (Deshaies and Joazeiro, 2009). The *Drosophila* genome encodes only one E1 enzyme (Watts, 2003), 32 E2 enzymes (Michelle, 2009) and roughly 150 E3 enzymes (Du, 2011).

### 1.3.2 Diversity of ubiquitylation

Ubiquitylation of substrate protein emerges in different ways. The posttranslational modification of lysine residues can be carried out on a single lysine (monoUb), multiple lysines (multi-monoUb) or a single lysine with a polymeric chain of ubiquitin (polyUb) (Figure 12; Strieter and Korasick, 2012). A significant layer of complexity is added to the ubiquitin signaling network by the fact that formation of polyUb chains bears the opportunity to form diverse branched chains and linkages. As all seven lysine residues (K6, K11, K27, K29, K33, K48, K63) and the N-terminal methionine residue of the ubiquitin molecule can serve as acceptors of further ubiquitin molecules, various chains with different types of linkages and lengths may arise *in vivo* (Xu, 2009; Dammer, 2011).

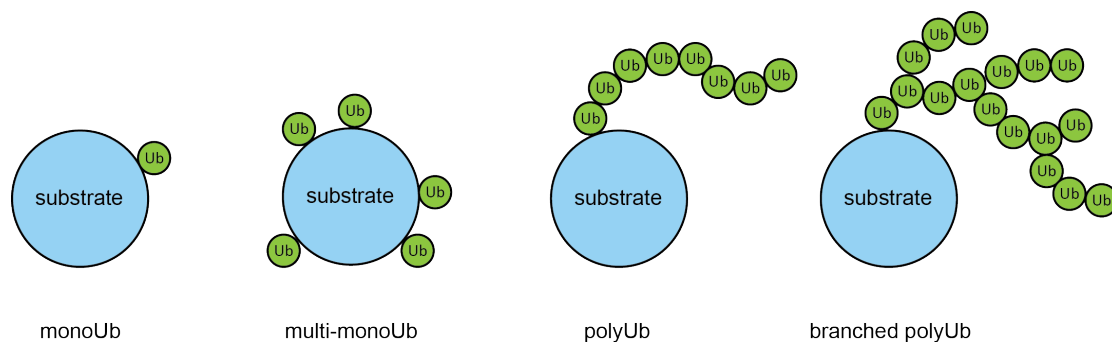


**Figure 12: Types of ubiquitylation.** Ubiquitin modifications can be arranged in various ways on the substrate protein. Addition of a single ubiquitin molecule results in monoubiquitylation (monoUb). Addition of more than one ubiquitin moiety to different sites on the target protein is referred to as multi-monoubiquitylation (multi-monoUb). Conjugation of ubiquitin chains to a distinct target residue is considered a polyubiquitylation (polyUb). If the ubiquitin molecules within a chain are linked always via the same residue it will result in linear polyubiquitin chains. In contrast branched polyubiquitin chains (branched polyUb) result if the ubiquitin molecules are linked via different lysines on ubiquitin.

### 1.3.3 Biological consequences of ubiquitylation

Whereas attachment of ubiquitin is still considered to be a classical proteolytic signal recent achievements in the field highlight that ubiquitylation is a complex signal that can lead to a variety of biological signals. Monoubiquitylation of a target protein is implicated in diverse processes such as modulation of protein-protein interactions, cellular localization transcription regulation or modulation of cell differentiation (Husnjak, 2012; Mosesson, 2009; Sussman, 2013). In contrast, addition of multiple monoubiquitylation to substrate protein was linked to endocytosis and cell signaling (Chen and Sun, 2009; Haglund, 2003). The main role for polyubiquitin chains can still be attributed to the labeling of target protein for proteasomal degradation via the 26S proteasome (Xu, 2009). For example lysine 11, 29 and 48 polyubiquitin chains mediate proteasome-dependent degradation of target protein (Johnson, 1995; de Bie, 2010; Matsumoto, 2010) whereby a tetramer of K48-linked Ub-chains was described to be the minimal proteolytic signal (Hershko and Ciechanover, 1998).

Polyubiquitin chains are composed of identical subunits, yet ubiquitin chains linked through K48 and K63 exhibit conformational differences. These differences in structure are crucial for interactions of the modified target with distinct ubiquitin-binding proteins (Dikic, 2009) and may explain the different properties and functions. K63-linked chains are not only involved in non-proteolytic actions by regulating the target's function during DNA repair (Chen and Sun, 2009) but also typically facilitate protein-protein interactions required for signal transduction (Skaug, 2009). Moreover, intracellular trafficking to the lysosome/vacuole, activation of transcription factors and regulation of histones was described to be dependent on K63 mediated ubiquitylation (Braun and Madhani, 2012; Praefcke, 2012). The atypical lysine 6-linked polyubiquitin chains have been linked to autoubiquitylation activity of specific E3 ligases such as the Polycomb complex protein RING1B (Ben-Saadon, 2006). It is obvious that ubiquitin conjugation is a highly complex network that regulates crucial processes of distinct nature. Thus, study of ubiquitin modifications is an important yet challenging task

In *Drosophila* the MSL2 RING domain is able to exhibit ubiquitylation activity on the MSL-DCC. While this function is crucial to maintain a balanced stoichiometry of the dosage compensation complex, MSL2-dependent ubiquitylation might fulfill roles apart from proteasomal targeting. Likewise, human MSL2 (hMSL2) was suggested to ubiquitylates the tumor suppressor p53 promoting cytoplasmic p53 localization without affecting the stability (Kruse and Gu, 2009). In addition, MSL2 together with MSL1 acts as a histone ubiquitin ligase that specifically ubiquitylates H2B at lysine 34, a modification involved in the *trans*-regulation of H3K4 and H3K79 methylation (Wu, 2011). Moreover, hMSL2 was implicated in the modification and stabilization of 53BP1 a key repair protein that acts in response to DNA damage (Lai, 2013).

## 1.4 Objective

While it has been shown that MSL2-mediated ubiquitylation of the MSL-DCC proteins is used to maintain a balanced stoichiometry of the complex (Villa, 2012), MOF ubiquitylation could play an additional role apart from proteasomal targeting. The attachment of ubiquitin is still considered to be a classical proteolytic signal, however achievements in the field reveal that ubiquitylation is a complex modification that can lead to a variety of biological signals. MSL2-related ubiquitylation of MOF thus might be involved in roles apart from proteasomal targeting. This thesis provides a comprehensive analysis of MOF ubiquitylation. To analyze the functions of MOF ubiquitylation Lys to Arg (K>R) point mutants were generated and characterized both *in vivo* and *in vitro* using recombinant protein, stable cell lines and transgenic flies, respectively. Recombinant MOF mutant protein was employed in *in vitro* ubiquitylation assays to analyze modification pattern of both MSL2-mediated and MSL2-independent ubiquitylation. Furthermore, histone acetylation assays were performed to estimate enzymatic activity of generated MOF mutants. Stable cell lines were generated to analyze MSL-DCC assembly and X-territorial targeting. Transgenic fly lines expressing MOF mutants were analyzed for their male viability. Using a mass spectrometry-based approach the first comprehensive analysis of MOF ubiquitylation pattern *in vitro* and *in vivo* was generated. Furthermore the first ubiquitylome from S2 cells has been obtained highlighting the complexity and magnitude of ubiquitylation present in *Drosophila*.

Previous experiments performed in collaboration with Tiziana Bonaldi (IFOM-IEO Campus, Milan) revealed that MSL2 targets potential substrates outside of the MSL-DCC as well. Due to its involvement in transcriptional elongation SPT6 was chosen as a candidate protein. Monoclonal antibodies directed against SPT6 were generated and characterized in Western blot and immunofluorescence. Expression and purification of recombinant SPT6 was employed for *in vitro* ubiquitylation assays in the presence of MSL2.



## **2 MATERIALS & METHODS**

### 2.1 Materials

#### 2.1.1 Chemicals

Acetic acid (VWR); Acrylamide Rotiporese Gel 30 (Roth); Agarose (Bio & Sell); Ampicillin (Roth); Anti-FLAG M2 Agarose beads (Sigma); ATP (Sigma); Bovine serum albumin, (Sigma); Bromophenol blue (Serva); 2-Chloroacetamide (Sigma); Complete Protease Inhibitor Cocktail Tablets (Roche); Coomassie Brilliant Blue (Sigma); DAPI (4',6-diamidino-2-phenylindole), (Invitrogen); DMSO (Dimethylsulfoxide), (Sigma); dNTP mix (NEB); DTT (Dithiotreitol), (Roth); Effectene Transfection Reagent (Quiagen); ECL Advance Western Blotting Detection Kit (VWR); EDTA (Sigma); EDTA (Ethylenediaminetetraacetic acid), (Sigma); EGTA (Ethylenglycol-bis(2-aminoethyl)-N,N,N',N'-tetraacetic acid), (Sigma); Ethanol (Sigma), Ethidium bromide (Sigma); Fetal bovine serum (Sigma); GFP-Trap A (Chromo Tek GmbH); Glycerol (Merck);  $\beta$ -glycerophosphate (Sigma); Glycogen (Roche); GST-Mdm2/HDM2 (R&D Systems); Hepes (N-(2-hydroxyethyl)piperazine-H<sup>+</sup>-(2-ethanesulfonic acid), (Roth); His6-Ubiquitin (R&D Systems); Hygromycin B (Life Technologies); IPTG (Isopropyl-D-thiogalactopyranoside), (Sigma); Isopropanol (Sigma); LB Agar (Serva); Magnesium chloride (VWR);  $\beta$ -mercaptoethanol (Sigma); Methanol (Sigma); MG 132 (Enzo Life Sciences); NEM (N-Ethylmaleinimid), (Thermo Fisher Scientific); Normal Donkey Serum (Dianova); Normal Goat Serum (Dianova); NP-40 (Igepal CA-630), (Sigma); Orange G (Sigma); Paraformaldehyde (Life Technologies); Peptone (BD Biosciences); PMSF (Sigma); Potassium chloride (VWR); Protein A Sepharose, Protein G Sepharose (Helmholtz Centre Munich, E. Kremmer); Rotiporese® Gel 30 (Roth); Schneider's Drosophila medium (Life Technologies); SDS (Sodium dodecyl Sulfate), (Serva); Sf-900 II medium (Invitrogen); SILAC Drosophila medium -Arg/-Lys (Dundee Cell Products); Sodium bicarbonate (Sigma); Sodium carbonate (Sigma); Sodium chloride (Serva); Sodium deoxycholate (Sigma); Sodium fluoride (Sigma); Sodium orthovanadate (Sigma); Penicillin/Streptomycin (Sigma); PMSF (Phenylmethanesulfonyl fluoride), (Sigma); TEMED (N,N,N',N'-Tetramethylethylenediamine), (Roth); Tris (Diagonal); Triton X-100 (Sigma); Tween 20 (Sigma); Yeast extract (BD Biosciences).

**2.1.2 Enzymes, Kits and Markers**

100 bp DNA marker (NEB), 1 kb DNA marker (NEB); Duolink detection reagent (#DUO92013, Sigma), Duolink PLA probe anti-mouse minus (#DUO92004, Sigma); Duolink PLA probe anti-rabbit plus (#DUO92002, Sigma); Fast SYBR® Green Master Mix (Applied Biosciences); GeneElute PCR Clean-up Kit (Sigma); MEGAscript T7 kit (Ambion); Midi- and Midiprep Kit (Marchery Nagel); Novex Colloidal Blue Staining Kit (Invitrogen); PCR cleanup Kit (Marchery Nagel); peqGOLD Protein Marker IV (Peqlab); Pfu Turbo DNA Polymerase (Agilent); Phusion DNA Polymerase (Biolabs); Proteinmarker III (Serva); Restriction enzymes (NEB); RNeasy Kit (Qiagen); SuperSkript III First Strand Synthesis System (Life Technologies); Taq DNA Polymerase (Biolabs); UbcH5c/E2 enzyme (R&D Systems); UBE1/ E1 enzyme (R&D Systems).

**2.1.3 Consumables**

1.5 ml and 2 ml reaction tubes (Greiner, Sarstedt), 1.5 ml low binding tubes DNA (Sarstedt); 1.5 ml low binding tubes Protein (Sarstedt); 15 ml and 50 ml tubes (Sarstedt); Amplify solution (Amersham); Cell culture flasks (Sarstedt, Greiner); Cell culture plates (Sarstedt, Greiner); Cover slips (Roth); Cryovials (Roth); Filter paper Whatman 3 mm (Whatman); Filter tips (Biozym, Gilson, Sorenson); Glass pipettes 5 ml and 10 ml (Hirschmann); Glassware (Schott); Laboratory film (Parafilm); LightCycler R 480 Multiwell plate, white (Sarstedt); LightCycler R 480 Sealing foil (Sarstedt); Microscope slides SuperFrost (Roth); Micro-Spin columns (Bio Rad); Nitrocellulose membrane (Amersham); p81 filter paper (Millipore); Pasteur pipettes (Brand), Petridishes (Greiner); Pipette tips (Biozym, Greiner, Sarstedt); Protein gel cassettes (Invitrogen); Protein gels precast (Serva); Vectashield Mounting Medium (Vector Laboratories); X-ray films (Fujifilm).

**2.1.4 Antibodies**

**Table 1: Primary antibodies employed in this study**

Name	Type	Application	Dilution	Supplier
ms aFLAG	monoclonal, M2	WB	1:5000	Sigma (#F3165)
		IF	1:200	
rb aFLAG	polyclonal	IF	1:200	Sigma (#F7425)
ms aGFP	monoclonal	IF	1:200	Roche (#11814460001)
rat aGFP	monoclonal 3H9	WB	1:1000	ChromoTek (#ABIN398304)
rb aGFP	polyclonal	IF	1:200	Acris (#TP401)
ms aLamin	T40	WB	1:500	H. Saumweber
gp aMLE	polyclonal GP_16	WB	1:300	C. Regnard (Eurogentec)
rat aMLE	monoclonal 6E11	WB	1:1000	E. Kremmer (Helmholtz)
		IF	1:400	
rat aMOF	monoclonal 4D4	IF	1:9	E. Kremmer (Helmholtz)
rb aMOF	polyclonal (SA4897)	WB	1:2000	Akthar and Becker, 2000
		IF	1:400	
rb aMSL1	polyclonal	WB	1:1000	E. Schulze
		IF	1:400	
gp aMSL2	polyclonal	WB	1:2000	C. Regnard (Pineda)
rat aMSL2	monoclonal 1D6	WB	1:500	E. Kremmer (Helmholtz)
		IF	1:200	
rb aMSL2	polyclonal (SABC)	WB	1:1000	Gilfillan et al., 2006
		IF	1:400	
rat aMSL3	monoclonal 1C9.5	WB	1:50	E. Kremmer (Helmholtz)
		IF	1:10	
ms aSPT6	monoclonal 26D12	WB	1:1000	this thesis
		IF	1:400	
ms aSPT6	monoclonal 25C6	WB	1:1000	this thesis
		IF	1:400	
ms aSPT6	monoclonal 28C3	WB	1:50	this thesis
ms aSPT6	monoclonal 27C1	WB	1:50	this thesis
ms aUbiquitin	monoclonal, FK2	WB	1:1000	Merck Millipore (#04-263)
		IF	1:200	
rb aUbiquitin	polyclonal	IF	1:200	Merck Millipore (#662099)

**Table 2: Secondary antibodies employed in this study**

Name	Application	Dilution	Supplier
a ms HRP	WB	1:20000	VWR (#NA931)
a rat HRP	WB	1:20000	VWR (#NA935)
a rb HRP	WB	1:20000	VWR (#NA934)
a gp HRP	WB	1:50000	Dianova (#706-035-148)
a ms iRDye 680	WB	1:10000	LI-COR Biosciences (#926-68070)
a rat iRDye 700	WB	1:10000	Biomol (#612-730-120)
a rb iRDye 800	WB	1:10000	LI-COR Biosciences (#926-32211)
a gp iRDye 680	WB	1:10000	LI-COR Biosciences (#925-68077)
a ms 488	IF	1:400	Jackson Immuno Research (#715-545-151)
a ms Rhodamine-Red-X	IF	1:400	Jackson Immuno Research (#715-296-151)
a rat Cy3	IF	1:400	Jackson Immuno Research (#712-165-153)
a rb 647	IF	1:400	Jackson Immuno Research (#711-605-152)

**2.1.5 Oligonucleotides**

Oligonucleotides were purchased from Biomers (Ulm, Germany), Eurofins MWG Operon (Ebersberg, Germany) or Sigma-Aldrich (Taufkirchen, Germany).

**Table 3: Oligonucleotides: for molecular cloning**

Name	Sequence 5' – 3'	Description
MOF_1_AgeI_rv (SS059)	<b>AACCGGT</b> GCCATGGTCAAGGCATCATC	Subcloning of MOF point and deletion mutants from pFastBac1 to pHspEGFP
MOF_2_KpnI_fw (SS060)	GGGG <b>TACCA</b> TGTCTGAAGCGGAGCTGG	
MOF_3_KpnI_fw (SS061)	GGGG <b>TACCA</b> TGGAGCACGACAACACTTC	
MOF_4_AgeI_rv (SS062)	<b>AACCGGT</b> GCGCCGGAATTTCCCGGAG	
MOF_K372R_K381R_fw (SS022)	AATAGAT <b>CCT</b> TGTCGGGATTTTCGCTTAT	Site directed mutagenesis of MOF
MOF_K372R_K381R_rv (SS021)	ATCGAT <b>CCT</b> TTGCATC GATGCAA <b>AGG</b> ATCGATATAAGCGAAAAT CCCGAC <b>AGG</b> ATCTATT	
MOF_K532_fw (SS043)	CAGGCGGCGCTGGAG <b>AGG</b> GAGCACGAGT CCATT	Site directed mutagenesis of MOF
MOF_K532_rv (SS044)	AATGGACTCGTGCT <b>CCT</b> TCCAGCGCC GCCTG	
MOF_K706R_K715R_fw (SS045)	CTGTTCGCGC <b>AGG</b> GAGGGCGTAATCGGTA GTCCGGAG <b>AGAC</b> CGCTCTCG	Site directed mutagenesis of MOF
MOF_K706R_K715R_rv (SS046)	CGAGAGCGGG <b>TCT</b> TCCGGACTACCGATT ACGCCCT <b>CCT</b> GCGCGACAG	
MOF_K539R_K541R_K545R_fw (SS047)	CACGAGTCCATTACG <b>AGG</b> ATC <b>AGG</b> TACA TTGAT <b>AGG</b> CTGCAGTTTGGCAAC	Site directed mutagenesis of MOF
MOF_K539R_K541R_K545R_rv (SS047)	GTTGCCAAACTGCAG <b>CCT</b> ATCAATGTAC <b>CTGATCCT</b> CGTAATGGACTCGTG	
MOF_K694R_fw (SS048)	CGTAAGGGATTTGGA <b>AGG</b> CTACTAATAG CCTTTAG	Site directed mutagenesis of MOF
MOF_K694R_rv (SS049)	CTAAAGGCTATTAGTAG <b>CCT</b> TCCAAATC CCTTACG	
MOF_K773R_K776R_fw (SS050)	TCCATGAAGATGATC <b>AGG</b> TATTGG <b>AGG</b> GCCAGAATGTCATTTGC	Site directed mutagenesis of MOF
MOF_K773R_K776R_rv (SS051)	GCAAATGACATTCTGGCC <b>CCT</b> CCAATAC <b>CTGATCATCT</b> CATGGA	

**Table 4: Oligonucleotides for RNA interference**

Name	Sequence 5' – 3'	Description
GST_fw	TTAATACGACTCACTATAGGGAGAATGTCCCCTA TACTAGGTTA	Control siRNA
GST_rv	TTAATACGACTCACTATAGGGAGAACGCATCCAG GCACATTG	
MOF_fw	TTAATACGACTCACTATAGGGAGAATGTCTGAAG CGGAGCTGGAAC	siRNA targeting of MOF mRNA
MOF_rv	TTAATACGACTCACTATAGGGAGATTTCTGCTTC TGCGGCTGC	
MOF3'UTR_fw	TTAATACGACTCACTATAGGGAGAAATAAGCTAT TCTATTGCACC	siRNA targeting of endogenous MOF mRNA
MOF3'UTR_rv	TTAATACGACTCACTATAGGGAGATTTAACAAGT CCAGAGTTTT	
MSL2_fw	TTAATACGACTCACTATAGGGAGAATGGCCAGA CGGCATAC	siRNA targeting of MSL2 mRNA
MSL2_rv	TTAATACGACTCACTATAGGGAGACAGCGATGTG GGCATGTC	

**Table 5: DNA for *in vitro* ubiquitylation assay**

Name	Sequence 5' – 3'	Description
DBF12-L15	TGCGGCCATCTCTTTTCGTTTTGATGTTTCTACGC CATGTG	Generation of dsDNA
DBF12-L15	CACATGGCGTAGAAACATCAAAACGAAAGAGATG G	

### 2.1.6 Plasmids

All plasmids were sequenced at GATC (Konstanz, Germany) or Eurofins MWG Operon (Ebersberg, Germany). Cloning procedures of the individual plasmids listed in Table 6 are described in section 2.3 Molecular biology methods.

## 2 MATERIAL & METHODS

**Table 6: Plasmids employed in this study**

Name	Source	Description	Marker		
pBluescript II SK-noLys	Gene Cust	Synthesized DNA for subcloning	Amp		
pBluescript II SK-3Lys	Gene Cust	to pFastBac1			
pMT-SPT6-GFP	Heun Lab	Expression of C-terminally GFP-tagged proteins in S2 cells	Amp		
pIB-SPT6-GFP	Heun Lab				
pFastBac1-MOF wt-FLAG	Becker Lab	Expression of C-terminally GFP-tagged proteins in S2 cells	Amp		
pFastBac1-MOF-2KN-FLAG	this study				
pFastBac1-MOF-3KN-FLAG	this study				
pFastBac1-MOF-5KN-FLAG	this study				
pFastBac1-MOF-7KN-FLAG	this study				
pFastBac1-MOF-9KN-FLAG	this study				
pFastBac1-MOF-3KC-FLAG	this study				
pFastBac1-MOF-9KC-FLAG	this study				
pFastBac1-MOF $\Delta$ N-FLAG	this study				
pFastBac1-MOF Nt-FLAG	this study				
pFastBac1-SPT6 fl-FLAG	this study				
pFastBac1-SPT6[1]-FLAG	this study				
pFastBac1-SPT6[2]-FLAG	this study				
pEGFP-hsp-MOF wt-GFP	this study			Expression of C-terminally GFP-tagged proteins in S2 cells	Kan
pEGFP-hsp-MOF-2KN-GFP	this study				
pEGFP-hsp-MOF-3KN-GFP	this study				
pEGFP-hsp-MOF-5KN-GFP	this study				
pEGFP-hsp-MOF-7KN-GFP	this study				
pEGFP-hsp-MOF-9KN-GFP	this study				
pEGFP-hsp-MOF-3KC-GFP	this study				
pEGFP-hsp-MOF-9KC-GFP	this study				
pEGFP-hsp-MOF $\Delta$ N-GFP	this study				
pEGFP-hsp-MOF Nt-GFP	this study				
pUAST-AttB-MOF wt-FLAG	this study	Site directed insertion of MOF mutants to the fly genome	Amp		
pUAST-AttB-MOF-2KN-FLAG	this study				
pUAST-AttB-MOF-3KN-FLAG	this study				
pUAST-AttB-MOF-5KN-FLAG	this study				
pUAST-AttB-MOF-7KN-FLAG	this study				
pUAST-AttB-MOF-9KN-FLAG	this study				
pUAST-AttB-MOF-3KC-FLAG	this study				
pUAST-AttB-MOF-9KC-FLAG	this study				
pUAST-AttB-MOF $\Delta$ N-FLAG	this study				
pUAST-AttB-MOF Nt-FLAG	this study				

### 2.1.7 Insect cell lines and bacterial strains

#### 2.1.7.1 *E.coli* strains

**Table 7: Bacterial strains employed in this study**

Strain	Genotype	Supplier
<i>E.coli</i> DH5a	<i>fhuA2</i> $\Delta(\text{argF-lacZ})$ U169 <i>phoA</i> <i>glnV44</i> $\Phi$ 80 $\Delta(\text{lacZ})$ M15 <i>gyrA96</i> <i>recA1</i> <i>relA1</i> <i>endA1</i> <i>thi-1</i> <i>hsdR17</i>	NEB
<i>E.coli</i> Stellar	<i>F</i> <sup>-</sup> , <i>endA1</i> , <i>supE44</i> , <i>thi-1</i> , <i>recA1</i> , <i>relA1</i> , <i>gyrA96</i> , <i>phoA</i> , $\Phi$ 80d <i>lacZ</i> $\Delta$ M15, $\Delta(\text{lacZYA} - \text{argF})$ U169, $\Delta(\text{mrr} -$ <i>hsdRMS</i> - <i>mcrBC</i> ), $\Delta$ <i>mcrA</i> , $\lambda$ -	Clontech
<i>E.coli</i> DH10Bac	<i>F</i> <sup>mcrA</sup> $\Delta(\text{mrr-hsdRMS-mcrBC})$ $\Phi$ 80 <i>lacZ</i> $\Delta$ M15 $\Delta$ <i>lacX74</i> <i>recA1</i> <i>endA1</i> <i>araD139</i> $\Delta(\text{ara, leu})$ 7697 <i>galU</i> <i>galK</i> $\lambda$ <i>rpsL</i> <i>nupG</i> /pMON14272/pMON7124	Life Technologies

#### 2.1.7.2 Insect cell lines

**Table 8: Insect cell lines employed in this study**

Strain	Organism	Origin	Source
Kc	<i>D. melanogaster</i>	embryonic, dorsal closure stage	DGRC
L2-4	<i>D. melanogaster</i>	S2 clone, late embryonic stage	Patrick Heun
Sf21	<i>S. frugiperda</i>	pupal ovarian tissue	Invitrogen

2.1.7.3 Stable *Drosophila melanogaster* cell lines

**Table 9: Stable cell lines obtained in this study**

Cell line	Plasmid	Source
L2-4 MOF wt	pHspEGFP	This thesis
L2-4 MOF-2KN	pHspEGFP	
L2-4 MOF-3KN	pHspEGFP	
L2-4 MOF-5KN	pHspEGFP	
L2-4 MOF-7KN	pHspEGFP	
L2-4 MOF-9KN	pHspEGFP	
L2-4 MOF Nt	pHspEGFP	
L2-4 MOF ΔN	pHspEGFP	
L2-4 MOF-3KC	pHspEGFP	
L2-4 MOF-9KC	pHspEGFP	
Kc MOF wt	pHspEGFP	This thesis
Kc MOF-3KC	pHspEGFP	
Kc MOF-9KC	pHspEGFP	
L2-4 SPT6-MT	pMT/V5-His/ <i>lacZ</i>	This thesis
L2-4 SPT6-IB	pIB	

## 2.1.8 Technical devices

Description	Supplier
- 20°C Freezer	Liebherr
- 80°C Freezer	Thermo Scientific
4°C Fridge	Liebherr, Siemens
CASY Cell counter	Innovatis
Cell culture hood	B-[MaxPro] <sup>2</sup> -160, Berner
Centrifuges	Avanti JXN-26 (25-50 rotor) Eppendorf 5415R Heraeus Megafuge 2.0 Heraeus Pico17 Sorvall RC6 Plus (SS-34 rotor) Thermo Scientific Multifuge X3R
Gel documentation system	ChemiDoc, Bio-Rad Peqlab
Gel dryer	583 Gel Dryer, Bio-Rad
Developer machine	Curix, AGFA
Incubator Drosophila Cell culture	HettCube 600R, Hettich
Incubator Drosophila Fly culture	MLR-352H-PE, Panasonic
Incubation Shaker	Infors, Brunswick
LightCycler 480 II	Roche
Microscopes	Axiovert 200M epifluorescence, Zeiss Leica DMIL LED AxioStar plus, Zeiss Stemi 2000, equipped with KL1500 LCD, Zeiss
Mini Trans-Blot Electrophoretic Transfer Cell	Bio-Rad
pH 720 pH-meter	inoLab
Pipetboy	Neolab
Pipettes	Gilson
Proteingel chamber	Novex Mini-Cell System, Invitrogen
Scales	Sartorius
Sonifier	Branson MD-250
Spectrophotometer	Peqlab Nanodrop ND1000
Thermomixer	Eppendorf 5436
Vortex VR2	Bachofer

### 2.1.9 Software

Device/ Application	Software
ChemiDoc	Bio-Rad Image Lab Software 5.2.1
Image processing	Adobe Illustrator, Adobe Photoshop, Axio Vision (Zeiss), FIJI, ImageJ
LI-COR	Odyssey 2.1 (LI-COR)
Phylogeny analyses	Protein BLAST (web browser-based)
Sequence Alignments	MacVector, ApE, Serial Cloner
Visualization of protein structures	PyMOL (DeLano Scientific LLC)

## 2.2 Standard buffers and solutions

Established standard buffers are listed below. Additional buffers used in individual methods are included in their respective method section.

Agarose gel	TAE buffer
	1% Agarose
	Ethidium Bromide (6 $\mu$ l)
Ampicillin stock solution	100 mg/ml Ampicillin (1000x)
Chloramphenicol stock solution	34 mg/ml Chloramphenicol in Ethanol (1000x)
Coomassie destaining solution	10% Acetic acid (v/v)
Coomassie fixing solution	10% Acetic acid (v/v)
	50% Methanol (v/v)
Coomassie staining solution	10% Acetic acid (v/v)
	50% Methanol (v/v)
	0.1% Coomassie Brilliant Blue R (w/v)
Ethidium bromide stock solution	10 mg/ml Ethidium bromide (20000x)
Kanamycin stock solution	10 mg/ml Kanamycin (1000x)
5x Lämmli loading buffer	250 mM Tris pH 6.8
	50% Glycerol (v/v)
	10% SDS (w/v)
	0.05% Blue Bromophenol (w/v)
	0.5 M DTT
LB agar plates	LB medium
	2% Agar (w/v)
LB medium	1% Peptone (w/v)
	0.5% Yeast extract (w/v)
	1% NaCl (w/v)
PBS(T) buffer	137 mM NaCl
	2.7 mM KCl
	10 mM Na <sub>2</sub> HPO <sub>4</sub> x 12 H <sub>2</sub> O
	2 mM KH <sub>2</sub> PO <sub>4</sub>
	(0.1% Tween-20 (w/v))
RIPA extraction buffer	0,1% SDS (w/v)
	0,5% Deoxycholate (w/v)
	0,5% NP40 (v/v)
	1 mM EDTA
	50 mM Tris pH 7.5
	150 mM NaCl

## 2 MATERIAL & METHODS

---

SDS-PAGE running buffer	25 mM Tris base 192 mM Glycine 0.1% SDS (w/v)
Separating gel (7%)	23% Rotiporese® 375 mM Tris/HCl pH 8.8 0.1% SDS 0.07% TEMED 0.1% Ammonium persulfate
Stacking gel	17% Rotiporese® 126 mM Tris/HCl pH 6.8 0.1% SDS 0.1% TEMED 0.1% Ammonium persulfate
Transfer buffer	25 mM Tris base 192 mM Glycine 20% Methanol (v/v)
Urea sample buffer	9 M Urea 1% SDS (w/v) 25 mM Tris pH 6.8 1 mM EDTA 100 mM DTT
TAE buffer	40 mM Tris pH 7.6 20 mM acetic acid 1 mM EDTA
TE buffer	10 mM Tris pH 8 1mM EDTA

## 2.3 Molecular biology methods

### 2.3.1 General molecular biology methods

Standard molecular biology methods like polymerase chain reaction (PCR) for amplification of nucleic acids, enzymatic restriction and ligation of DNA fragments were performed according to standard protocols (Green and Sambrook, 2012). Preparation and transformation of chemically competent *E. coli* cells were performed according to Inoue (1990). Preparation of plasmid DNA was carried out using plasmid purification kits from Macherey-Nagel. DNA fragments from agarose gels and PCR reactions used for cloning were isolated and purified using the NucleoSpin® Gel and PCR clean-up kit (Macherey-Nagel).

### 2.3.2 Cloning of FLAG-tagged expression constructs

For expression of recombinant protein in Sf21 cells different MOF-FLAG wildtype and mutant constructs were cloned to pFastBac-1.

#### 2.3.2.1 Generation of MOF deletion mutants

MOF  $\Delta$ N was obtained after restriction of pFastBac1 MOF wt with NcoI/EcoRI, while MOF Nt was digested using NcoI/SacI, respectively. Klenow Polymerase was used for the fill in of 5'-overhangs and removal of 3'-overhangs. Obtained DNA fragments were purified from gel and ligated using Quick T4 DNA Ligase.

#### 2.3.2.2 Generation of N-terminal MOF mutants

Generation of MOF K>R point mutants in the N-terminus of MOF was carried out by DNA synthesis and site directed mutagenesis. To this end two MOF sequences with either 3 or 7 lysine to arginine point mutations were synthesized and placed into the pBSR2 vector. To obtain pFastBac MOF-3KN and pFastBac MOF-7KN synthesized DNA fragments were subcloned from pBSR2 to pFastBac1 using NarI and XbaII restriction sites. Two additional K>R (K372R, K381R) point mutations were inserted using specific primers (listed in Table 3) for site directed mutagenesis on pFastBac MOF wt, pFastBac MOF-3KN and pFastBac MOF-7KN to obtain pFastBac MOF-2KN, pFastBac MOF-5KN and pFastBac MOF-9KN, respectively.

#### 2.3.2.3 Generation of C-terminal MOF mutants

Generation of MOF K>R point mutants in the C-terminus of MOF was carried out by successive site directed mutagenesis. Specific primers (listed in Table 3) were used on pFastBac MOF wt to obtain pFastBac MOF-3KC and pFastBac MOF-9KC.

### **2.3.3 Cloning of GFP-tagged expression constructs**

For expression of recombinant protein in *Drosophila* cell lines MOF inserts were amplified from respective pFastBac1 constructs using suitable primer with AgeI and KpnI restriction sites (listed in Table 3). Obtained PCR products were purified using Quiagen quick spin Clean-up Kit. pHspEGFP vector and amplified inserts were digested using AgeI and KpnI restriction enzymes. Vector was further dephosphorylated using SAP (Shrimp alkaline phosphatase). Inserts and dephosphorylated vector were purified from gel and ligated using T4 DNA Ligase.

### **2.3.4 Cloning of FLAG-tagged constructs to pUAST-attB**

For site directed insertion of MOF mutants into the fly genome MOF mutant inserts were subcloned from respective pFastBac constructs to pUAST-attB (Bischof, 2007) using KpnI and EcoRI restriction. Inserts and dephosphorylated vector were purified from gel and ligated using T4 DNA Ligase.

## 2.4 Cell biological methods

### 2.4.1 Maintenance of *D. melanogaster* and *S. frugiperda* cell lines

Tissue culture work was performed under sterile conditions. Media and solutions were preheated to room temperature prior to use. Determination of cell number was carried out using the CASY cell counter system. To obtain the average cell density of a given cell culture flask 50  $\mu$ l of cell suspension was mixed with 10 ml of CasyTon solution and measured using a program adjusted to SL2 or Sf21 cell counting parameters, respectively.

*Drosophila* cells were cultivated at 26°C in Schneider's *Drosophila* medium containing L-glutamine, additionally supplemented with Penicillin, Streptomycin and 10% (v/v) fetal calf serum (FCS). Sf21 cells were cultivated at 26°C in Sf-900 II medium supplemented with Penicillin, Streptomycin and 10% (v/v) fetal calf serum (FCS). Cell density was maintained between  $0.5 \times 10^6$  and  $5 \times 10^6$  cells/ml to ensure exponential cell growth.

### 2.4.2 Cryopreservation and thawing of *Drosophila* cells

Cells were seeded to a density of  $1 \times 10^6$  cells/ml in a 175 cm<sup>2</sup> culture flask 3 days prior to freezing. Collection of cells was carried out by centrifugation at 500 g for 5 min at room temperature. After resuspending the cell pellet in 5 ml freezing medium (FCS + 10% (v/v) DMSO) cells were distributed to aliquots of 1 ml each in Cryo vials. To decelerate the freezing process vials were placed to an isopropanol freezing chamber and stored at -80°C. For long term preservation cells were maintained in liquid nitrogen.

To thaw cells a frozen stock was thawed rapidly in a water bath set to room temperature. Cells were transferred to 20 ml of cultivation medium in a 75 cm<sup>2</sup> culture flask. Maintenance and further cultivation was performed as described above.

### 2.4.3 Generation of stable SL2 and Kc cell lines

Stable *Drosophila* cell lines were generated by cotransfection of the expression vector and the pCoHygro selection vector. One day prior to transfection  $1 \times 10^6$  cells were seeded onto two 10 cm plates in 10 ml growth medium and incubated as described previously. The next day 2  $\mu$ g of expression vector and 100 ng of selection vector were transfected to the cells using Effectene reagent. In order to transfect two plates per construct double amounts of the transfection mix were prepared. Vectors were diluted in EC buffer to a final volume of 300  $\mu$ l. Subsequently 16  $\mu$ l of Enhancer was added and vortexed for 1 sec. After incubation for 5 min at room temperature 60  $\mu$ l Effectene was added, vortexed for 10 sec and again incubated for 15 min at room temperature. In the meantime 7 ml of fresh media was carefully replaced to the 10 cm culture plates. After the last incubation the transfection mix was

supplemented with 3 ml of growth medium and added dropwise to the cells. After 48-72 h the two plates were combined in a 75 cm<sup>2</sup> culture flask to a final volume of 20 ml, to start the selection Hygromycin B was added (300 µg/ml). 5 ml of selection medium (300 µg/ml Hygromycin B) was added weekly to the cells for about 3 weeks. Afterwards the selection medium was removed and the stable cell line was routinely maintained in 75 cm<sup>2</sup> flasks as described above.

### **2.4.4 Whole cell extracts from SL2 and Kc cells**

Analysis of protein content was carried out after preparation of whole cell extract. To this end 5x10<sup>6</sup> cells were collected and washed once with cold PBS. The pellet was resuspended in 200 µl RIPA extraction buffer supplemented with 1 mM Protease Inhibitor, 5 mM N-Ethylmaleinimid and 15 µM MG132. After 15 min on ice with occasional vortexing the cell suspension was cleared by centrifugation at 13000 rpm for 30 min at 4°C. After centrifugation 5x Lämmli sample buffer was added to the supernatant and boiled at 85°C for 10 min. For subsequent protein analysis by Western blotting 0.25x10<sup>6</sup> cells were loaded per lane for SDS-PAGE.

### **2.4.5 RNA interference in SL2 and Kc cells**

Genomic DNA or a DNA plasmid containing *gst* cDNA was used as a template in a PCR reaction to amplify a PCR product for SXL, MOF or GST RNAi, respectively. Used primers contain a binding site for T7 RNA polymerase and are listed in Table 4. Purification of PCR products was carried out using the PCR Clean-up Kit according to the manufacturer's guide. The obtained PCR products were used to transcribe dsRNA *in vitro* using the MEGAscript T7 kit according to the manufacturer's guide. Secondary structures were denatured by heating the RNA for 10 min at 85°C. To support formation of dsRNA duplexes the RNA was slowly cooled down to room temperature.

For knockdown experiments 2x10<sup>6</sup> exponentially growing cells were seeded to a 6-well plate in 1 ml of Schneider's *Drosophila* medium without FCS. 10 µg of dsRNA was added per well and placed onto a shaking platform for 10 min at room temperature followed by 50 min of incubation at 26°C. Afterwards 2 ml of growth medium was added. To achieve efficient knockdown of the target protein cells were incubated for additional 4-7 days at 26°C. Cells were collected for immunostaining and Western blot analysis.

### 2.4.6 Immunofluorescence on SL2 cells

For analysis by immunostaining  $0.8 \times 10^6$  cells were seeded onto coverslips and allowed to attach for 1 h at room temperature. Cells were washed briefly with PBS and subsequently fixed in 2% (v/v) Formaldehyde in PBS for 7.5 min on ice. Permeabilization of the cells in PBS supplemented with 0.25% (v/v) Triton X-100 and 1% (v/v) Formaldehyde was carried out for additional 7.5 min on ice. Afterwards, cells were washed twice with PBS and blocked in PBS containing 3% (w/v) BSA for 1 h at room temperature. All subsequent steps of the protocol were performed at room temperature. Cells were incubated for 1 h with appropriate primary antibody diluted in blocking solution supplemented with 0.01% (v/v) Triton X-100 and 1.2% Normal Donkey Serum. Following two washing steps of 5 min each in PBS cells were incubated for an additional hour with secondary antibody. Again cells were washed twice with PBS for 5 min. DNA was counterstained with DAPI ( $1 \mu\text{g}/\mu\text{l}$  in PBS) for 2 min. Finally, cells were washed two times with PBS and mounted using  $10 \mu\text{l}$  Vectashield mounting medium. The coverslip was sealed to the object slide by nail polish. Detection of immunofluorescence was carried out using a Zeiss Axiovert 200 epifluorescence microscope equipped with a CDD Camera (AxioCamMR, Zeiss). Images were level adjusted in FIJI and edited using Adobe Photoshop CS5 and Adobe Illustrator CS5.

### 2.4.7 Immunoprecipitation experiments

#### 2.4.7.1 Immunoprecipitation of transgenic MOF-GFP from stable cell lines

Whole cell extract from  $110 \times 10^6$  cells was prepared as previously described in section 2.4.4. Whole cell extracts from SL2 and Kc cells using  $1000 \mu\text{l}$  RIPA lysis buffer.  $30 \mu\text{l}$  of equilibrated GFP-binder slurry was added to the obtained protein extract and incubated for 3 h on a rotating wheel at  $4^\circ\text{C}$ . Following washing steps were carried out by inverting the sample tube 20 times using PBS + 0.1% Triton-X, PBS + 0.1% Triton-X 300 mM NaCl, PBS + 0.1% Triton-X and finally PBS. 0.25% of extract before immunoprecipitation (input) and 50% of beads were separated by 7% SDS-PAGE as described above. Detection of protein was carried out using Western blot analysis.

#### 2.4.7.2 Immunoprecipitation of transgenic MOF-GFP for mass spectrometry

Expansion of  $1.5 \times 10^9$  cells was carried out using  $175 \text{ cm}^2$  cell culture flasks. After collection cells were washed once with cold PBS and snap frozen in liquid nitrogen. The cell pellet was resuspended in 5 ml cold RIPA extraction buffer supplemented with 1 mM Protease Inhibitor, 5 mM N-Ethylmaleinimid and  $15 \mu\text{M}$  MG132. After 10 min incubation on ice cells were lysed on ice using sonification at an amplitude of 15% (3 x 10 s pulses, 20 s pause, Branson Digital Sonifier 250D). Lysate was incubated another 15 min on ice with occasional

vortexing. Finally the cell suspension was cleared by centrifugation at 13000 rpm for 30 min at 4°C. 100  $\mu$ l of equilibrated GFP-binder slurry was added to the obtained protein extract and incubated for 3 h on a rotating wheel at 4°C.

Washing steps were carried out by inverting the sample tube 20 times using PBS + 0.1% Triton-X, followed by 3 rounds of washing with PBS enriched for 8 M Urea and 1% SDS. Finally beads were washed once more with each PBS + 0.1% Triton-X and PBS. 25% of the sample was boiled with 5x Lämmli-DTT and subjected to Western blot analysis together with 0.02% of extract before immunoprecipitation (input).

For mass spectrometry analysis 75% of the sample was boiled in 5x Lämmli buffer supplemented with 1 mM DTT. After incubation with 5.5 mM 2-Chloroacetamide for 45 min at room temperature in the dark the sample was separated by 7% SDS-PAGE. Coomassie staining was carried out overnight at room temperature with gentle shaking using Novex Colloidal Blue Staining Kit. After destaining the gel with high purity water cut gel slices were subjected to mass spectrometry analysis performed by Petra Beli at the Institute of Molecular Biology in Mainz.

### **2.4.8 Precipitation of proteins for ubiquitylome analysis**

Confluent L2-4 or Kc cells were harvested from 4-5 175 cm<sup>2</sup> cell culture flasks and washed twice in ice-cold PBS. Cell pellet was lysed using a modified lysis buffer (50 mM Tris-HCl, pH 7.5, 150 mM NaCl, 1 mM EDTA, 1% NP-40, 0.1% Na-deoxycholate) supplemented with protease inhibitors, phosphatase inhibitors and cysteine peptidase inhibitor N-Ethylmaleimide prior to use (1:1000 Roche complete protease inhibitor cocktail, 5 mM  $\beta$ -glycerophosphate, 5 mM NaF, 1 mM Na-orthovanadate, 10 mM N-Ethylmaleimide). Cells were incubated for 10 min on ice and centrifuged at 16,000 $\times$ g for 15 minutes at 4°C. Protein concentration of the supernatant was determined using Bradford. 200-250 mg of protein were employed for ubiquitylome analysis by mass spectrometry. 4 volumes of ice-cold acetone were added to the supernatant and proteins were precipitated overnight at -20°C. Samples were shipped on dry ice and further processed by Petra Beli at the Institute of Molecular Biology in Mainz.

## 2.5 *Drosophila melanogaster* studies

### 2.5.1 Generation of transgenic fly lines

Injection of manipulated pUAST-attB-MOF mutant plasmids was carried out by Genetic Services Inc. (Sudbury, USA) and BestGene Inc. (Chino Hills, USA). Fly Stocks were maintained at 18°C on standard medium.

### 2.5.2 Fly crosses for male viability assays

Complementation of the male-lethal *mof*<sup>2</sup> was carried out at 25°C. Transgene expression was induced by crossing female flies of the genotype *mof*<sup>2</sup>/*Fm7a*; *P{armadillo-GAL4}* to male *y/w*; *{w<sup>+</sup> MOF-FLAG-UAS}*. Relative male survival was scored as ratio of male *mof*<sup>2</sup>/*y*; *P{armadillo-GAL4}*/*{w<sup>+</sup> MOF-FLAG-UAS}* to female *mof*<sup>2</sup>/*+*; *P{armadillo-GAL4}*/*{w<sup>+</sup> MOF-FLAG-UAS}*. Fly strains generated in this study are listed in Table 9.

### 2.5.3 Immunostaining of polytene chromosomes

For optimal conditions larvae were raised at 18°C until they reached the 3<sup>rd</sup> instar stage. Salivary glands were dissected in PBS. Homogenous fixation of the glands was carried out for 30 sec with gentle moving in solution A (3.7% PFA, 1% Triton-X in PBS). Tissue was subsequently transferred to solution B (3.7% PFA, 50% acetic acid in PBS) and incubated for 2.30 min on a cover slip. A poly-L-lysine coated slide was used to take up the coverslip. To disrupt cells and nuclei the slide was tapped with a pencil, moved back and forth and finally heavily pressed on a blotting paper with the thumb. After snap freezing the slide in liquid nitrogen the cover slip was removed using a razor blade and slides were transferred to PBS. Prepared chromosome squashes may be stored in 100% methanol at -20°C at this point.

For immunostaining the slide was incubated in blocking solution (3% BSA, 0.2% NP40, 0.2% Tween20, 10% non fat dry milk in PBS) with gentle shaking for 1 h. Primary antibodies diluted in blocking solution were added onto the slide, covered with a coverslip and incubated in a humid chamber for 1 h at room temperature or overnight at 4°C. Slides were rinsed twice for 5 min in PBS at room temperature. Two washing steps were carried out for each 15 min at room temperature by thoroughly shaking the slides, washing 1 (300 mM NaCl, 0.2% NP40, 0.2% Tween20 in PBS), washing 2 (400 mM NaCl, 0.2% NP40, 0.2% Tween20 in PBS). Again, slides were rinsed in PBS for 5 min. Secondary antibodies were diluted in blocking solution and incubated for 1 h in the dark at room temperature. Again, washing steps were carried out as described previously (5 min rinse in PBS, followed by washing 1 and washing 2 for each 15 min at room temperature with heavy shaking). DNA was counterstained with

DAPI for 10 min at room temperature followed by another wash in PBS for 5 min. Finally, chromosomes were mounted using 40  $\mu$ l VectaShield.

Detection of immunofluorescence was carried out using a Zeiss Axiovert 200 epifluorescence microscope equipped with a CDD Camera (AxioCamMR, Zeiss). Images were level adjusted in FIJI and edited using Adobe Photoshop CS5 and Adobe Illustrator CS5.

### **2.5.4 Preparation of protein extracts from salivary glands**

Salivary glands of 3<sup>rd</sup> instar larvae were dissected in PBS and subsequently transferred to 2.5x Lämmli-DTT. After macerating the glands carefully the sample was boiled for 10 min at 85°C with heavy shaking. For subsequent Western blot analysis 3-5 pairs of salivary glands were loaded to SDS-PAGE.

## 2.6 Biochemical methods

### 2.6.1 SDS-polyacrylamide gel electrophoresis (SDS-PAGE)

Reducing SDS-PAGE was carried out for separation of proteins using the Novex Mini-Cell system (Invitrogen). Samples complemented with Lämmli sample buffer were loaded to suitable polyacrylamide gels. SDS-PAGE was carried out according to standard protocols at 30-60 mA at room temperature for varying time. Protein size was determined using various molecular weight standards purchased from Peqlab or Serva. Afterwards SDS-polyacrylamide gels were used for either Coomassie staining or Western blotting.

### 2.6.2 Coomassie staining of protein gels

Following SDS-PAGE polyacrylamide gels were fixed in fixing solution for 30 min at room temperature. Proteins were stained with Coomassie Brilliant Blue G-250 (0.0025% (w/v)) in fixing solution for 1 h and finally destained with 10% (v/v) Acetic acid until protein bands became visible.

### 2.6.3 Western Blot

Proteins separated by reducing SDS-PAGE were transferred to a nitrocellulose membrane using a wet transfer system (Mini-PROTEAN). Wet transfer was performed in transfer buffer at a constant current of 300 mA (6.25 mA/cm<sup>2</sup>) for 80 min at 4°C. To minimize background by unspecific protein-protein interactions the membranes were blocked in 3% (w/v) BSA in PBS for 30 min at room temperature. Membranes were probed with an appropriate dilution of primary antibody overnight at 4°C. Removal of unspecific bound proteins was achieved by extensive washing (3x 10 min) with PBS-T. Subsequently, the membranes were incubated with horseradish- or infrared dye-coupled secondary antibody for 1h at room temperature. After repeated washing antigen-antibody complexes were detected using the enzymatic activity of the horseradish peroxidase conjugated to the secondary antibody. Chemiluminescence was detected using ECL Immobilon Western reagent in combination with X-ray films or the Chemidoc detection system. When using infrared dye-coupled secondary antibodies the membranes were dried prior to detection of proteins using the LI-COR Odyssey Infrared Imaging System.

### **2.6.4 *In vitro* ubiquitylation assay**

Assays were carried out in 20  $\mu$ l of reaction buffer (25 mM HEPES pH 7.6, 70 mM KCl, 5 mM ATP, 0.6 mM DTT) in the presence of 55 ng E1 (Boston Biochem, E-305), 263 ng E2 (Boston Biochem, E2-627), 500 ng MSL2, and 1 mg of substrate protein at 30°C. Reaction was stopped after 1 h by addition of 5x Lämmli loading buffer. Sample was subjected to SDS-PAGE and immunoblotting. *In vitro* ubiquitylation assays in the presence of nucleic acids contained 1  $\mu$ M of annealed DBF12-L15 dsDNA. dsDNA was obtained by annealing equimolar concentrations of complimentary oligonucleotides in annealing buffer (10 mM Tris-HCl pH 7.5, 50 mM NaCl, 0.1 mM EDTA). To support formation of dsDNA duplexes the DNA was slowly cooled from 95°C down to room temperature.

### **2.6.5 Histone acetylation assay**

HAT assays were performed using 1.5  $\mu$ g of recombinant histone H4 or 0.44  $\mu$ g of nucleosomal histones, respectively. In addition 3 $\mu$ M [<sup>3</sup>H]acetyl-CoA, 200 ng of recombinant MOF protein were combined in a final volume of 20  $\mu$ l containing 50 mM KCl, 50 mM Tris (pH 7.8) and 0.1 mM EDTA. Samples were incubated for 1 h at 26°C. Half of each reaction was spotted onto p81 filters, washed three times with 50 mM Na-Carbonate (pH 9.3) and the filters were counted in a scintillation counter. Incorporation of [<sup>3</sup>H]acetate was determined as a general measure of HAT activity. The remainder of the reaction was used to visualize [<sup>3</sup>H]acetylated proteins by 4-20% SDS-PAGE. The gel was treated with amplify solution and incubated on a shaker for 30 min. For autoradiography the gel was dried and X-ray films were exposed for 5-7 days at -80°C.

## 2.7 Expression and purification of MSL-DCC proteins in Sf21 cells

### 2.7.1 Generation of recombinant Baculovirus

Recombinant Baculoviruses were obtained using suitable pFastBac1 vectors and the Bac-to-Bac expression system according to the manufacturer's instructions (Invitrogen). In this study Baculoviruses for protein expression of MOF K>R point mutants as well as MOF deletion mutants and SPT6 protein were obtained. Baculoviruses for MSL2 expression were generated in the lab before.

### 2.7.2 Infection of Sf21 cells with Baculovirus

Expression of C-terminally FLAG-tagged proteins was performed using recombinant Baculoviruses. Sf21 cells (100 ml,  $1 \times 10^6$  cells/ml) were infected with the optimal amount for each virus, previously determined in test expressions. Cells were harvested after 3 days of protein expression. The cell pellet was washed with ice-cold PBS, snap frozen in liquid nitrogen and stored at  $-80^\circ\text{C}$ .

### 2.7.3 Preparation of Sf21 cell extracts

For preparation of whole cell extracts obtained Sf21 cell pellet was rapidly thawed in a water bath at room temperature and subsequently placed on ice. 10 ml of lysis buffer was added and cells were carefully resuspended.

Lysis buffer: 50 mM HEPES pH 7.6  
0.3 M KCl  
5% (v/v) Glycerol  
0.05% (v/v) NP-40  
1 mM  $\text{MgCl}_2$   
0.5 mM EDTA

Lysis buffer was further supplemented with protease inhibitors prior to use.

For MSL2 purification 0.05 mM  $\text{ZnCl}_2$  was added to the lysis buffer.

After incubation for 10 min on ice cells were lysed on ice by sonication (4 x 10 sec, 15% amplitude, 20 sec pause) using Branson Digital Sonifier. To remove cell debris the lysate was centrifuged 30 min at 16000 rpm and  $4^\circ\text{C}$ , followed by a second centrifugation step for another 15 min. Obtained supernatant containing the soluble protein fraction was subjected to protein purification using anti-FLAG M2 Agarose beads.

### **2.7.4 Purification of FLAG-tagged MSL-DCC proteins from Sf21 cell extracts**

200  $\mu$ l of anti-FLAG M2 Agarose slurry was equilibrated with lysis buffer, added to the obtained soluble protein fraction and incubated for 2.5 h at 4°C on a rotating wheel. Following incubation washing steps were carried out using at least 10 ml of chilled buffer. First, beads were briefly washed with lysis buffer, followed by a second washing step for 5 min at 4°C on a rotating wheel. A high salt (1 M KCl) washing step of 10 min at 4°C on a rotating wheel reduced non-specific protein interactions with the beads. Finally the beads were washed another time with lysis buffer for 5 min followed by two quick washes in appropriate elution buffer. Elution buffer is composed as the lysis buffer but contained 50 mM KCl for MOF and SPT6 purification and 100 mM KCl/ 0.05 mM ZnCl<sub>2</sub> for MSL2 purification, respectively.

Elution of the FLAG-tagged proteins from the beads was achieved by addition of 0.5 mg/ml FLAG-peptide in a total volume of 400  $\mu$ l. After incubation at 4°C on a rotating wheel for 3 h the eluted protein was separated from the FLAG-beads using Micro-Spin columns. Protein yield after elution was usually high for MOF and full length SPT6 while MSL2 and SPT6[1] needed further concentration, which was carried out using Amicon Ultra-4 centrifugal filter devices. Obtained proteins were snap frozen as small aliquots and stored at -80°C.

## **3 RESULTS**

### 3.1 *In vitro* characterization of MOF ubiquitylation

#### 3.1.1 MOF is ubiquitylated by MSL2 *in vitro*

It was previously reported that FLAG-tagged *Drosophila* MSL2 from recombinant protein expression exhibits robust ubiquitylation activity on MOF and the other DCC subunits *in vitro* (Villa, 2012). To identify MOF ubiquitylation sites recombinant MOF was subjected to *in vitro* ubiquitylation assays. Ubiquitylation assays contained MOF substrate, MSL2 (E3 ligase), recombinant E1 and E2 enzymes, His-ubiquitin and ATP. Modified MOF was digested with trypsin and subjected to mass spectrometry (Petra Beli, IMB Mainz). Ubiquitylated peptides were identified by the characteristic mass shift resulting from the attachment of two glycine residues that originate from the C-terminus of ubiquitin on the branched peptide (Figure 13). Analysis of three biological replicates revealed that ubiquitylated lysine residues are distributed all over MOF (Figure 14A).

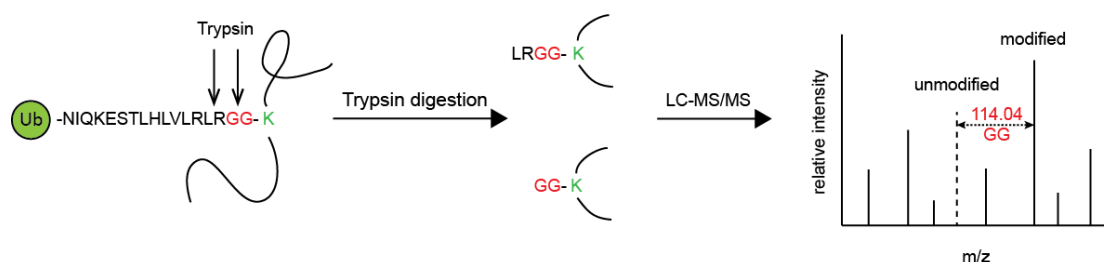


**Figure 13: Detection of ubiquitylation sites using mass spectrometry.** Ubiquitylated proteins are digested with trypsin. Tryptic peptides are fractionated, desalted and subjected to LC-MS/MS analysis. Ubiquitylated peptides characterized by a diglycine modification on the lysine residue are identified using MaxQuant software.

To further evaluate MOF ubiquitylation FLAG-tagged MOF lysine to arginine (K>R) point mutants either in the N-terminus (KN) or the C-terminus (KC) were employed (Figure 14B). Ubiquitylation is a highly promiscuous modification and targets other lysines as well, if the favored site is not accessible anymore. Consequently, not only the lysines identified by mass spectrometry were modified but also the few surrounding lysine residues in the N-terminus. As there are only nine lysine residues present within the first 400 aa of MOF, the introduction of N-terminal mutants was particularly easy. In total five N-terminal MOF K>R point mutants were obtained (Figure 14B; 2KN, 3KN, 5KN, 7KN and 9KN). On the contrary, the C-terminal part of MOF is highly structured and displays multiple lysine residues. Using the structural prediction of human MOF HAT domain (Kadlec, 2011) homologous lysines were identified in the *Drosophila* MOF and assessed according to their accessibility. Finally, two C-terminal MOF point mutants with either 3 or 9 K>R point mutations were generated (Figure 14B; 3KC and 9KC). In addition, two deletion mutants were generated, either

exhibiting the MOF N-terminus alone (Nt) or lacking the N-terminus ( $\Delta$ N). Recombinant MOF mutant protein was purified from a C-terminal FLAG tag using the Sf21 expression system in combination with Baculovirus infection. Coomassie-stained protein preparations are depicted in Figure 14C. Recombinant proteins were subjected to *in vitro* ubiquitylation and histone acetylation assays.

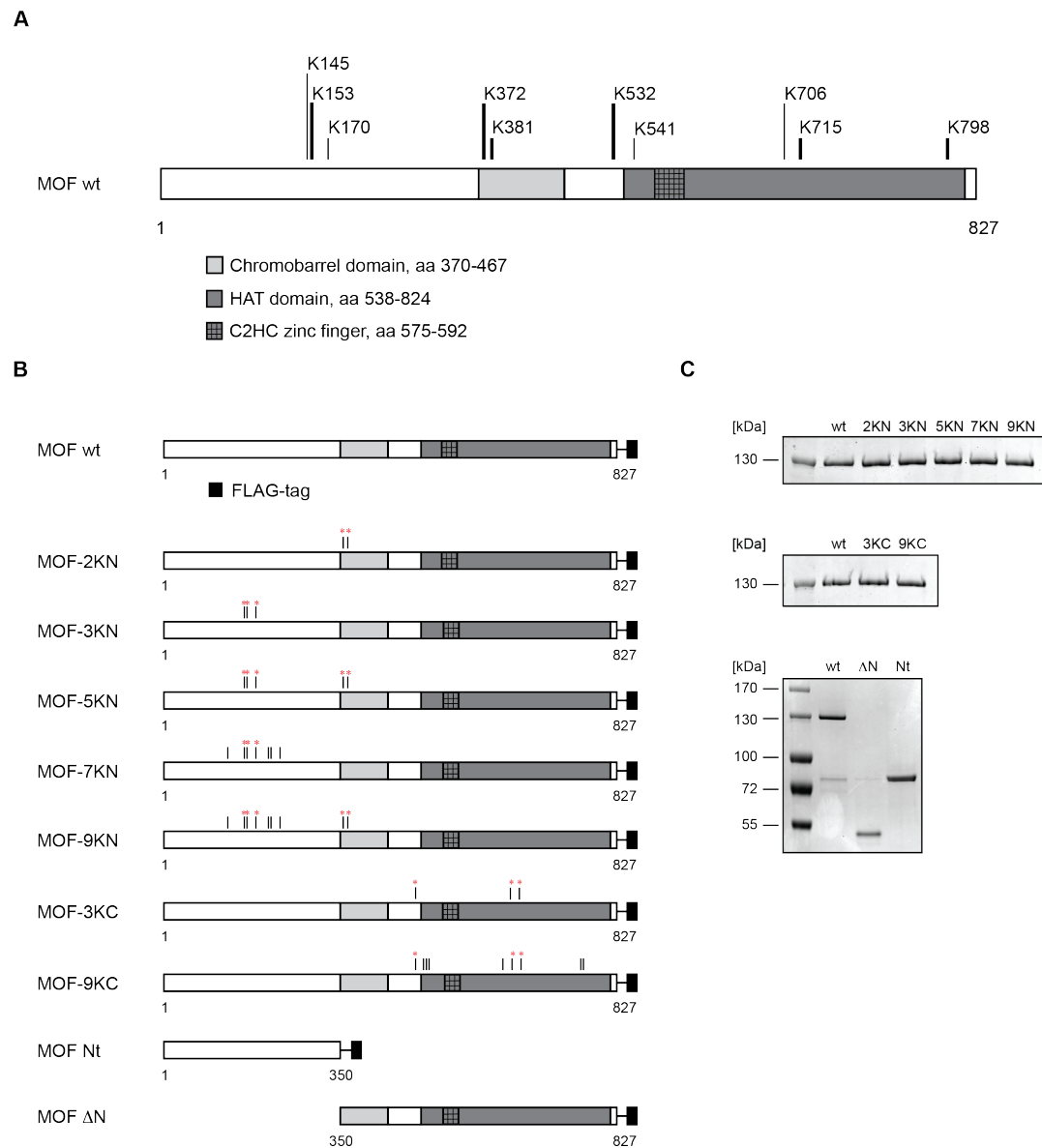


**Figure 14: Investigation of recombinant MOF protein *in vitro*.** (A) Schematic representation of MOF wt protein. MOF contains an unstructured N-terminal domain and two globular domains: chromobarrel domain and histone acetyltransferase domain (light and dark gray boxes). A C2HC zinc finger is located within the HAT domain (dashed box). Black bars indicate lysine residues identified by mass spectrometry after *in vitro* ubiquitylation reaction of MOF wt in presence of MSL2. Bold and light bars represent residues found ubiquitylated in 3 out of 3 and 1 out of 3 biological replicates, respectively. (B) Schematic representation of domain structure in MOF wt, N-terminal (KN) MOF K>R point mutants, C-terminal (KC) MOF K>R point mutants and MOF deletion mutants. Recombinant MOF mutant protein was purified from the C-terminal FLAG-tag (black boxes). Black bars indicate mutated lysine residues. Asterisks indicate modified lysine residues identified by mass spectrometry after *in vitro* ubiquitylation reaction of MOF wt in presence of MSL2. (C) Coomassie-stained SDS-PAGE gels of recombinant MOF proteins obtained after FLAG-purification. Positions of molecular mass marker proteins are indicated to the left (kDa). Full-length MOF protein migrates at 130 kDa, the deletion mutants MOF  $\Delta$ N and Nt migrate at 55 and 80 kDa, respectively.

### 3.1.2 *In vitro* ubiquitylation of MOF mutants by MSL2

Previous results obtained from mass spectrometry indicated that *in vitro* MSL2 modifies lysine residues all over MOF. To further investigate MOF ubiquitylation pattern recombinant MOF wt, K>R point mutants,  $\Delta$ N and Nt mutants obtained after FLAG-purification were subjected to *in vitro* ubiquitylation assays in the presence of MSL2 as described above. Using a dual-color infrared imaging system (LI-COR) bands from anti-ubiquitin antibody were aligned with corresponding bands from MOF-specific antibody to identify ubiquitylated species of MOF in Western blot (Figure 15). Western blot analysis revealed that MSL2 ubiquitylates MOF wt, 2KN, 3KN and 5KN to similar extents, while ubiquitylation of 7KN and 9KN was dramatically reduced (Figure 15A). anti-MOF background signal observed without MSL2 present in the reaction is displayed in lane 7 (Figure 15A). A hallmark of E3 ligases is the ability to exhibit autoubiquitylation activity. This characteristic feature can be observed as MSL2 is placed into an ubiquitylation reaction without any further substrate protein (Ctrl, lane 8). Autoubiquitylation of MSL2 was also detected in reactions 5 and 6 as reduced ubiquitylation activity on 7KN and 9KN results in changed substrate specificity of MSL2. Interestingly, loss of potential C-terminal ubiquitylation sites did not change the overall amount of ubiquitylated MOF species, as MOF wt, 3KC and 9KC were ubiquitylated by MSL2 to similar extents (Figure 15B). Upon deletion of the unstructured N-terminus ubiquitylated forms of MOF were not detectable anymore (Figure 15C). In contrast, MOF Nt acted as a substrate for MSL2 *in vitro* ubiquitylation (Figure 15D). Taken together these observations demonstrate that *in vitro* MOF is modified by MSL2 predominantly in the N-terminus.

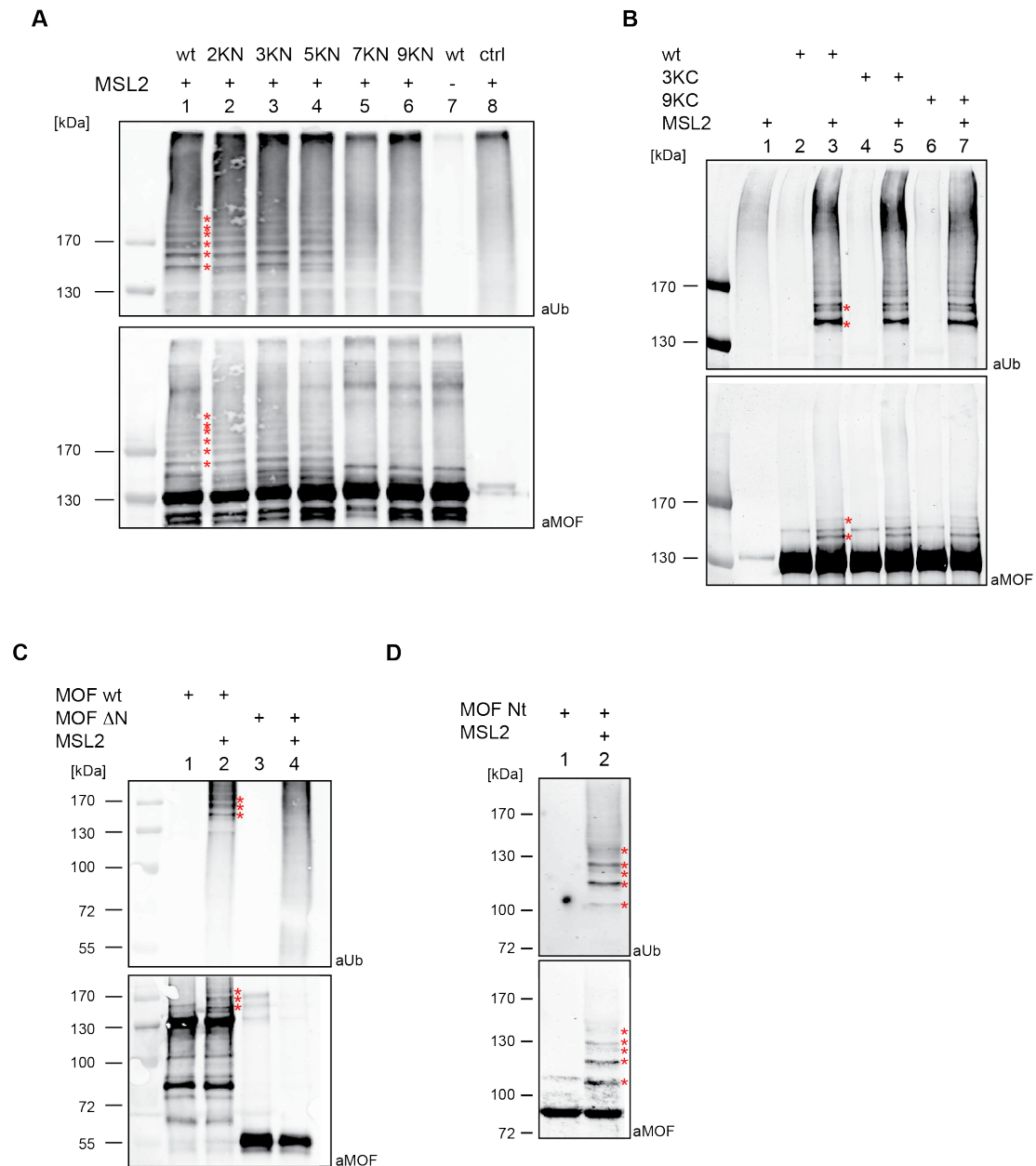


**Figure 15: *In vitro* ubiquitylation of recombinant MOF mutants.** (A) *In vitro* ubiquitylation assay using recombinant MOF wt and N-terminal K>R MOF point mutants. Ubiquitylation assays contained recombinant E1 and E2 enzymes, His-ubiquitin and ATP. MSL2 and different MOF substrates were added to the reactions as indicated. Ubiquitylated proteins were detected using anti-ubiquitin (aUb, top) and anti-MOF (aMOF, bottom) antibodies. Positions of molecular mass marker proteins are indicated to the left (kDa). Asterisks indicate bands that correspond to ubiquitylated forms of MOF protein. MSL2 ubiquitylates MOF wt, 2KN, 3KN and 5KN, ubiquitylation of 7KN and 9KN is impaired. In the absence of MSL2 MOF wt is not ubiquitylated. Without substrate present in the reaction autoubiquitylation of MSL2 is observed (Ctrl). (B) *In vitro* ubiquitylation assay using recombinant MOF wt and C-terminal K>R MOF point mutants. MSL2 ubiquitylates MOF wt, 3KC and 9KC to same extents. (C) *In vitro* ubiquitylation assay using recombinant MOF wt and MOF ΔN deletion mutant was performed as described previously. MOF ΔN is not ubiquitylated by MSL2 *in vitro*. (D) *In vitro* ubiquitylation assay using recombinant MOF Nt demonstrates that MOF Nt is a substrate for MSL2 ubiquitylation *in vitro*.

**3.1.3 MOF is ubiquitylated by a DCC-unrelated E3 ligase *in vitro***

In the presence of MSL2 N-terminal MOF point mutants exhibiting either seven or nine K>R replacements demonstrated a decent reduction of ubiquitylation *in vitro* (Figure 15A). Despite numerous lysine residues present in the C-terminal part of the protein, both 7KN and 9KN as well as MOF  $\Delta$ N failed to get ubiquitylated by MSL2, highlighting that the N-terminus is the predominant site for MOF modification by MSL2 *in vitro*. To evaluate whether N-terminal MOF ubiquitylation by MSL2 can be attributed to a distinct MSL-DCC-related pattern, ubiquitylation assays with a MSL-DCC-unrelated E3 ligase were performed. To this end Mdm2 was employed, an E3 ligase known to promiscuously modify a diverse set of proteins. Moreover, 9KN mutant was employed in Mdm2 *in vitro* ubiquitylation assays to evaluate whether an E3 ligase with different properties than MSL2 might be able to modify this mutant *in vitro* (Figure 16). In comparison to MSL2 Mdm2 exhibited a more pronounced ubiquitylation activity both on itself as well as on putative substrates (Figure 16A, lanes 1 and 2). Ubiquitylation on MOF wt was considerably higher when placed by Mdm2 (lane 5). While MSL2 failed to ubiquitylate 9KN (lane 7), the MSL-DCC-unrelated Mdm2 readily modified 9KN *in vitro* (lane 8).

In order to investigate whether Mdm2 targets different lysines than MSL2 and may exhibit an MSL-DCC unrelated ubiquitylation pattern, the ubiquitylation sites were mapped. To this end half of the reaction was loaded for Western blot analysis and the other half was subjected to mass spectrometry. In addition, MOF 9KN was employed to determine whether loss of N-terminal ubiquitylation sites led to increased C-terminal ubiquitylation by Mdm2 to compensate for the lack of N-terminal modification. Again, Mdm2 exhibited robust ubiquitylation activity on MOF wt and was also able to modify 9KN as shown by Western blot analysis (Figure 16B). Modified lysine residues on MOF wt after Mdm2 ubiquitylation were found all over the protein with a similar pattern like found on MOF ubiquitylated by MSL2 *in vitro* before: 8 out of 10 Mdm2 sites were found after MSL2 ubiquitylation as well (Figure 15C). Two C-terminal sites were found exclusively after Mdm2 but not after MSL2 ubiquitylation. One N-terminal site was unique to MSL2 ubiquitylation, however this lysine was found ubiquitylated in only one biological replicate (K145, Figure 14B). As proposed, MOF-9KN acquired additional ubiquitylation sites: compared to MOF wt four additional lysines were ubiquitylated by Mdm2 in the C-terminus.

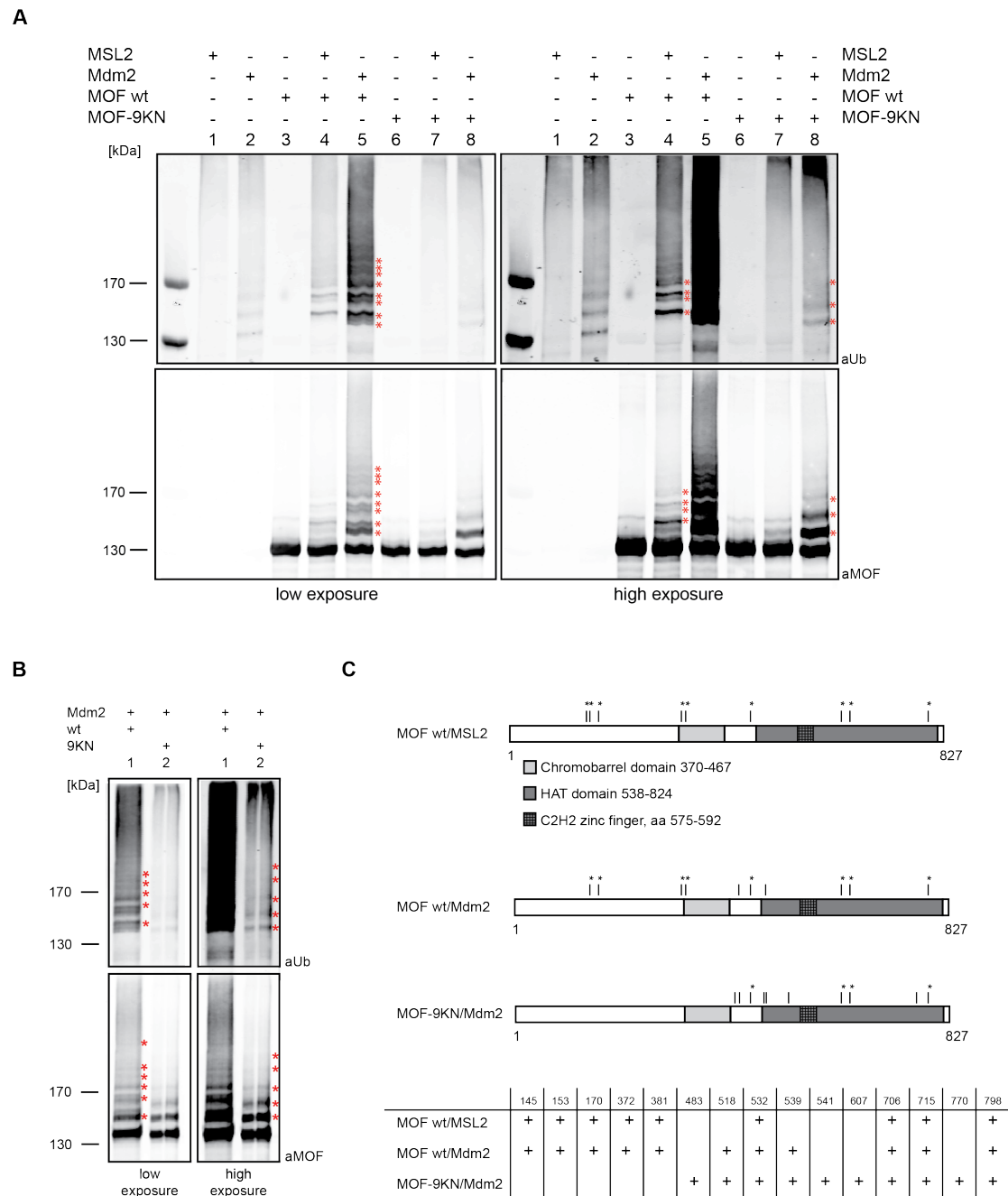


**Figure 16: MOF is ubiquitylated by an MSL-DCC unrelated E3 ligase *in vitro*.** (A) MOF wt and 9KN were subjected to *in vitro* ubiquitylation reaction using either MSL2 or Mdm2 as described previously. Ubiquitylated proteins were detected using anti-ubiquitin (aUb, top) and anti-MOF (aMOF, bottom) antibodies. Positions of molecular mass marker proteins are indicated to the left (kDa). Asterisks indicate bands that correspond to ubiquitylated forms of MOF protein. Two different exposures (low and high) are shown. (B) *In vitro* ubiquitylation assay of MOF wt and 9KN by MSL2 and Mdm2, respectively. Ubiquitylation assays were carried out as described previously and subjected to mass spectrometry. Ubiquitylated proteins were detected using anti-ubiquitin (aUb, top) and anti-MOF (aMOF, bottom) antibodies. Positions of molecular mass marker proteins are indicated to the left (kDa). Two different exposures are provided (low and high exposure). Asterisks indicate bands that correspond to ubiquitylated forms of MOF protein. (C) Schematic representation of modified lysine residues in MOF wt and 9KN after ubiquitylation with indicated E3 ligases *in vitro*. MOFwt/MSL2 ubiquitylation pattern as already depicted in Figure 14A is provided for comparison. Black bars indicate ubiquitylated lysine residues. Asterisks indicate modified lysine residues identified by mass spectrometry after *in vitro* ubiquitylation reaction of MOF wt in presence of MSL2.

### 3.1.4 Allosteric modulation of MSL2 ubiquitylation activity

MSL2 directly interacts with HAS DNA *in vitro* and *in vivo* (Straub, 2008; Fauth, 2010; Zheng, 2014; Villa, 2016), it was explored whether the E3 ligase activity of MSL2 would be modulated by DNA binding. To this end *in vitro* ubiquitylation assays on MOF wt in the presence of saturating amounts of DNA (Fauth, 2010; 3XDBF-12-L15) were performed (Figure 17). MSL2 exhibits robust ubiquitylation activity on MOF wt while addition of DNA to the reaction dramatically reduced MOF ubiquitylation pattern. This experiment suggests that the enzymatic activity of MSL2 can be allosterically modulated by DNA binding, a reaction that might contribute to regulated MSL-DCC assembly *in vivo*.

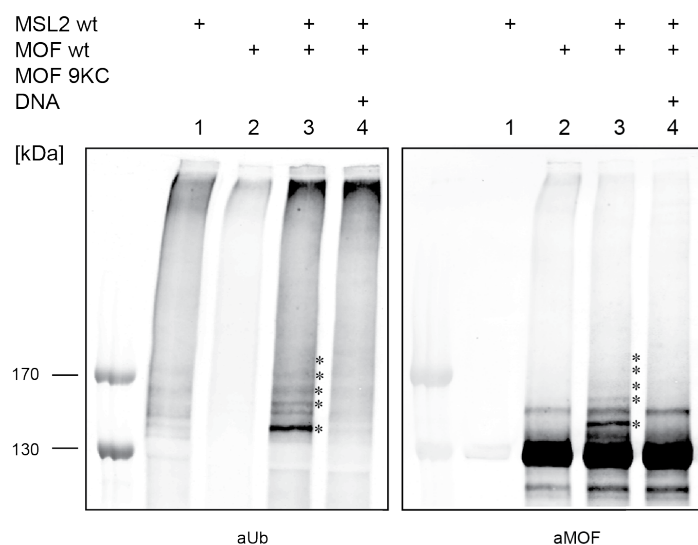


**Figure 17: Allosteric modulation of MSL2 ubiquitylation activity.** *In vitro* ubiquitylation assay in presence of DNA. Assays were performed as described previously. Saturating amount of DNA (1  $\mu$ M; 3XDBF-12-L15) was added to the reaction as indicated. Ubiquitylated proteins were detected using anti-ubiquitin (aUb, top) and anti-MOF (aMOF, bottom) antibodies. Positions of molecular mass marker proteins are indicated to the left (kDa). Asterisks indicate bands that correspond to ubiquitylated forms of MOF protein. The experiment was repeated at least 3 times with same outcome.

### 3.1.5 Enzymatic activity of MOF derivatives

To determine enzymatic and functional consequences of K>R or deletion mutants, respectively, the most prominent MOF mutants were employed in histone acetylation assays on both free H4 histones and nucleosomes. To this end, incorporation of [ $^3$ H]acetyl was analyzed using *in vitro* histone acetylation assays as a readout of enzymatic activity. In a first screen recombinant protein was subjected to HAT assays on purified histone H4. MOF wt and H4 were added as negative controls exhibiting no detectable HAT activity (Figure 18, lanes 1 and 6). MOF Nt alone had barely detectable acetylation activity as the HAT domain is missing from this deletion mutant (Figure 18, lane 5). Interestingly, MOF wt, 9KN and  $\Delta$ N were able to acetylate H4 (Figure 18, lanes 2-4) even in the absence of MSL1 and MSL3

which is in contrast to previous findings that indicated that activity of MOF is stimulated only upon addition of MSL1 and MSL3 (Morales, 2004). Furthermore, hyperacetylation activity of MOF  $\Delta$ N on histone H4 as described in literature (Conrad, 2012) was not observed in this experimental setup.

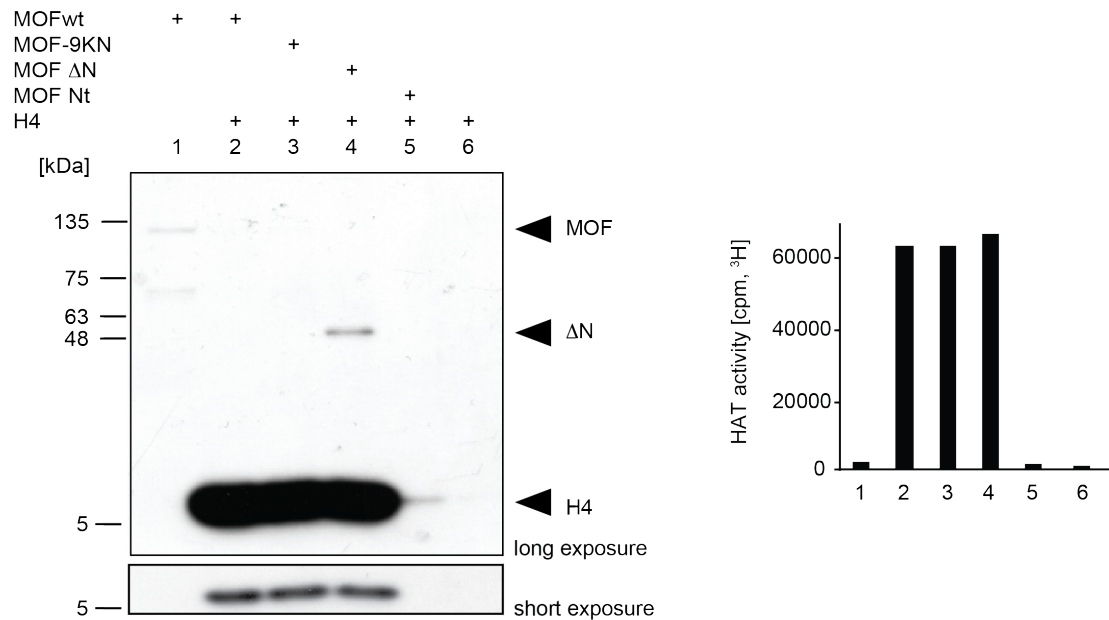


**Figure 18: HAT activity of selected MOF derivatives on H4 histones *in vitro*.** HAT assays were performed using 1.5  $\mu$ g of recombinant histone H4, 3  $\mu$ M [ $^3$ H]acetyl-CoA, 200 ng of each recombinant MOF wt and MOF mutant protein in a 20  $\mu$ l reaction containing 50 mM KCl, 50 mM Tris (pH 7.8) and 0.1 mM EDTA. Samples were incubated for 1 h at 26°C. Half of each reaction was used for autoradiography to visualize [ $^3$ H]acetylated proteins (left panel) and the other half was used to determine incorporation of [ $^3$ H]acetate as a general measure of HAT activity (right panel). Positions of molecular mass marker proteins are indicated to the left (kDa). Arrowheads indicate migration of H4,  $\Delta$ N and respective MOF full-length derivatives. The experiment was performed in 2 biological replicates with the same outcome.

Next, HAT assays on nucleosomal substrates in the presence of MSL3 and MSL1 were performed as interaction of MOF with an MSL1-MSL3 subcomplex was described to increase specificity and efficiency of the acetyltransferase reaction (Morales, 2004). To this end MOF wt, the most dramatic N-terminal mutants (9KN and  $\Delta$ N) as well as both C-terminal MOF mutants (3KC and 9KC) were employed.

In accordance with literature, addition of MOF alone did not have any detectable acetylation activity (Figure 19, lane 8). Upon addition of MSL1-MSL3 to the acetylation reaction MOF exhibits autoacetylation as well as acetylation of MSL3 and MSL1 (Figure 19, lane 7), whereby most of the acetyl groups are incorporated into MSL1. Once nucleosomes are added to the reaction, acetyl groups are also incorporated into histone H4 (lane 1). As MOF-9KN mutant is employed incorporation of acetyl groups was comparable to MOF wt (Figure 19, lane 4). In contrast, C-terminal MOF K>R mutants displayed subtle changes in enzyme

### 3 RESULTS

activity compared to MOF wt. While 9KC, exhibited slightly increased acetylation activity on histone H4, the mutant with fewer point mutations (3KC) surprisingly acetylated both MSL1 and histone H4 to a higher extent (Figure 19, lane 2 and 3).

In conclusion, N-terminal mutation of lysine residues does not affect MOF acetylation activity *in vitro* neither on free histone H4 nor on histone H4 in a nucleosomal context in the presence of an MSL1-MSL3 subcomplex. However, C-terminal MOF mutants that carry point mutations within the HAT domain, exhibited changes in substrate specificity.

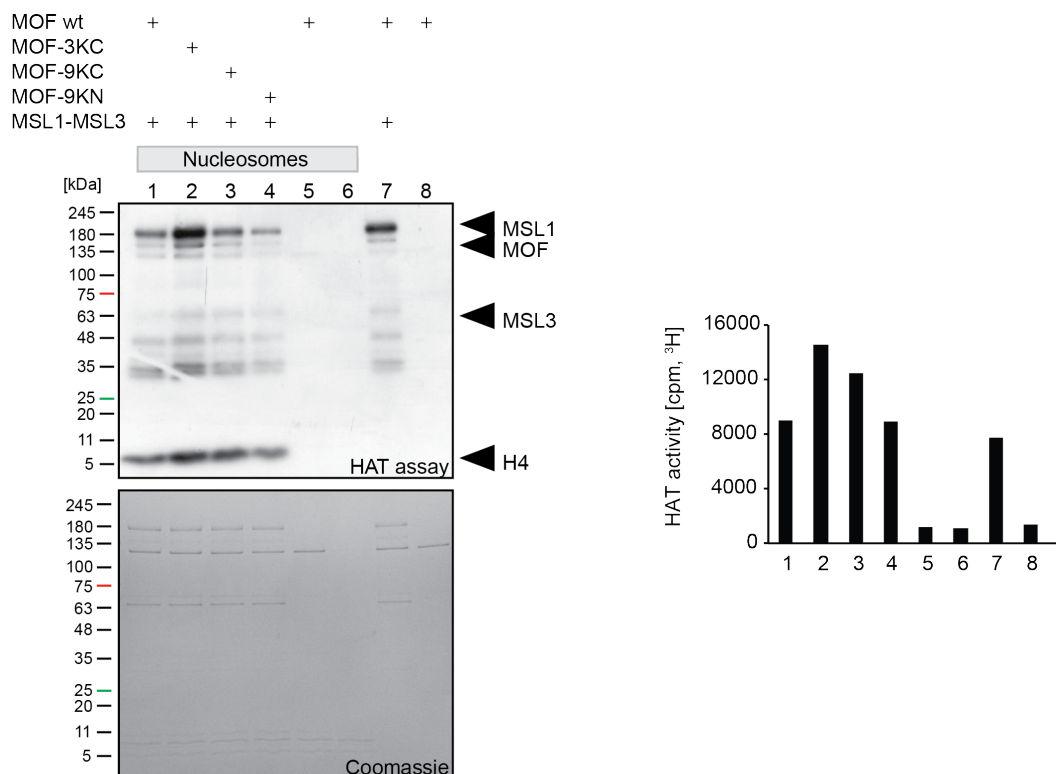


**Figure 19: HAT activity of MOF wt, 3KC, 9KC and 9KN on nucleosomes *in vitro*.** (A) HAT assays were performed using 0.44 µg of nucleosomal substrates, 3µM [<sup>3</sup>H]acetyl-CoA, 1.5 pmol of each recombinant MSL1-MSL3 subcomplex, MOF wt and MOF K>R mutants as indicated (3KC, 9KC, 9KN) in a 20 µl reaction containing 50 mM KCl, 50 mM Tris (pH 7.8) and 0.1 mM EDTA. Samples were incubated for 1 h at 26°C. Half of each reaction was used for autoradiography to visualize [<sup>3</sup>H]acetylated proteins (left panel) and the other half was used to determine incorporation of [<sup>3</sup>H]acetate as a general measure of HAT activity (right panel). Positions of molecular mass marker proteins are indicated to the left (kDa). Arrowheads indicate migration of H4, MSL3, respective MOF full-length derivatives and MSL1. The experiment was performed in 2 biological replicates with same outcome.

## 3.2 *In vivo* characterization of MOF ubiquitylation

### 3.2.1 MOF is ubiquitylated *in vivo*

Ubiquitylation assays on recombinant MOF protein clearly demonstrated that MOF can be modified by the two employed E3 ligases, MSL2 and Mdm2, *in vitro*. In order to examine to which extent MOF is ubiquitylated *in vivo* both endogenous as well as transgenic MOF mutants were analyzed using different approaches.

Proximity ligation assays (PLA) are more sensitive and specific than traditional immunosassays and allow the detection of protein-protein interactions as well as protein modifications. Fixed cells that stably express MSL2-GFP were stained with anti-MOF and anti-ubiquitin antibodies. Oligonucleotides (PLA-probes) attached to secondary antibodies hybridize and form a circular DNA molecule if the probes are in close proximity ( $\leq 40$  nm). The DNA circle is amplified using rolling circle amplification and incorporation of fluorescently labeled oligonucleotides is used to visualize the PLA signal. Ubiquitylated MOF protein was detected in MSL2-GFP cell lines as PLA signals that represent interaction foci of MOF and ubiquitin (Figure 20A). Suitable controls were included to assess the specificity of anti-MOF/anti-ubiquitin PLA staining (Figure 20B). The first row depicts a representative PLA experiment using anti-MOF and anti-ubiquitin primary antibodies. Multiple interaction foci (PLA) distributed all over the nuclei and the cytoplasm indicate the colocalization of MOF and ubiquitin. PLA signal was gone when only one antibody was utilized or when the cell was depleted for MOF by RNA interference demonstrating the specificity of this method.

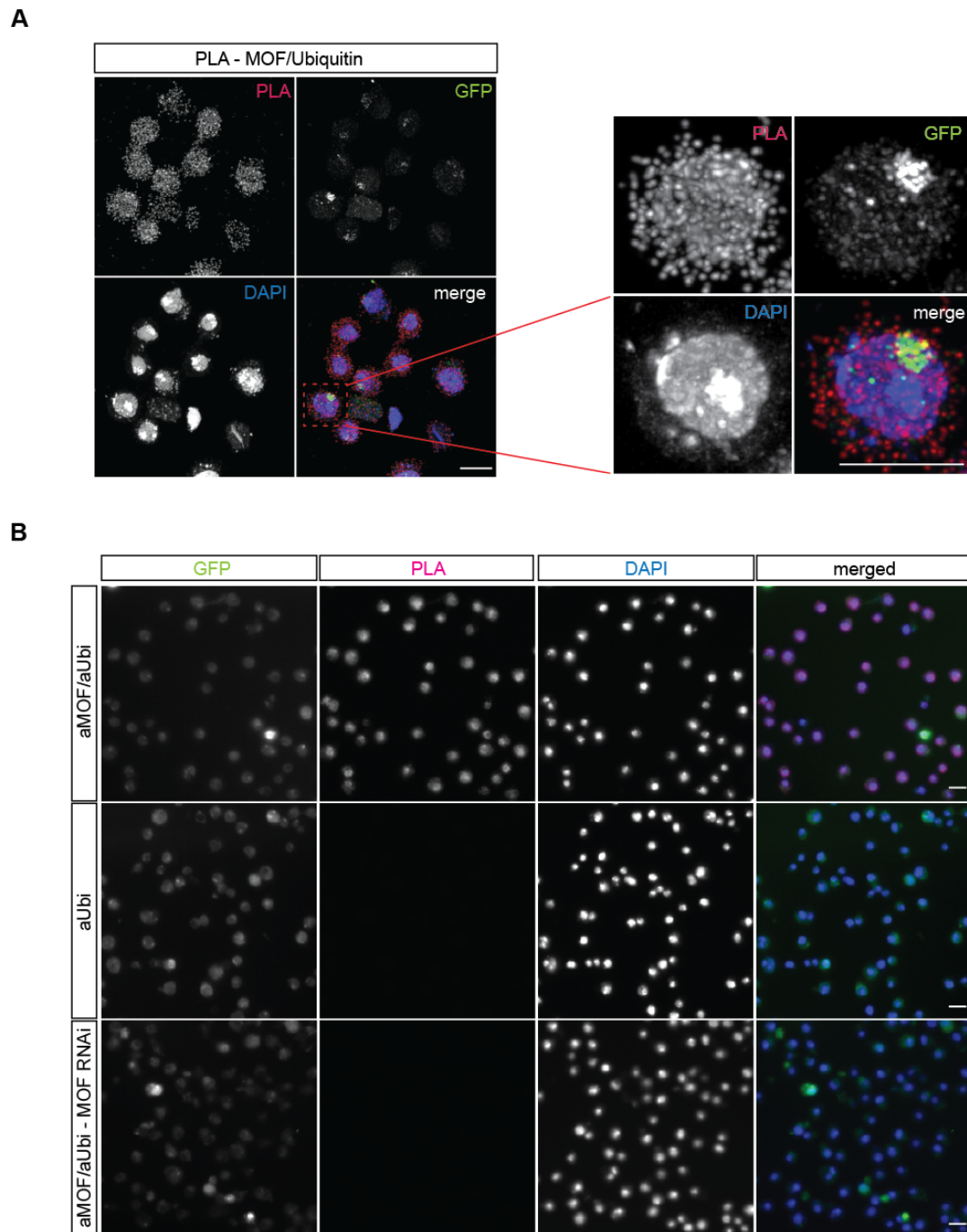


**Figure 20: Detection of MOF ubiquitylation *in vivo*.** (A) Cell lines stably expressing MSL2-GFP were subjected to PLA assays to detect MOF ubiquitylation *in vivo*. The proximity of MOF and ubiquitin is visualized by interaction foci (red dots, PLA). GFP stains transgenic MSL2-GFP, DNA was counterstained with DAPI. Magnification highlights the localization of MOF/ubiquitin interaction foci (PLA) throughout the cell. MSL2 enriches at the X-territory (GFP). Scale bars represent 1 $\mu$ m. (B) Assessment of PLA specificity using anti-MOF (aMOF) and anti-ubiquitin (aUb) antibodies. To test specificity of anti-MOF/anti-ubiquitin PLA staining MSL2-GFP cell lines were employed. The PLA signal is gone upon staining with anti-ubiquitin only (second row). Loss of PLA signal is also observed using anti-MOF and anti-ubiquitin antibodies on cells depleted for MOF protein after 7 days of MOF RNAi (third row). GFP stains transgenic MSL2-GFP, DNA was counterstained with DAPI. Scale bars represent 1 $\mu$ m.

Since proximity ligation cannot be used to identify at which residues MOF is modified, an ubiquitylome from S2 cells was generated using mass spectrometry. To this end proteins from

whole cell extracts were precipitated and ubiquitylated proteins were enriched using di-glycine antibodies. Mass spectrometry of the immunoprecipitated protein fraction revealed an ubiquitylome that comprises more than 1000 proteins (preliminary data, one data set only). Within the sample, MOF was found to be modified on 7 lysine residues distributed within the C-terminal region of MOF chromobarrel and HAT domain (Figure 21). Interestingly, 4 of the lysine residues were also found to be ubiquitylated by MSL2 *in vitro* before (Figure 14A; K372, K532, K715, K798).

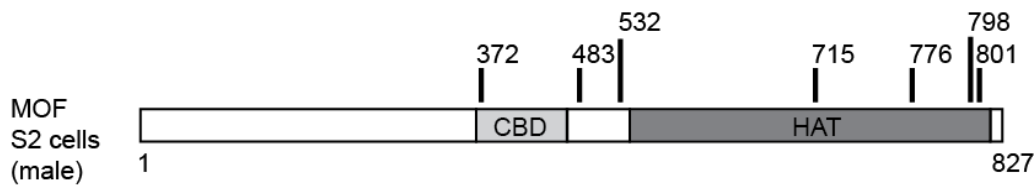


**Figure 21: Ubiquitylome from S2 cells reveals MOF ubiquitylation sites *in vivo*.** Ubiquitylated protein fraction was isolated from S2 cells using di-glycine antibody and subjected to mass spectrometry. Black bars indicate modified lysine residues on the MOF protein. CBD (chromobarrel domain), HAT (histone acetyltransferase domain).

To determine whether identified lysine residues are modified in a dosage compensation-related manner, yet another mass spectrometry approach was followed. MOF-GFP was stably transfected into both male (S2) and female (Kc) cell lines. Using the GFP-trap resin MOF was recovered from whole cell extracts and subjected to Coomassie staining (Figure 22B). High molecular weight bands above the unmodified MOF-GFP protein fraction were considered to be ubiquitylated forms of MOF. In fact, Western blot analysis using anti-ubiquitin and anti-MOF antibodies together with the dual color infrared system (see above) revealed that the high molecular weight bands correspond to ubiquitylated forms of MOF (Figure 22A). Slow migrating protein bands were isolated from Coomassie gels, trypsin digested and subjected to mass spectrometry. In the course of 4 (S2 cells) and 2 (Kc cells) biological replicates, respectively, N-terminal MOF ubiquitylation was never detected (Figure 22C). Instead, C-terminal MOF ubiquitylation seems to dominate *in vivo*. When comparing MOF ubiquitylation patterns derived either from male or female cells no lysine residues were found that are modified only in males but not in females. In fact, there is even one additional site ubiquitylated on MOF derived from female cells.

In summary, a large pool of ubiquitylated MOF was detected both in the nucleus and cytoplasm of *Drosophila* cells. Interestingly, modified lysine residues detected on MOF-GFP after immunoprecipitation were predominantly found in the C-terminus, but not in the N-terminus *in vivo* highlighting a discrepancy between MOF ubiquitylation *in vitro* and *in vivo*. Similarities in ubiquitylation pattern between MOF derived from either male or female cells suggest that MSL2-independent ubiquitylation dominates *in vivo*.

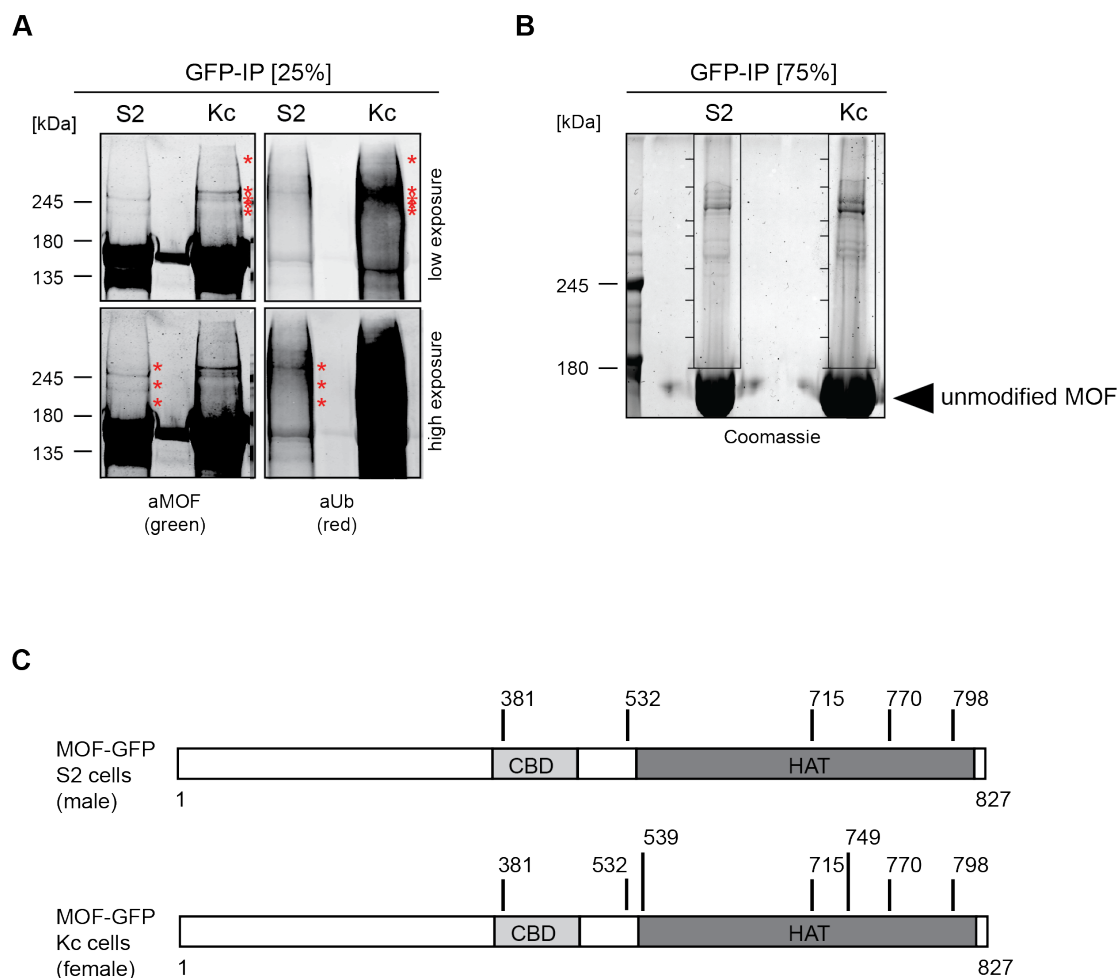


**Figure 22: *In vivo* ubiquitylation pattern on MOF derived from male and female cells.** (A) MOF-GFP was recovered from male (S2) and female (Kc) cells stably transfected with MOF-GFP using the GFP-trap resin. Ubiquitylated species of MOF were detected in Western blot using anti-MOF (aMOF, left) and anti-ubiquitin (aUb, right) antibodies. Asterisks indicate bands that correspond to ubiquitylated forms of MOF protein. Western blots were exposed at either low (top) or high (bottom) exposure. Positions of molecular mass marker proteins are indicated to the left (kDa). (B) Sample preparation for mass spectrometry of MOF *in vivo* ubiquitylation sites. MOF-GFP was recovered from male (L2-4) and female (Kc) cells stably transfected with MOF-GFP using the GFP-trap resin. 75% of the sample was loaded to 7% SDS-PAGE for coomassie staining and modified protein fraction was cut from the gel as indicated by black boxes. Proteins were trypsin digested followed by subsequent analysis of ubiquitylated lysine residues by mass spectrometry. (C) Schematic representation of MOF *in vivo* ubiquitylation sites identified by mass spectrometry after isolation of MOF-GFP from stably transfected cell lines (S2, male; Kc, female). MOF ubiquitylation sites detected in S2 and Kc cells are displayed as black bars, numbers indicate modified lysine residues. The experiment in S2 cells was carried out in 4 biological replicates, 2 biological replicates were performed in Kc cells. CBD (hromobarrel domain), HAT (histone acetyltransferase domain).

### 3.2.2 Analysis of MSL2-dependent MOF ubiquitylation *in vivo*

Previous analyses had revealed that MOF is readily ubiquitylated both *in vitro* and *in vivo*. However, *in vivo* it has to be assumed that MOF is not only modified by MSL2 but also by several other E3 ligases present in the cell. A common approach to determine whether ubiquitylation of a given substrate is dependent on a distinct E3 ligase has been provided by target-specific double stranded RNAs that abolish the synthesis of the respective E3 ligase. Despite efficient dsRNA have already been successfully employed to specifically deplete MSL2 in S2 cells, a major limitation of the approach arises from the fact that any interference with MSL-DCC composition results in codepletion of associated complex members. However, in the context of both endogenous MOF and MOF-GFP, the transgenic protein might be less affected by MSL2 depletion. To study MOF-GFP ubiquitylation in dependency of MSL2 an RNAi mediated approach was employed using a dsRNA, spanning 400 bp of the *msl2* cDNA to deplete for MSL2 protein in stably expressing MOF-GFP cells. As a control for non-specific effects of RNA interference, cells were treated with as dsRNA that specifically targets the mRNA of glutathione-S-transferase (GST).

While in the context of a stably transfected MOF-GFP cell line it was observed that endogenous MOF levels were co-depleted as expected, amounts of transgenic MOF-GFP were mostly unaffected as shown by in Western blot analysis (Figure 23A). Using these observations PLA experiments were carried out on stable MOF-GFP cells to assay the amount of ubiquitylation on MOF in dependency of MSL2. To this end cells depleted for either MSL2 or GST were fixed according to standard procedures and stained with suitable primary antibodies directed against GFP and ubiquitin. To estimate the amount of ubiquitylation on transgenic MOF-GFP PLA was applied as described previously. Remarkably, the number of interaction foci seemed to be independent of MSL2 (Figure 23B) suggesting that MOF is susceptible to modifying E3 ligases also outside the MSL-DCC. Still, it has to be taken into account that the proportion of MOF-GFP after MSL2 RNAi might also reflect the fraction of MOF-GFP outside the MSL-DCC.

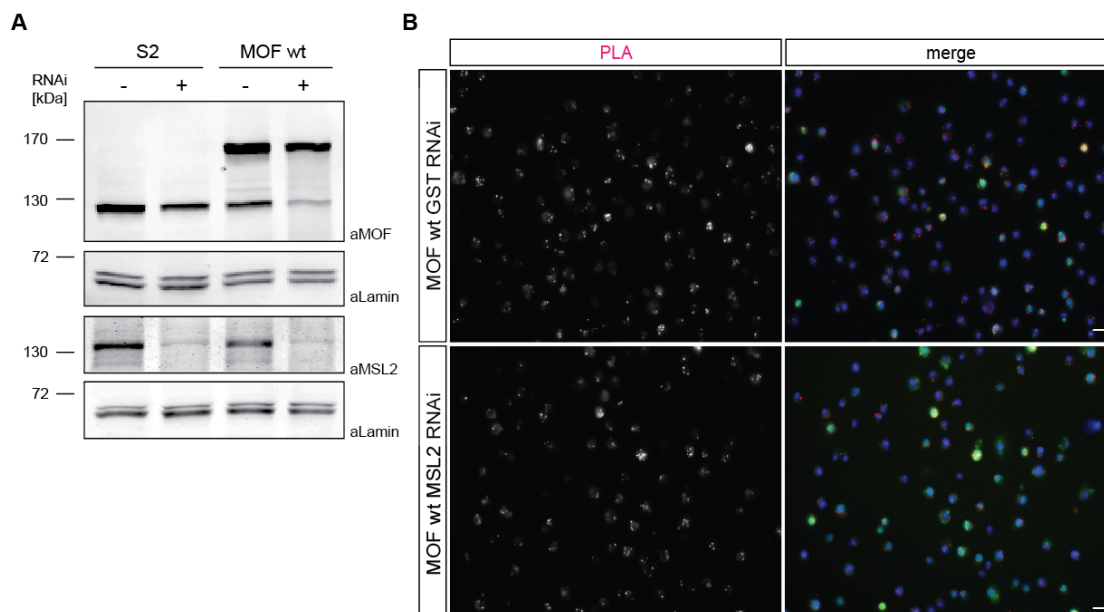


**Figure 23: RNAi of MSL2 in transgenic MOF-GFP cell lines.** (A) Transgenic S2 MOF-GFP cell lines were treated with dsRNA targeting the mRNA of GST or MSL2, respectively. Western blot analysis was performed after 7 days of RNAi.  $0.25 \times 10^6$  cells were loaded per lane and probed with anti-Lamin (aLamin), anti-MOF (aMOF) and anti-MSL2 (aMSL2) antibodies. Positions of molecular mass marker proteins are indicated to the left (kDa). (B) Cell lines stably expressing MOF-GFP were subjected to PLA assays to detect MSL2-dependent MOF ubiquitylation *in vivo*. The proximity of MOF and ubiquitin is visualized by interaction foci (PLA-signal). GFP stains transgenic MOF wt-GFP, DNA was counterstained with DAPI. Scale bars represent 1  $\mu$ m.

### 3.2.3 Analysis of proteasome-related MOF ubiquitylation *in vivo*

To highlight MSL2-independent ubiquitylation sites on MOF, stable MOF-GFP cell lines were treated with the proteasome inhibitor MG132 (Figure 24). Treatment of small numbers of cells consistently illustrated the accumulation of ubiquitin signal and MOF-GFP upon proteasome inhibition (Figure 24A). In order to obtain satisfactory protein amounts for ubiquitin remnant profiling large amounts of cells were raised and treated accordingly.

Despite several efforts and adjustments ubiquitylated species of MOF-GFP never accumulated to comparable amounts as seen before in the small-scale setup (Figure 24B, input). In an attempt to analyze ubiquitylation sites after proteasome inhibition, MOF-GFP was purified using the GFP-trap, trypsin-digested and subjected to LC-MS/MS (Figure 24B, GFP-IP). Analysis of ubiquitin remnants revealed only one ubiquitylated lysine residue (K715) on MOF-GFP after MG132 treatment (Figure 24C). The reasons for this poor accumulation of ubiquitylated MOF after proteasome inhibition are unclear, as one might have expected to detect more ubiquitylation sites as found before on MOF-GFP in steady state (Figure 24B). Since amount and quality of detected ubiquitylated peptides also depends very much on the performance of the mass spectrometer, biological and technical replication is highly recommended.

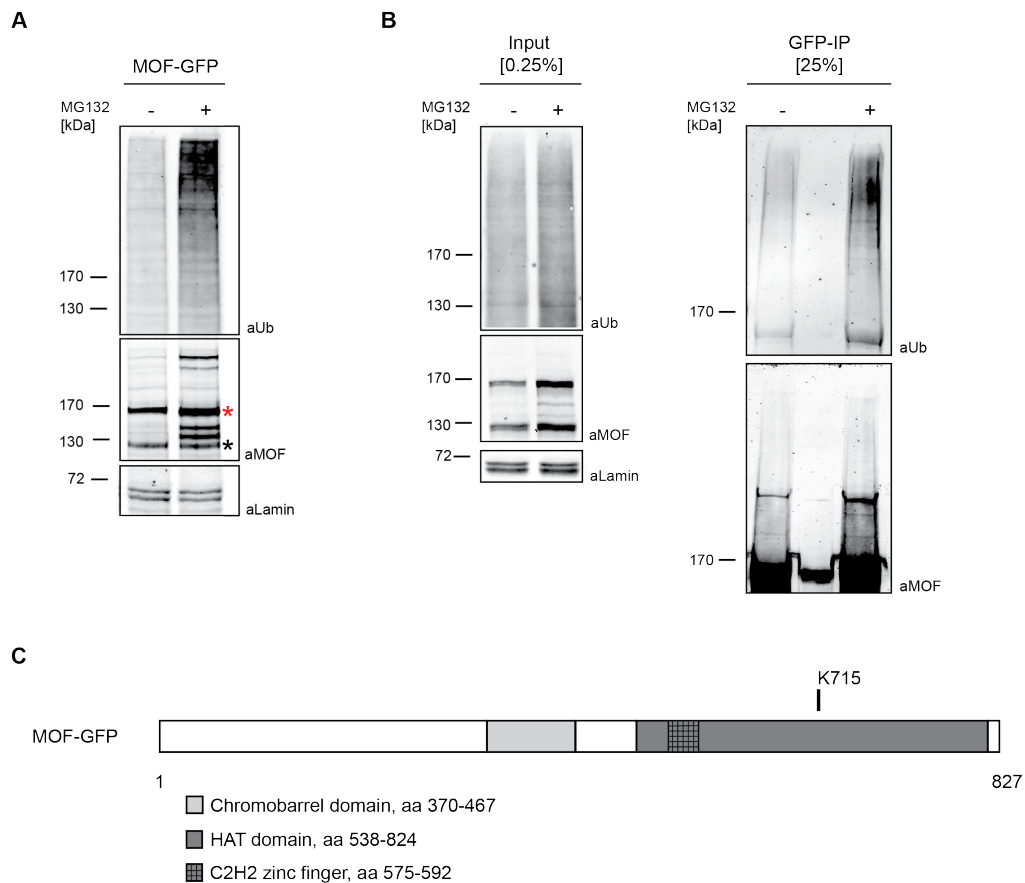


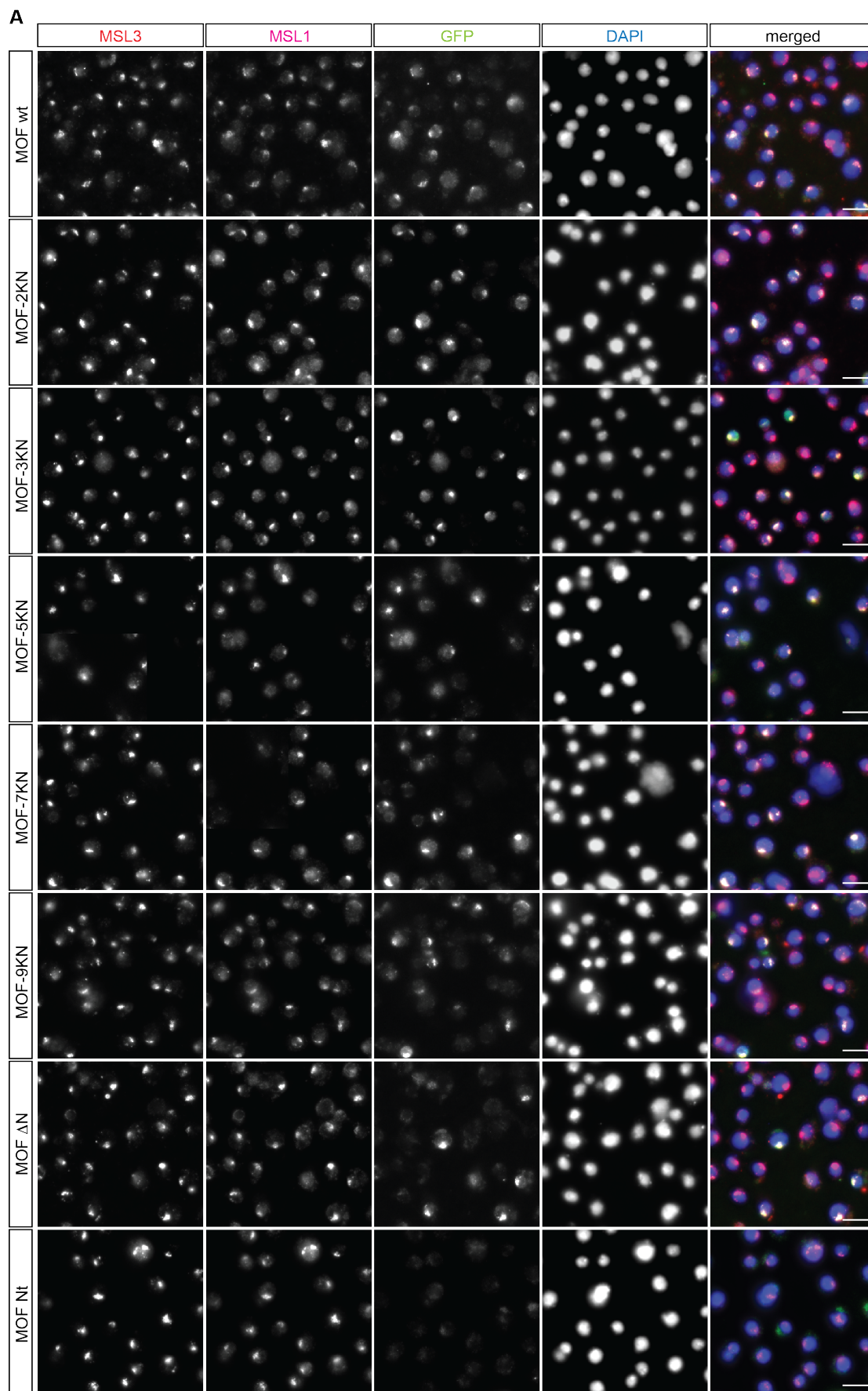
**Figure 24: Proteasome inhibition in stable S2 MOF-GFP cells.** Stable MOF-GFP cells were incubated with 10  $\mu\text{M}$  MG132 for 6 h prior to harvesting. (A) Protein extracts referring to  $0.25 \times 10^6$  of each untreated and treated cells were loaded for SDS-PAGE and subjected to Western blot analysis. Membranes were probed with anti-Lamin (aLamin), anti-MOF (aMOF) and anti-ubiquitin (aUb) antibodies. Positions of molecular mass marker proteins are indicated to the left (kDa). Red asterisk indicates MOF-GFP, black asterisk indicates endogenous MOF. (B) MOF-GFP was recovered from cells stably transfected with MOF-GFP using the GFP-trap resin. 0.25% of input and 25% of IP were loaded to SDS-PAGE and subjected to Western blot analysis. Membranes were probed with anti-Lamin (aLamin), anti-MOF (aMOF) and anti-ubiquitin (aUb) antibodies. Positions of molecular mass marker proteins are indicated to the left (kDa). (C) Schematic representation of MOF-GFP. MOF ubiquitylation site identified by mass spectrometry is displayed as black bar, number indicates modified lysine residue. One biological replicate is depicted.

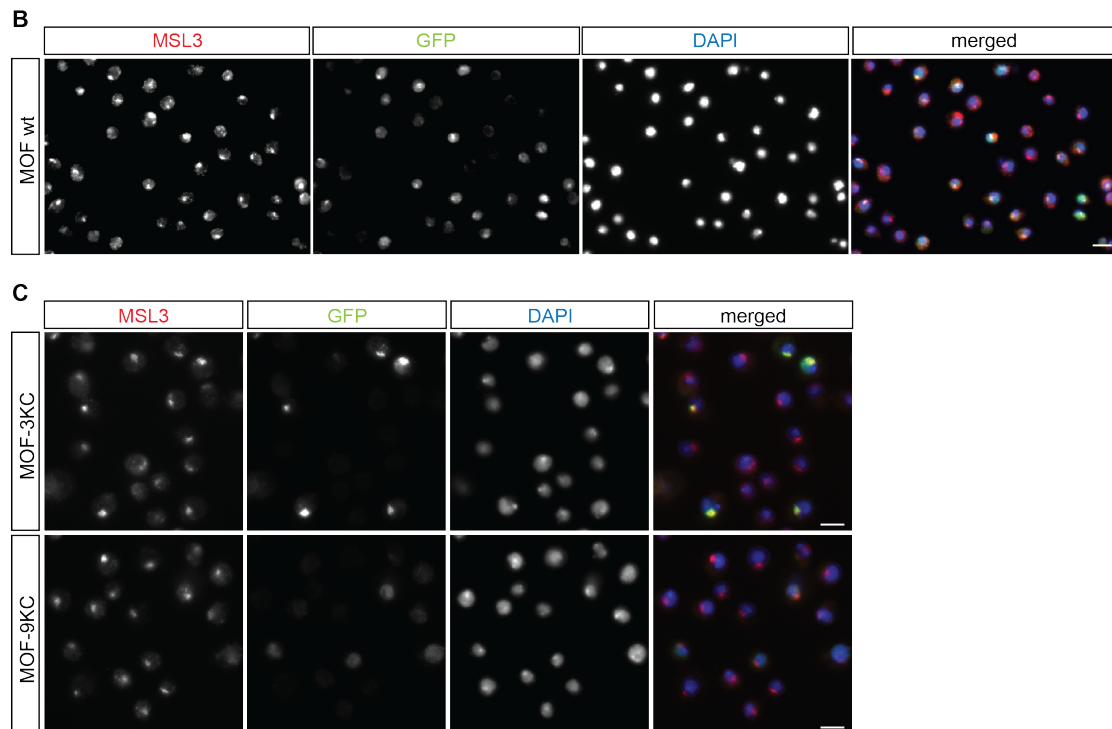
### 3.2.4 Characterization of MOF mutants *in vivo* using immunofluorescence

Previous experiments revealed a discrepancy of the ubiquitylation pattern obtained on MOF *in vitro* and *in vivo*. To investigate whether the modifications placed on MOF play a role in dosage compensation MOF mutant constructs were employed in S2 cells. Transgenic cell lines were established using stable transfection of pHsp70-EGFP MOF derivative constructs. MOF-GFP mutant cell lines were subjected to immunofluorescence staining to ascertain their X-territory targeting and association with the MSL-DCC (Figure 25). Immunostaining of stable cell lines expressing N-terminal MOF-GFP K>R point mutants revealed proper targeting to the X-territory and co-localization with associated MSL-DCC proteins. MOF  $\Delta$ N-GFP was slightly reduced on the X-territory, whereas MOF Nt no longer targets the X-territory (Figure 25A). MSL-DCC localization to the X-territory does not seem to be affected by the expression of N-terminal MOF mutant transgenes.

C-terminal MOF mutant cell lines were employed using stable transfection of pHsp70-EGFP constructs as already mentioned above. However, in this case the cell lines were established using a different transfection reagent (Effectene, Quiagen). Accordingly, faithful MOF-GFP expression and X-territory targeting were confirmed once more (Figure 25B). Immunofluorescence staining of C-terminal MOF K>R mutants revealed that 3KC faithfully targeted the X-territory and co-localized with MSL3, whereas for 9KC this was not the case (Figure 25C).

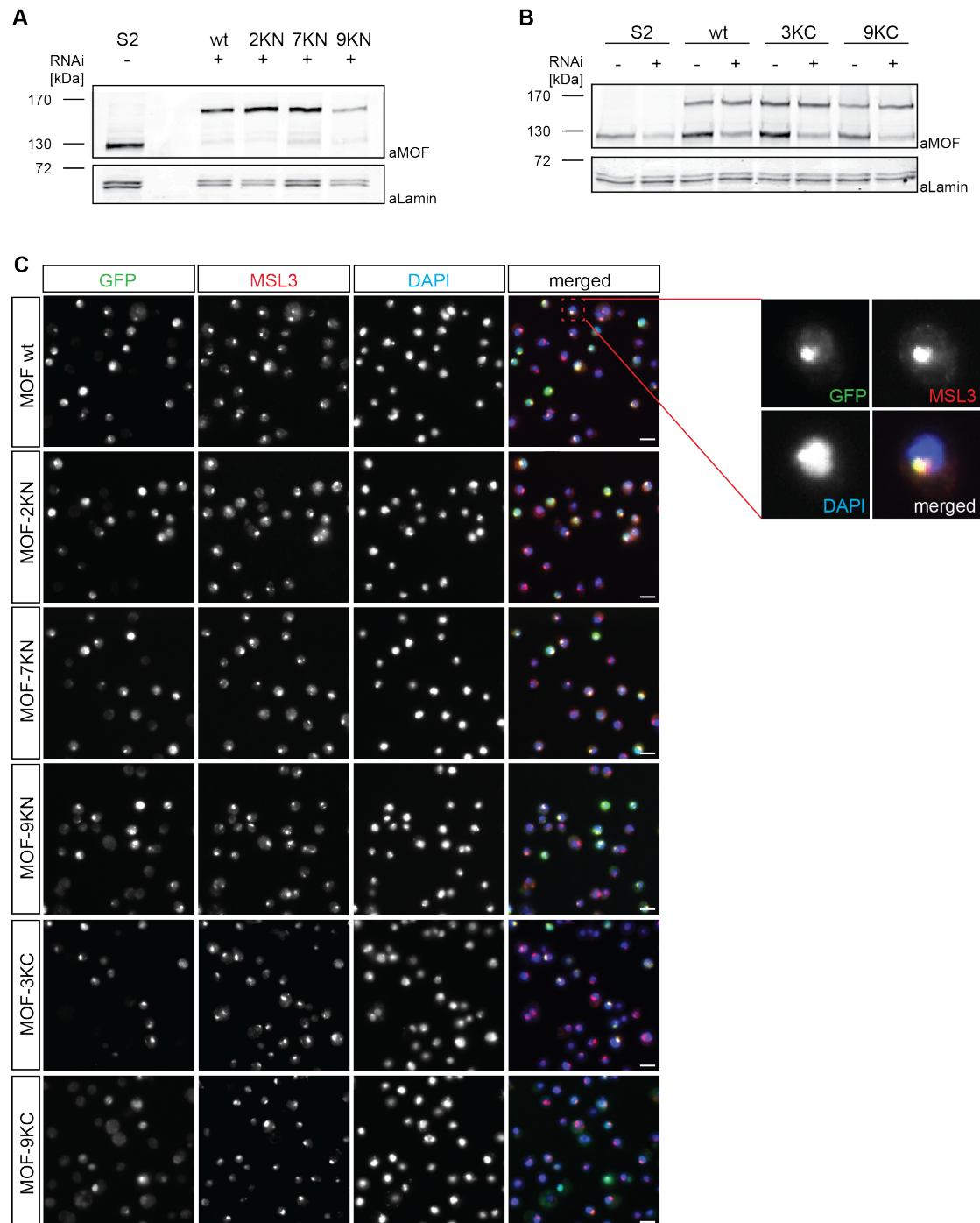
Since transgenic cell lines still contained the functional endogenous MOF protein incorporation of the transgenes might be incomplete and cells are not fully challenged to incorporate potential impaired MOF-GFP derivatives into the MSL-DCC. To analyze the MOF mutants in the absence of endogenous MOF protein RNA interference was employed to favor incorporation of the MOF-GFP transgenes into the MSL-DCC. Using suitable primers a dsRNA spanning 300 bp within the 3' untranslated region of the *mof* gene was designed. As a control for non-specific effects of RNA interference, cells were treated with dsRNA that specifically targets the mRNA of glutathione-S-transferase (GST). A subset of K>R mutants was selected for RNAi experiments. Due to previous observations from *in vitro* ubiquitylation assays N-terminal 2KN, 7KN and 9KN were of particular interest. While 2KN represents the loss of the lysines within the chromobarrel domain, 7KN might phenocopy MOF  $\Delta$ N. 9KN is a combination of the latter two mutants exhibiting loss of all lysines within the first 400 aa of MOF. To analyze the impact of loss of C-terminal lysines, both 3KC and 9KC were employed.





**Figure 25: Nuclear localization of MOF mutants.** (A) Nuclear localization of N-terminal MOF point mutants and MOF deletion mutants. Stable cell lines expressing either MOF-GFP or the indicated MOF-GFP mutants were stained with antibodies against MSL3, MSL1 and GFP as indicated. DNA was counterstained with DAPI. Scale bars represent 1  $\mu$ m. (B) Confirmation of MOF-GFP localization upon changed employment of transfection reagent. Cell lines stably expressing MOF-GFP were stained with antibodies against MSL3 and GFP as indicated. DNA was counterstained with DAPI. Scale bars represent 1  $\mu$ m. (C) Nuclear localization of C-terminal MOF point mutants. Stable cell lines expressing either MOF 3KC-GFP or MOF 9KC-GFP were stained with antibodies against MSL3 and GFP as indicated. DNA was counterstained with DAPI. Scale bars represent 1  $\mu$ m.

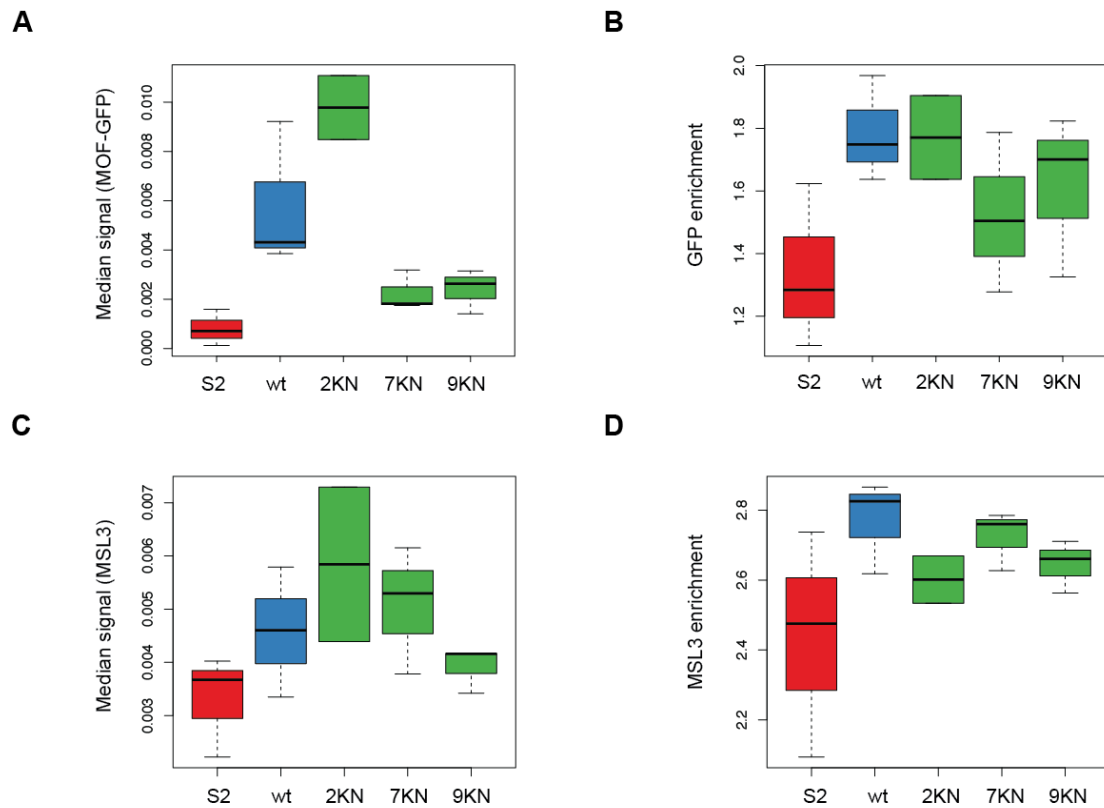
After 7 d of RNAi endogenous MOF levels were substantially reduced in the N- and C-terminal K>R point mutants as shown by immunoblotting of whole cell extracts (Figure 26A and B). Stable cell lines depleted for the endogenous MOF protein were subjected to immunofluorescence experiments. It had previously been demonstrated that MOF transgenes enrich significantly better to the X-territory upon depletion of endogenous MOF protein. MOF wt, 2KN, 7KN, 9KN and 3KC target the X-territory as assessed by co-localization with MSL3 (Figure 26C). While loss of three potential C-terminal ubiquitylation sites (3KC) is still well tolerated, loss of 9 lysine residues (9KC) within the MOF HAT domain resulted in loss of GFP signal from the X-territory.



**Figure 26: Depletion of endogenous MOF protein in transgenic cell lines using RNA interference.** (A, B) Transgenic S2 cell lines (MOF wt, 2KN, 7KN, 9KN, 3KC and 9KC) were treated with dsRNA targeting the 3' mRNA of the endogenous MOF protein. Western blot analysis was performed after 7 days of endogenous MOF RNAi.  $0.25 \times 10^6$  cells of control (S2) and knockdown samples were loaded per lane and probed with anti-Lamin (aLamin) and anti-MOF (aMOF) antibodies. Positions of molecular mass marker proteins are indicated to the left (kDa). (C) Nuclear localization of K>R MOF point mutants upon knockdown of endogenous MOF protein. Stable cell lines expressing either MOF-GFP wt or the indicated MOF-GFP point mutants were stained with antibodies against GFP and MSL3 as indicated. DNA was counterstained with DAPI. Scale bars represent 1  $\mu$ m.

### 3 RESULTS

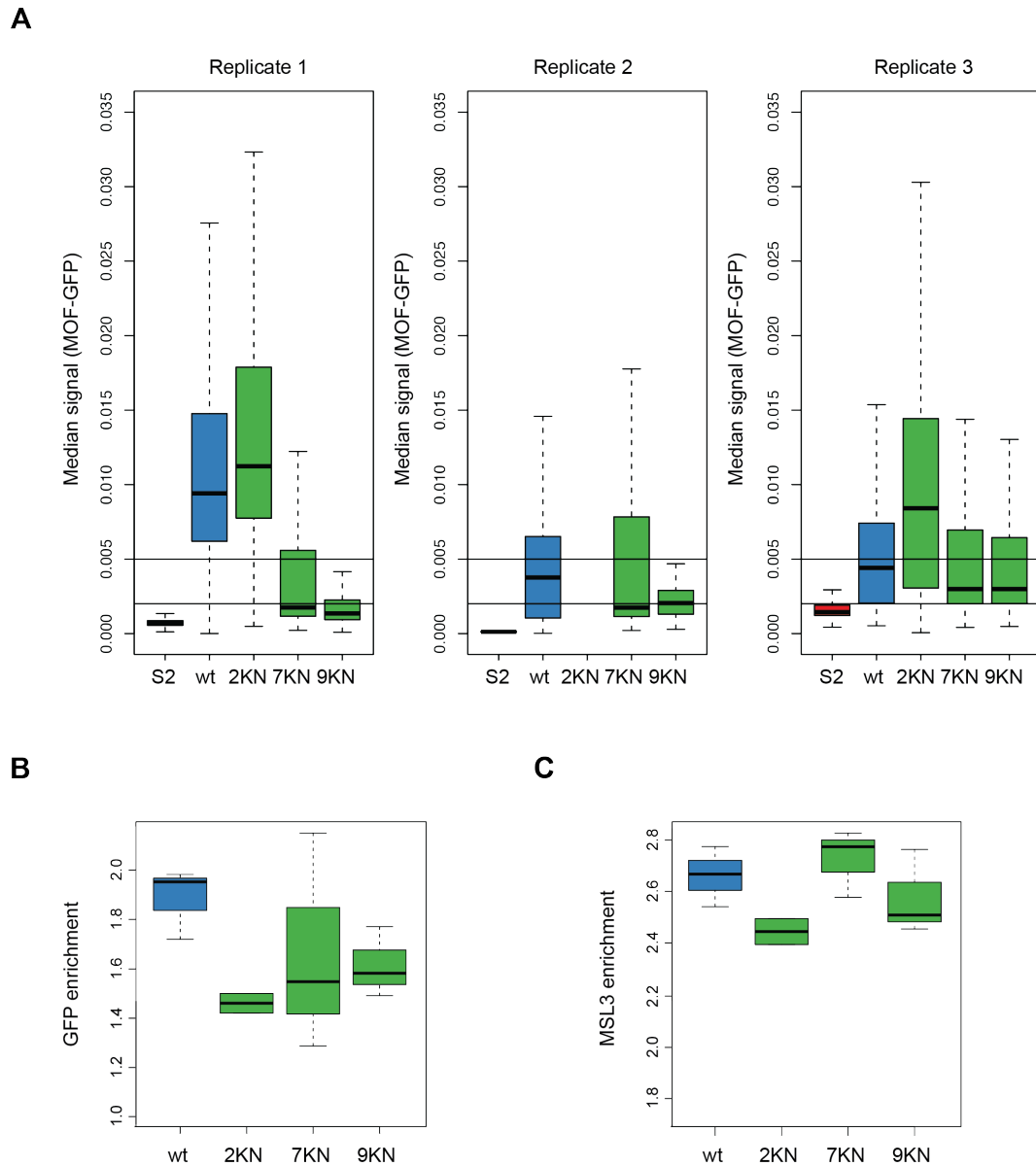
To assess differences of X-territory enrichment of both MOF-GFP mutant transgenes and MSL3 a quantitative approach was applied. Since the effect upon expression of C-terminal MOF mutants was very obvious quantification was restrained to the N-terminal (KN) mutants. Using CellProfiler three biological replicates were quantified upon RNAi of endogenous MOF protein in S2, wt, 7KN and 9KN, two biological replicates were processed for 2KN (Figure 27).



**Figure 27: Analysis of X-chromosomal territories in S2 cells stably expressing MOF-GFP K>R point mutants after RNAi of endogenous MOF protein.** (A) Quantification of median MOF-GFP signal using GFP antibody. For each cell line the median GFP-signal within the nuclei (segmented on the DAPI staining) is plotted. S2 cell line served as non-transfected GFP-negative control. The black bar indicates median signal for each cell line, the box plot presents standard deviation. Scaling of the y-axis is logarithmic. (B) Quantification of the X-chromosomal territories in transgenic cell lines using GFP antibody. For each staining log enrichment ratios were calculated as territorial signals computationally segmented on the MSL3 staining and the mean intensity of the nuclei (segmented on the DAPI staining). The black bar indicates average GFP enrichment for each cell line. Scaling of the y-axis is logarithmic. (C) Quantification of median MSL3 signal in transgenic cell lines using MSL3 antibody. For each cell line the median MSL3-signal within the nuclei (segmented on the DAPI staining) is plotted. Scaling of the y-axis is logarithmic. (D) Quantification of the X-chromosomal territories in transgenic cell lines using MSL3 antibody. For each staining log enrichment ratios were calculated as territorial signals computationally segmented on the MSL3 staining and the mean intensity of the nuclei (segmented on the DAPI staining). The black bar indicates average MSL3 enrichment for each cell line. Scaling of the y-axis is logarithmic.

Quantification of median MOF-GFP signals within the nuclei (segmented on the DAPI staining) revealed major differences in the expression levels of the MOF-GFP derivatives, which was also visible in Western blot, and immunofluorescence microscopy of representative areas of the imaged slides. Compared to MOF wt-GFP median levels of 2KN-GFP were substantially higher, while in 7KN- and 9KN-GFP cell lines median GFP levels were particularly low (Figure 27A). GFP-enrichment on the X-territory seemed to follow this tendency as MOF wt-GFP and 2KN-GFP enriched to similar extent on the X chromosome, while 7KN- and 9KN-GFP enrichment was reduced (Figure 27B). When checked for the median MSL3 signal within the nuclei (segmented on the DAPI staining), 2KN-GFP exhibited highest MSL3 levels, followed by 7KN-, wt- and 9KN-GFP, lowest MSL3 median levels were detected in S2 control cells (Figure 27C). At the same time MSL3 enrichment on the X-territory was highest for wt-GFP, followed by 7KN-, 9KN- and 2KN-GFP, while MSL3 enrichment on the X-territory was least efficient in S2 control cells (Figure 27D). In summary, all K>R mutants display reduced MSL3 enrichment on the X-territory when compared to MOF wt, however the biological relevance of these observations remain to be discussed.

Notably, median GFP expression levels substantially varied between the employed MOF K>R mutants (Figure 27A). Hence, MSL3 enrichment on the X-territory might be dependent on relative amounts of the GFP transgenes present in the cells. To evaluate whether median GFP-levels affected GFP and MSL3 enrichment on the X-territory, cutoffs on median MOF-GFP signal in single biological replicates were employed to constrain the analysis to signals that represent moderate expression of MOF-GFP (Figure 28A). Remarkably, the replicates were quite different regarding the GFP expression levels of the individual MOF mutant cell lines. Still, evaluation of average GFP and MSL3 enrichment after application of the cutoffs confirmed the previous observations: all K>R point mutants enrich less on the X territory than the wt (Figure 28B) and MSL3 enrichment on the X-territory followed the same tendency as previously described in Figure 27D (Figure 28C). In summary, varying GFP-expression levels cannot be linked to the overall reduction of MSL3 enrichment on the X-territory in the K>R mutants.

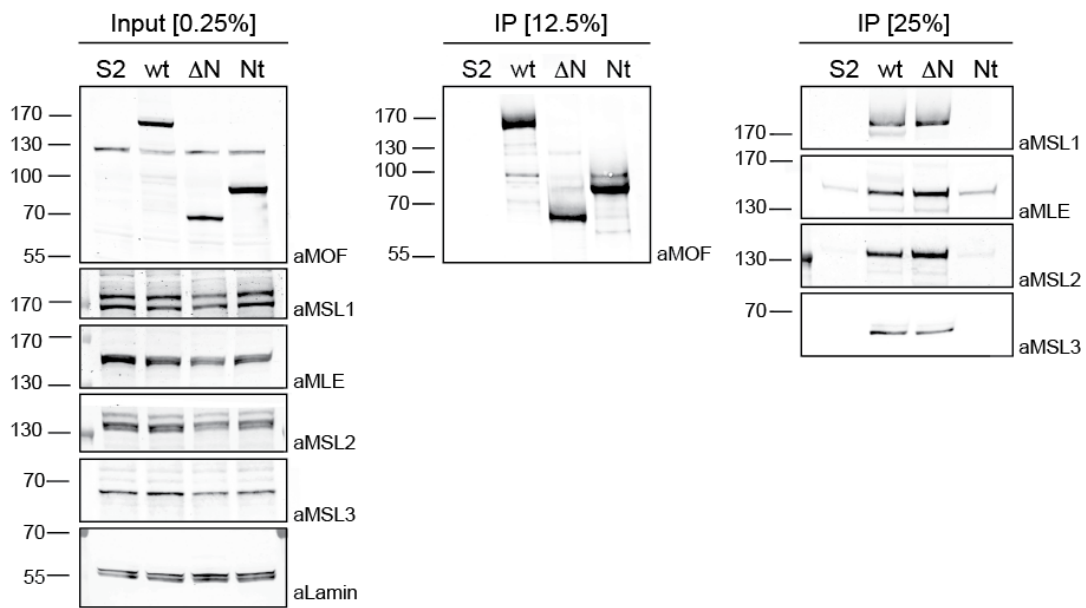
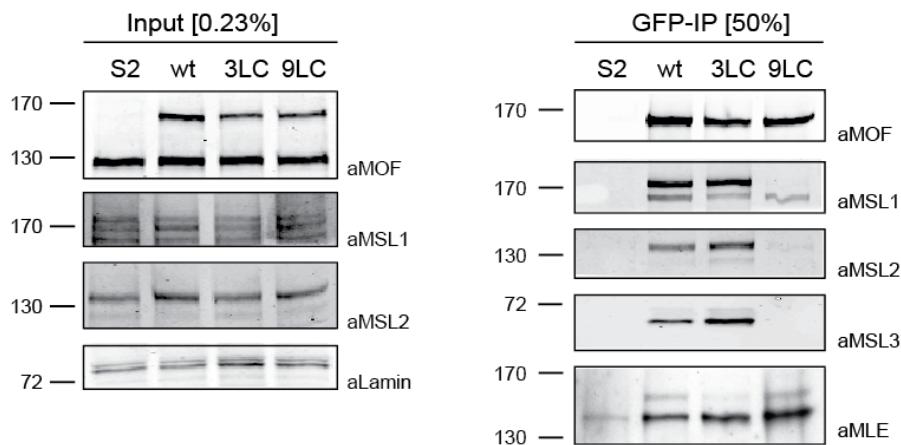


**Figure 28: Analysis of X-chromosomal territories in S2 cells stably expressing MOF-GFP K>R point mutants after RNAi of endogenous MOF protein.** The box plots present standard deviation. Scaling of the y-axes are logarithmic. (A) Employed cutoffs on median MOF-GFP signal in the single biological replicates. MOF-GFP signals within the nuclei (segmented on the DAPI staining) were constrained to signals that represent moderate expression of MOF-GFP. Plots depicted in **Figure 27B-C** were assessed on cells within the cutoff area between the indicated horizontal bars. The bold black bar indicates median MOF-GFP signal for each cell line. (B) Quantification of the X-chromosomal territories in transgenic cell lines depleted for endogenous MOF protein using GFP antibody. The black bar indicates average GFP enrichment for each cell line. (C) Quantification of the X-chromosomal territories in transgenic cell lines depleted for endogenous MOF protein using MSL3 antibody. The black bar indicates average MSL3 enrichment for each cell line.

### 3.2.4 Association of MOF mutants with the MSL-DCC

Extensive mutation of C-terminal lysine residues resulted in loss of both MOF Nt-GFP and MOF-9KC-GFP from the X-territory as assessed by immunofluorescence (Figure 25A and C). This finding points to a diminished assembly of the MSL-DCC upon expression of transgenic MOF mutants *in vivo*. To confirm this assumption immunoprecipitation experiments were performed to study the assembly of the MOF mutants with the MSL-DCC. To this end MOF deletion mutants and C-terminal K>R point mutants were employed using the GFP-trap (Figure 29). Immunopurified MOF  $\Delta$ N-GFP is able to interact with the members of the MSL-DCC, whereas MOF Nt-GFP no longer exhibits any interactions with the complex. Signal observed in immunoprecipitation of MOF Nt-GFP with MLE is also observed in the non-GFP S2 control and can be attributed to background signal as a consequence of MLE sticking to the GFP-trap. Various studies point to a dimeric complex composition of the MSL-DCC. Within the MSL-DCC dimerization of MSL1 and the interaction with two MSL2 subunits is believed to initiate the assembly of the complex (Hallacli, 2012). Furthermore, it was proposed that MLE dimerizes *in vitro* (Izzo, 2008). To date, it is not fully proven whether MOF exhibits homodimerization as well. Immunoprecipitation experiments performed on transgenic MOF-GFP however did not reveal interaction of MOF-GFP and endogenous MOF (Figure 29A). Immunoprecipitation experiments performed on the C-terminal MOF K>R point mutants confirmed that immunopurified 3KC-GFP is able to exhibit substantial interaction with MSL1, MSL2, MSL3 and MLE (Figure 29B). 9KC-GFP on the contrary does not interact with MSL1, MSL2 and MSL3. However, 9KC-GFP surprisingly still interacts with MLE, which was unexpected since a direct interaction of MOF and MLE was not reported so far.

In summary, mutation of N-terminal lysine residues does not affect complex association on the X chromosome. On the contrary, both a MOF deletion representing the N-terminus only as well as extensive mutation of C-terminal lysine residues result in loss of localization on the X-territory as well as loss of complex association.

**A****B**

**Figure 29: Association of transgenic MOF-GFP mutants with the MSL-DCC.** Cell extracts from control cells (S2) and stably transfected cells with MOF-GFP derivatives as indicated were immunoprecipitated with the GFP-trap. Western blots of input lysates or immunoprecipitates were analyzed with antibodies against MOF, MSL1, MSL2, MSL3, MLE and Lamin as indicated. Positions of molecular mass marker proteins are indicated to the left (kDa). The experiments were repeated in biological triplicates with the same outcome. (A) Association of transgenic MOF-GFP deletion mutants with the MSL-DCC. MOF wt-GFP and MOF  $\Delta N$ -GFP associate with the MSL-DCC, MOF Nt-GFP fails to interact with the complex. (B) Association of transgenic C-terminal MOF-GFP K>R point mutants with the MSL-DCC. MOF wt-GFP and MOF 3KC-GFP associate with the MSL-DCC, MOF 9KC-GFP interacts with MLE only.

### 3.2.5 Male viability of MOF mutants

To analyze the functionality and impact of the MOF point mutants in the living organism transgenic fly lines were generated using site-directed integration of the MOF constructs. Transgenic flies harbor MOF mutant constructs on the third chromosome under the control of an upstream activating sequence (UAS), furthermore, they exhibit a C-terminal FLAG-tag and a *mini white* reporter construct ( $w^+$ ). To check for proper activation of transgene expression the UAS constructs were first induced using a salivary glands tissue specific GAL4 driver line. Flies homozygous for the transgene were crossed to flies comprising a GAL4 activator downstream of the *Sgs3* promoter. Relative expression levels of the MOF transgenes were assessed from each 2-4 salivary glands by Western blot analysis (Figure 30).

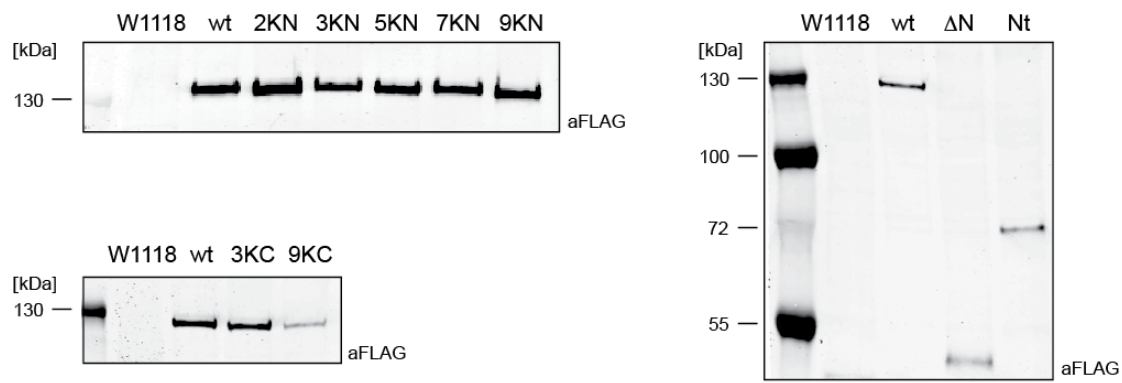


**Figure 30: Induction of MOF transgene expression in salivary glands.** Homozygous males carrying MOF transgenes were crossed to virgin flies carrying the tissue-specific *Sgs3*-Gal4 salivary gland driver. Salivary glands from isogenic W1118 flies were used as control. 2-3 pairs of salivary glands were dissected, boiled in sample buffer and subjected to Western blot analysis. Induced MOF transgenes were detected using anti-FLAG (aFLAG) antibody. Positions of molecular mass marker proteins are indicated to the left (kDa).

Next, the viability of the MOF mutants was assayed by complementation of the male-lethal *mof*<sup>2</sup> mutant (Figure 31). Similar to immunofluorescence experiments before, only a subset of MOF mutants was selected for complementation assays (wt, 2KN, 7KN, 9KN, 3KC, 9KC, ΔN and Nt). Transgene expression was induced at 25°C by crossing female flies of the genotype *mof*<sup>2</sup>/*Fm7a*; *P{armadillo-GAL4}* to male *y/w*;  $\{w^+ \text{ MOF-FLAG-UAS}\}$ . Relative male survival was scored as ratio of male *mof*<sup>2</sup>/*y*; *P{armadillo-GAL4}*/ $\{w^+ \text{ MOF-FLAG-UAS}\}$  to female *mof*<sup>2</sup>/*+*; *P{armadillo-GAL4}*/ $\{w^+ \text{ MOF-FLAG-UAS}\}$ . 2KN, 7KN and 9KN rescued male lethality of *mof*<sup>2</sup> to similar extent as the MOF wt transgene (Figure 31A). ΔN and Nt deletion mutants dramatically reduced male survival in accordance with literature (Conrad, 2012a) and were used as internal negative control.

*mof*<sup>2</sup> complementation efficiency of the C-terminal MOF mutants was observed to be dependent on the amount of larvae per vial (Figure 31B). As 100 1<sup>st</sup> instar were placed to a food vial per cross MOF wt, the N-terminal 9KN and the C-terminal 3KC mutant fully

### 3 RESULTS

restored male viability. Male viability was mildly affected upon expression of 9KC (72%) whereas  $\Delta N$  restored male viability only up to 17%. In contrast, placement of at least 400 1<sup>st</sup> instar larvae per food vial affected overall complementation efficiency of all MOF transgenes (Figure 31C). Still, MOF wt, 9KN and 3KC rescued male viability to similar extents. The effect of  $\Delta N$  complementation was more pronounced in the crowded vial as male viability drops to 2% compared to 17% in the non-crowded vials. Male viability was strongly challenged upon expression of 9KC in the crowded food vials and complements *mof*<sup>2</sup> only up to 33%.

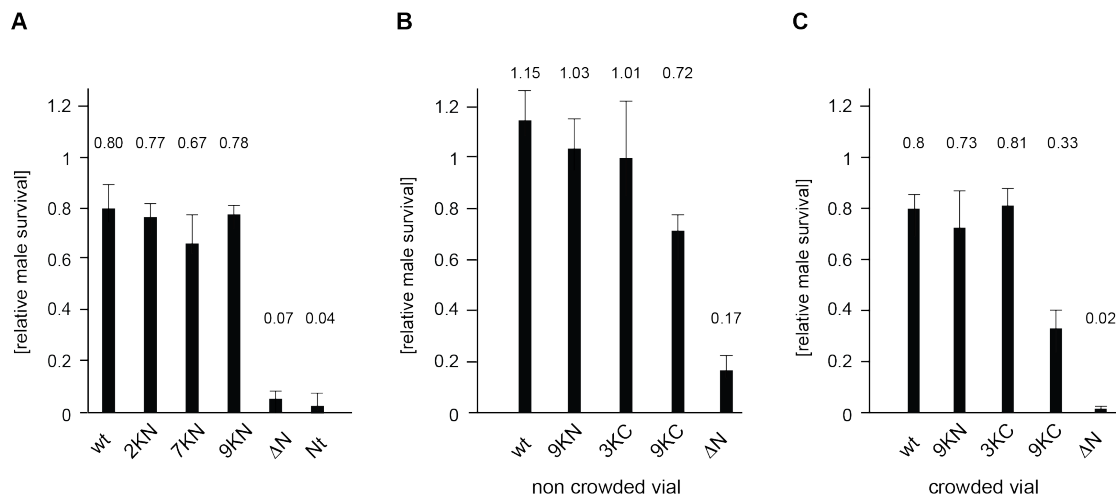


**Figure 31: Male viability of MOF mutants.** (A) Male viability upon expression of N-terminal MOF point mutants. Male survival was assayed upon expression of various MOF transgenes in the *mof*<sup>2</sup> male lethal background. Average ratios of male *mof*<sup>2</sup>/*y*; *P*{*armadillo-GAL4*}/*w*<sup>+</sup> *MOF-FLAG-UAS* flies compared to the number of female *mof*<sup>2</sup>/*+*; *P*{*armadillo-GAL4*}/*w*<sup>+</sup> *MOF-FLAG-UAS* flies (relative male survival) are shown. Error bars represent the standard error of the mean. The experiment was performed in biological triplicates. (B) Male viability upon expression of C-terminal MOF point mutants in non-crowded conditions. Average ratios of male *mof*<sup>2</sup>/*y*; *P*{*armadillo-GAL4*}/*w*<sup>+</sup> *MOF-FLAG-UAS* flies compared to the number of female *mof*<sup>2</sup>/*+*; *P*{*armadillo-GAL4*}/*w*<sup>+</sup> *MOF-FLAG-UAS* flies (relative male survival) are shown. Error bars represent the standard error of the mean. The experiment was performed in biological triplicates. (C) Male viability upon expression of C-terminal MOF point mutants in crowded conditions ( $\geq 400$  larvae per vial). Median ratios of male *mof*<sup>2</sup>/*y*; *P*{*armadillo-GAL4*}/*w*<sup>+</sup> *MOF-FLAG-UAS* flies compared to the number of female *mof*<sup>2</sup>/*+*; *P*{*armadillo-GAL4*}/*w*<sup>+</sup> *MOF-FLAG-UAS* flies (relative male survival) are shown. Error bars represent the standard error of the mean. The experiment was performed in 5 biological replicates.

### 3.3 MSL2-dependent ubiquitylation outside of the MSL-DCC

In order to explore whether the E3 ligase activity of MSL2 targets other substrates outside of the DCC an unbiased approach was employed previously in the laboratory in collaboration with Tiziana Bonaldi (IFOM-IEO Campus, Milan). A stable cell line (S2 cells) expressing His6-tagged ubiquitin under the control of a strong promoter was used to perform stable isotope labeling by amino acids in cell culture (SILAC). This stable cell line was treated with double-stranded interfering RNA for specific knockdown of MSL2 or control GST RNAi, respectively. To enrich for ubiquitylated proteins whole cell extracts were subjected to pull down experiments using Ni<sup>2+</sup> agarose beads. The SILAC analysis provided a set of putative substrates for MSL2 dependent ubiquitylation, yet none of the MSL-DCC proteins were detected either in input or in the enriched pull-down sample, which is most likely a consequence of their overall low cellular abundance. Due to its proposed role in transcriptional regulation at the step of elongation SPT6 was chosen as candidate protein for further investigations.

#### 3.3.1 Generation and characterization of SPT6 monoclonal antibodies

To study and characterize SPT6 in *Drosophila melanogaster*, monoclonal antibodies derived from rat and mouse were generated. Suitable epitopes were chosen from both the N-terminal and C-terminal part of the protein in accordance with a BLAST research for SPT6 specific peptides. Apparently aa 207-491 and aa 1525-1831 show no particular alignment with other *Drosophila* specific proteins so these parts of the protein were chosen for epitope search (Figure 32A). Commercial antibodies for both human and mouse SPT6 recognize epitopes within the C-terminus of the protein.

An epitope scan within the preselected regions of SPT6 yielded three potential epitopes suitable for antibody generation (Figure 32B). Peptides were synthesized and coupled via a cysteine group to ovalbumin by Peps4LS GmbH (Heidelberg). Dr. E. Kremmer (Service Unit Monoclonal Antibodies, Helmholtz Zentrum, Munich) employed obtained peptides for production of monoclonal antibodies.

**A**

```

1 MAEFLDSEAE ESEEEEELDV NERKRLKCLK AAVSDSSEEE EDDEERLREE
  LKDLIDDNPI EEDDGGGYDS DVGSGGKRRK KHEDDDLDDR LEDDDYDLIE
  ENLGVKVERR KRFKRLRRIH DNESDGEEQH VDEGLVREQI AEQLFDENDE
  SIGHRSESSH READDYDDVD TESDADDFIV DDNGRPIAEK KKKRRPIFTD
  ASLQEGQDIF GVDFDYDDFS KYEEDDYEDD SEGDEYDEDL GVGDDTRVKK
  KKALKKKVVK KTFDFIYEPS ELKRGHFTDM DNEIRKTDIP ERMQLREVPV
  TPVPEGSDEL DLEAEWIYKY AFCKHTVSEQ EKPESSREKMR KPPTTVNKKI
  QTLEFIRNQQ LEVFFIAFYR KEYVVKPELNI DDLWKVYYID GIWCQLNERK
  RKLKVLFEKM RQFQLDTLCA DTDQVPVDDV RLILDSDFER LADVQSMEEL
  KDVHMYFLLN YSHELPRMQA EQRRKAIQER REAKARRQAA AAENGDDAAE
  AIVVPEPEDD DPELIDYQL KQASNSPPYA VFRKAGICGF AKHFGLTPEQ
  YAENLRDNYQ RNEITQESIG PTELAKQYLS PRFMTTDEVI HAAKYVVARQ
  LAQEP LLRKT MREVFDRAR INIRPTKNGM VLIDENSPVY SMKYVAKKPV
  SDLFGDQFIK LMMAEEKLL EITFLEEFEG NACANGTPGD YVEESKALYQ
  LDQFAKHVQE WNKLAECVQ LALQKWVIPD LIKELRSTLH EEAQQFVLSR
  CTGKLYKWLK VAPYKQLPP DFGYEEWSTL RGIRVLGLAY DPHSVA AFC
  AVTTVEGDIS DYLRPLNLIK RKN SYNLEEK AQKLADLRKL SDFIKMKKPH
  IVVIGAESRD AQNIQADIKE ILHELETSEQ FPPIEVEIID NELAKIYANS
  KKGESDFKEY PPLLKQAASL ARKMQDPLVE YSQLCDADDE ILCLRYHPLQ
  ERVPREQLE QLSLQFINRT SEVGLDINLM VQNSRTINLL QYICGLGPRK
  GQALLKLLKQ SNQRLNRTQ LVTVCHLGPV VFINC SGFIK IDTSSLG DST
  EAYVEVL DGS RVHPETYEWA RKMAIDAMEY DDEETNPAGA LEEILES PER
  LKDLDLDAFA VELERQGF GS KSITLYDIRN ELSCLYKDYR TPYTKPSAEE
  LFDMLTKETP DSFYV GKCVT AMVTGFTYRR PQGDQLDSAN PVR LDSNESW
  QC PFCHKDDF PELSEVWNHF DANACPGQPS GVRVRENLG PGFIHIK NLS
  DRQVRNPEER VRV SQMIHVR I IKIDIDRFS VECSRTADL KDVNNEW RPR
  RDNYYDYVTE EQDNRKVS DA KARALKRRIY ARRVI AHPSF FNKSYAEVVA
  MLAEADQGEV ALRPSSKSKD HLTATWKVAD DIFQHIDVRE EGKENDFSLG
  RSLWIGTEEF EDLDEI IARH IMPMALAARE LIQYKYYKPN MVTGDENERD
  VMEKLLREEK ANDPKKIHYF FTASRAMP GK FLLSYLPKTK VRHEYVTVMP
  EGYRFRGQIF DTVNSLLRWF KEHWLDP TAT PASASASNLT PLHLMRPPPT
  ISSSSQTSLG PQAPYSVTGS VTGGTPRS GI SSAVGGGGSS AYSITQSI TG
  YGTSGSSAPG AGVSSSHYGS SSTPSFGAIN TPYTPSGQTP FMTPTYTPHAS
  QTPRYGHNV P SPSSQSSSQ RHHYGSSSGT GSTPRYHDMG GGGGGVGGG
  GGSNAYSMQP HHQQRAKENL DWQLANDAWA RRRPQQHQSH QSYHAQQQHH
  HSQQQPHMGM SMNMGITMSL GRGTGGGGGG GYGSTPVNDY STGGGHNRMG
  SSKASVRS TP RTNASPHSMN LGDATPLYDE N 1831
  
```

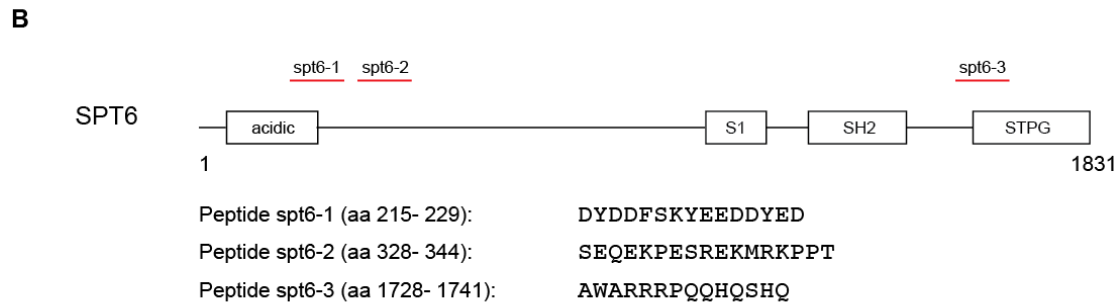


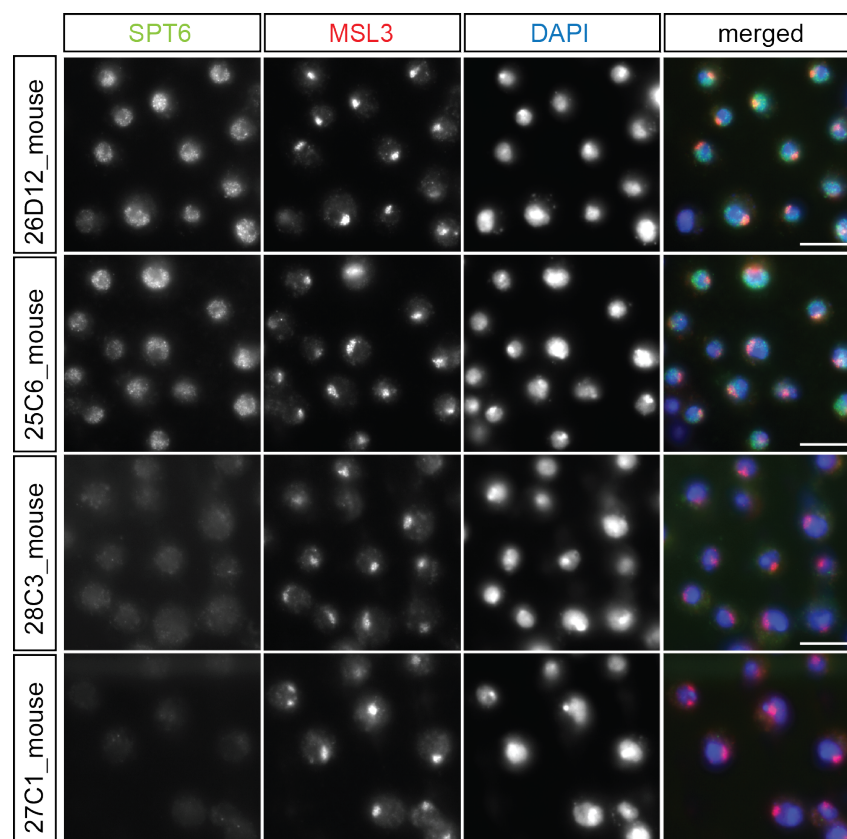
**Figure 32: Generation of SPT6 monoclonal antibodies.** (A) Protein sequence of *Drosophila* SPT6. Regions that do not exhibit alignments with other *Drosophila* proteins (BLASTp) are highlighted in red letters. (B) Schematic representation of SPT6 domain structure. Regions and sequences of selected peptides employed for generation of monoclonal antibodies are indicated.

About 100 supernatants were tested in a first screen for their reactivity in Western blot probing *Drosophila melanogaster* embryo extracts. Eight supernatants contained antigen-specific antibodies and were selected for further subcloning (Table 10).

**Table 10: monoclonal SPT6 antibodies.**

SPT6 antibody	epitope	host
26D12	spt6-1	mouse
25C6	spt6-1	mouse
13D4	spt6-1	rat
28C3	spt6-2	mouse
27C1	spt6-2	mouse
8C4	spt6-3	rat
14B8	spt6-3	rat
17C8	spt6-3	rat

In addition, reactivity of obtained monoclonal antibodies was assessed in immunofluorescence experiments on S2 cells. 26D12 and 25C6 hybridoma recognize a mostly nuclear protein while staining with 28C3, 27C1, 13D4, 8C4, 14B4 and 17C8 gave an unspecific background signal all over the nucleus and cytoplasm (Figure 33).



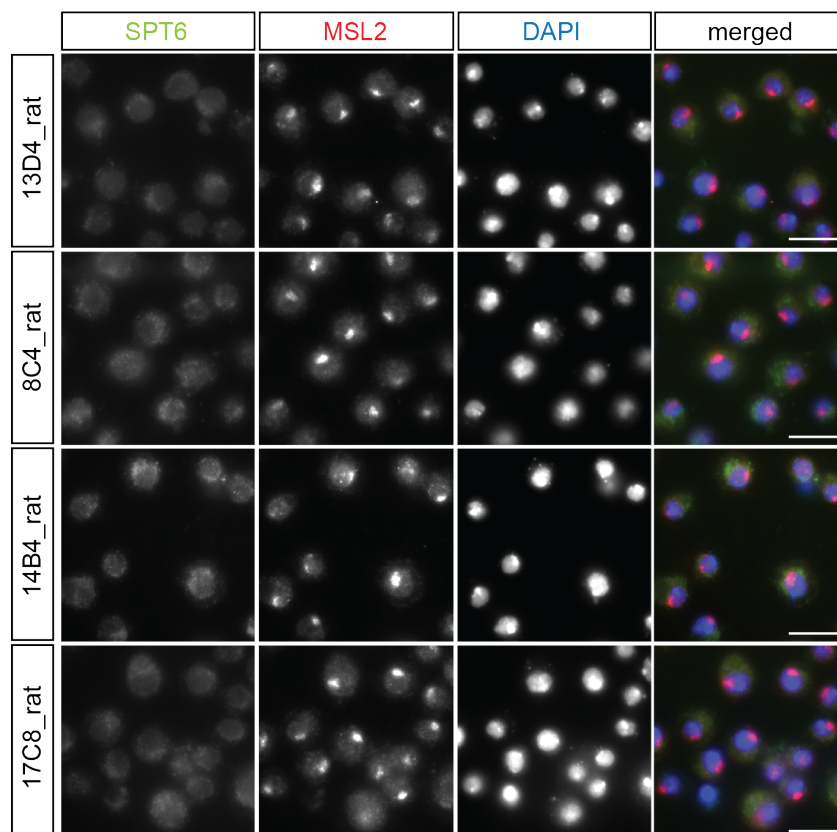


**Figure 33: SPT6 monoclonal antibodies in immunofluorescence.**  $0.8 \times 10^6$  S2 cells were stained with antibodies against SPT6, MSL3 or MSL2 as indicated. DNA was counterstained with DAPI. Scale bars represent 1  $\mu\text{m}$ .

Finally, the specificity of subcloned SPT6 monoclonal antibodies was further confirmed by Western blot analysis and immunofluorescence upon depletion of endogenous SPT6 using RNAi interference (Figure 34). A dsRNA, spanning 400 bp within the *spt6* cDNA was used to deplete SPT6 protein in S2 cells. As a control for non-specific effects of RNA interference, cells were treated with a dsRNA that specifically targets the mRNA of glutathione-S-transferase (GST). After 4 days of SPT6 RNAi protein levels were significantly depleted, whereas 7 days of RNAi treatment was lethal for the cells. Whole cell extracts from S2 cells depleted for GST or SPT6, respectively were subjected to Western blot analysis (Figure 34B). Supernatants 26D12 and 25C6 recognizing peptide spt6-1 and supernatants 28C3 and 27C1 recognizing peptide spt6-2, were found to specifically detect SPT6 from S2 whole cell extracts. Specificity of 26D12 and 25C6 monoclonal antibodies was also confirmed in immunofluorescence experiments on fixed S2 cells (Figure 34C).

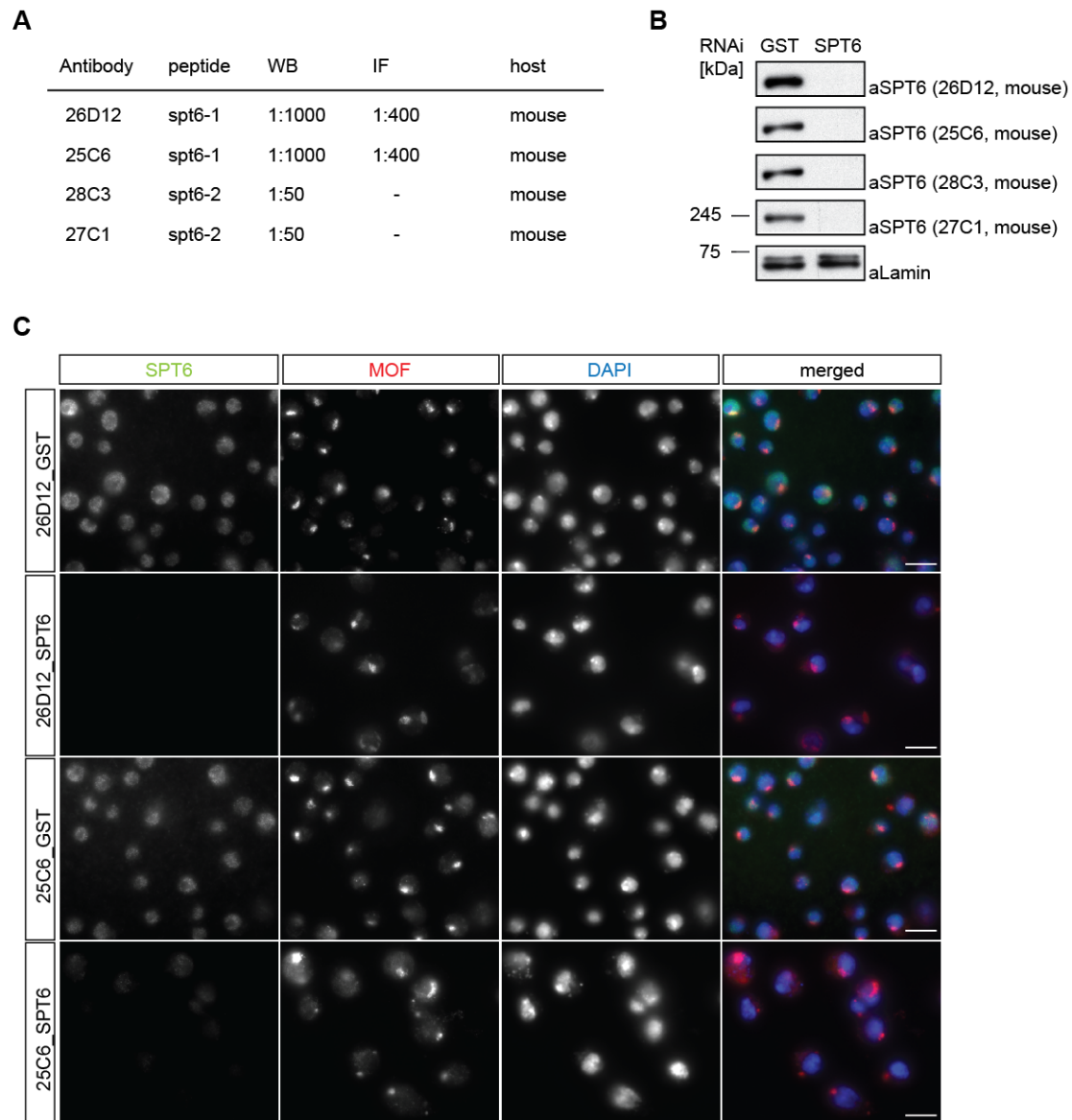


**Figure 34: Specificity of SPT6 monoclonal antibodies.** (A) Concentrations of different monoclonal SPT6 antibodies needed in Western blot and immunostaining experiments. (B) Western blot analysis after 4 days of GST and SPT6 RNAi, respectively.  $0.25 \times 10^6$  cells were loaded per lane and probed with anti-Lamin and indicated anti-SPT6 monoclonal antibodies. (C) 26D12 and 25C6 monoclonal SPT6 antibodies are specific in immunofluorescence experiments. S2 cell lines were treated with dsRNA against GST (ctrl) or SPT6, respectively.  $0.8 \times 10^6$  cells were stained with antibodies against SPT6 and MOF as indicated. DNA was counterstained with DAPI. Scale bars represent 1  $\mu$ m.

In summary, four specific monoclonal SPT6 antibodies were obtained recognizing the N-terminal epitopes spt6-1 and spt6-2, respectively. Unfortunately, immunization with the C-terminal spt6-3 peptide did not yield any specific antibodies. Future applications and analyzes of potential SPT6 deletion mutants have to consider the epitope specificity accordingly.

### 3.3.2 Purification of recombinant SPT6 protein

In order to investigate whether SPT6 is a substrate for MSL2-dependent *in vitro* ubiquitylation *spt6* cDNA was cloned into the pFastBac1 vector, comprising either aa 1-979 (SPT6[1]), aa 980-1831 (SPT6[2]) or the full-length sequence of SPT6. Using respective Baculoviruses recombinant protein was expressed in Sf21 cells. After 3 days of expression cells were harvested and protein was purified from a C-terminal FLAG-tag as described previously. For preparation of whole cell extracts cells were lysed, sonified and soluble protein fraction was obtained by centrifugation. SPT6, SPT6[1] and SPT6[2] proteins were readily expressed as seen from preparations of the cell pellet after centrifugation (Figure 35; P). On SDS-PAA gels the protein sizes of SPT6, SPT6[1] and SPT6[2] refer to 250, 160 and 120 kDa, respectively. While both SPT6 and SPT6[1] were found in the soluble fraction (S/N) after centrifugation, formation of inclusion bodies hampered SPT6[2] isolation. SPT6 and SPT6[1] proteins were eluted to satisfying amounts using 50 mM KCl elution buffer (E).

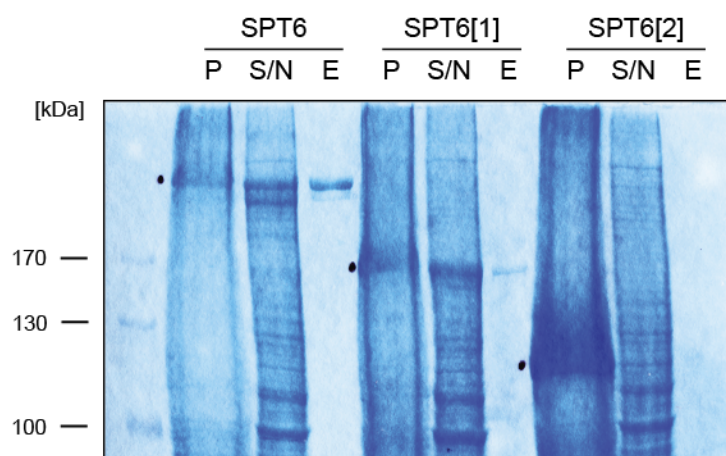


**Figure 35: FLAG-purification of SPT6.** Coomassie-stained SDS-PAA gel of pellet (P), obtained supernatant after centrifugation (S/N) and eluted protein fraction (E). Positions of molecular mass marker proteins are indicated to the left (kDa). Predicted positions of recombinant SPT6 derivatives are indicated as black dots. 2  $\mu$ l of eluted protein fraction were loaded to 7% SDS gels.

### 3.3.3 *In vitro* ubiquitylation of recombinant SPT6

To assess whether MSL2 exhibits ubiquitylation activity on SPT6 *in vitro* recombinant SPT6 proteins obtained from FLAG-purification were subjected to *in vitro* ubiquitylation assays as described previously (Figure 36). Employing both SPT6[1] and SPT6 full-length protein Western blot analysis revealed that SPT6 is ubiquitylated in the presence of MSL2 which was visualized by the detection of high molecular protein bands (Figure 36A). Suitable controls verified the specificity of MSL2-dependent SPT6 ubiquitylation (Figure 36B).

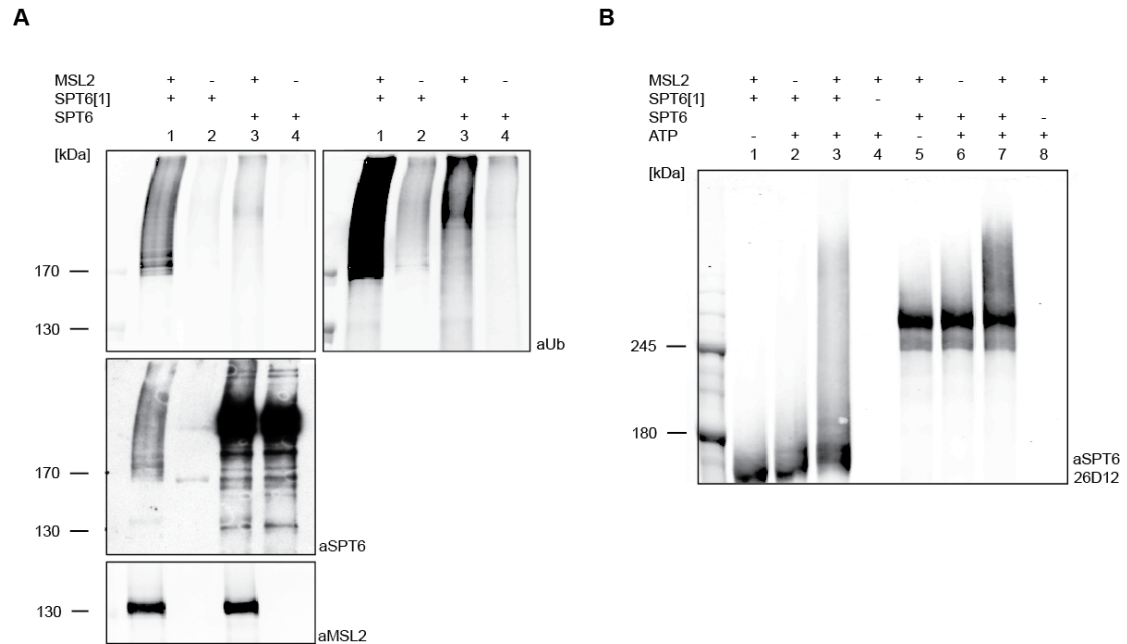


**Figure 36: *In vitro* ubiquitylation of SPT6 by MSL2.** *In vitro* ubiquitylation assay using recombinant SPT6[1] and full-length SPT6 was performed as described previously. Positions of molecular mass marker proteins are indicated to the left (kDa). (A) MSL2 and different SPT6 substrates were added to the reactions as indicated. Ubiquitylated proteins were detected using anti-ubiquitin (aUb (mouse), top), anti-SPT6 (aSPT6, guinea pig, middle) and anti-MSL2 (aMSL2 (rabbit), bottom) antibodies. (B) MSL2, different SPT6 substrates and ATP were added to the reactions as indicated. Ubiquitylated SPT6 was detected using anti-SPT6 (aSPT6, 26D12 mouse monoclonal) antibody.



## **4 Discussion**

### 4.1 MOF ubiquitylation

Almost any protein is modified by ubiquitylation at some point of its life cycle. While ubiquitylation is best known for its role in proteasomal turnover other ubiquitylation signals will not affect stability of the target protein. Within the past years reports on the functions of nonproteolytic substrate ubiquitylation have steadily accumulated (Kulathu and Komander, 2012; Keusekotten, 2013; Fiil, 2013; Corn and Vucic, 2014). The recent discovery that MSL2 is involved in homeostatic control of the associated dosage compensation complex proteins raised the question whether MSL2-mediated ubiquitylation of substrates is implicated in biological functions apart from proteasomal targeting (Villa, 2012). Previous analyses had already indicated that *in vitro* MSL2 preferentially ubiquitylates the N-terminal region of MOF (unpublished data, Villa). Interestingly, the large and unstructured N-terminus of MOF has been proposed to act as a regulator of dosage compensation, which controls the assembly of the MSL-DCC on the male X chromosome and modulates MOFs HAT activity (Conrad, 2012a). Combining these two findings – the N-terminus as a regulatory unit, preferentially ubiquitylated by MSL2 *in vitro* – the aim of the project was initially to explore whether ubiquitylation affects the function of the N-terminus and more systematically to characterize the involvement of MOF ubiquitylation in the context of dosage compensation. Combining biochemical analyses with genetic and cell approaches this study provides the first comprehensive characterization of MOF ubiquitylation.

#### 4.1.1 Discrepancies between MOF ubiquitylation *in vitro* and *in vivo*

MOF ubiquitylation by MSL2 *in vitro* is substantially different from ubiquitylation observed on MOF *in vivo*. *In vitro* ubiquitylation assays confirmed that MSL2 preferably ubiquitylates MOF within the first 400 aa. To determine whether this modification pattern is specific for MSL2-mediated ubiquitylation, the generic human E3 ligase Mdm2 was employed. Remarkably, both enzymes catalyzed highly similar ubiquitylation reactions. At the same time it has to be taken into account that Mdm2 exhibited higher enzymatic activity on the MOF substrate, which was reflected by the observation that Mdm2, in contrast to MSL2, was able to ubiquitylate MOF-9KN. It therefore remains unclear whether the nature of the difference between MSL2 and Mdm2 is qualitative (specificity) or quantitative (avidity).

To further study MOF ubiquitylation in general and MSL2-dependent MOF ubiquitylation in particular in a physiological setting, proximity ligation assays were employed. This approach is more specific and more sensitive than traditional immunoassays to detect protein-protein interactions or, as in this case, protein modifications (Weibrecht, 2013; Gomez, 2013). The appearance of MOF-ubiquitin interaction foci illustrated the presence of ubiquitylated MOF species *in vivo*. Interestingly, the number of interaction foci was not affected upon depletion

of MSL2, indicating that observed MOF ubiquitylation in the cell was placed by a different E3 ligase. Whereas PLA allows analyses of cell populations with single-cell resolution, it is not possible to identify the respective modified residues on MOF. To this end a mass spectrometry-based ubiquitylome approach was employed in S2 cells.

Technical advance within recent years provided refined methods for specific enrichment of ubiquitin remnant peptides as well as their detection using high-resolution mass spectrometry. Using the expertise of Dr. Petra Beli (IMB, Mainz) ubiquitylome analyses revealed more than 1000 ubiquitylated proteins in *Drosophila* S2 cells (preliminary data, one data set only). Within this dataset MOF was found modified on 7 lysine residues that clustered in the structured regions of HAT and CB domains. In a further attempt to investigate MSL2-specific MOF ubiquitylation male and female cells were stably transfected with tagged MOF, purified from cells, trypsin digested and subjected to LC-MS/MS. Since female cells lack MSL2 any ubiquitylation found there does not relate to dosage compensation. In a first approach MOF-FLAG was stably expressed in S2 and Kc cells, purified from protein extracts, trypsin digested and finally analyzed by LC-MS/MS. The sample complexity observed was very high, which prevented efficient identification of single modified lysine residues on MOF-FLAG. In an optimized approach high salt washing steps were employed using the GFP-trap to enrich MOF-GFP stably expressed in S2 or Kc cells. Reduced sample complexity allowed identification of ubiquitylated lysines on MOF-GFP in male or female cells and confirmed the data obtained from ubiquitylome analysis: modified lysine residues cluster around HAT and CB domain, whereas again N-terminal ubiquitylation could not be detected *in vivo*. Furthermore, the comparison of MOF-GFP ubiquitylation pattern derived from male and female cells did not highlight male-specific modifications. Instead, most of the modified lysines of MOF-GFP were shared in male and female cells. Moreover, MOF-GFP derived from female cells exhibited two additional ubiquitylation sites, yet this data has to be judged very carefully due to several technical issues.

Input samples revealed a stronger transgene expression on MOF-GFP derived from female cells when probed by Western blot analysis. To assess transgene expression within the population, cells were subjected to immunofluorescence microscopy revealing that transgenic MOF-GFP was strongly overexpressed in individual cells, male or female. Usually stable cell lines employed in this study comprised low numbers of cells with non-physiologically high levels of MOF-GFP. By contrast, in the samples dedicated to LC-MS/MS analysis it was observed that almost every cell expressed the GFP transgene and MSL3 localization from the X-territory in male cells was lost. In this context it has to be assumed that homeostasis of the MSL-DCC is highly affected resulting in malfunctioning dosage compensation. These cells had been cultivated in roller bottles in order to obtain higher cell numbers. However, in the

past these cultivation conditions have been observed to subject cells to stress that also lead to high overexpression of the transgene. As a consequence of disrupted MSL stoichiometry cells attempt to restore protein homeostasis via attachment of ubiquitin chains and subsequent degradation of excess protein through the proteasome.

We assume that this stress-induced and sex-independent ubiquitylation of high levels of ectopic MOF might dominate any low-level MSL2-dependent MOF ubiquitylation. Thus, to further determine whether the observed ubiquitylation pattern reflects the accumulation of MOF species designated for the proteasome the proteasome machinery was inhibited with MG132. Several studies demonstrated that inhibition of the proteasome leads to global perturbation of cellular ubiquitylation patterns and increased ubiquitylation of >40% of the quantified sites, which mediate proteasome-dependent degradation (Heidelberger, 2016; Kim, 2011; Wagner, 2011; Udeshi, 2012). Technical limitations however, prevented sufficient accumulation of MOF-GFP, which was reflected by the detection of only one single modified residue (K715). Notably, this ubiquitylation site was recurrently detected both in *in vitro* and *in vivo* mass spectrometry approaches employed in this study.

In summary, the predominating ubiquitylation pattern observed on MOF *in vivo* most likely is independent of dosage compensation and MSL2. Conceivably, MOF might be substrate to many different E3 ligases. In turn, this observation does not necessarily imply that MSL2-dependent MOF ubiquitylation does not exist. Instead, the contribution of MSL2-dependent ubiquitylation in the context of the MSL-DCC may be minute relative to abundant bulk MOF ubiquitylation designated for proteasomal turnover and escape detection, since the mass spectrometry approach is highly biased towards high abundant peptides.

### **4.1.2 MOF ubiquitylation - a male-specific role in dosage compensation?**

MSL2 is one of the key components of the MSL-DCC, implicated in the homeostatic control of complex stoichiometry and in targeting of substrate protein to the proteasome degradation system. The human homolog of MSL2 uses its E3 ubiquitin ligase activity to specifically ubiquitylate H2B, a modification involved in the regulation of transcriptional elongation, highlighting MSL2-mediated ubiquitylation as a crucial regulatory principle. Likewise, MSL2 ubiquitylation activity might play additional roles apart from proteasomal targeting in *Drosophila*.

Initially PLA experiments were performed to answer two questions: (1) Is there a difference in the amount of MOF/ubiquitin interaction foci in the nucleus and on the X-territory of cells expressing MOF K>R mutants? (2) Is MOF ubiquitylation dependent on MSL2? The first question was addressed by analysing selected MOF K>R mutants in cells depleted of endogenous MOF. Anti-GFP and anti-ubiquitin antibodies were employed to visualize the

interaction of MOF-GFP transgenes and ubiquitin. All MOF mutant cell lines employed in this approach exhibited similar numbers of MOF/ubiquitin interaction foci, suggesting that the levels of ubiquitylated MOF-GFP were either similar or only very mildly affected in a range that can not be distinguished by microscopy anymore (data not shown). Quantification of PLA foci on the X-territory in theory is an elegant approach to visualize ubiquitylated MOF in context of the MSL-DCC, but unfortunately it was not possible to properly discriminate and quantify the amounts of PLA foci on the X-territory. This was mainly due to technical limitations, such as inconsistent quality during sample preparation and staining. Moreover, the assay might have already been saturated thus not fully resolve increasing quantities beyond a certain threshold.

Addressing the second question it was observed that the numbers of MOF-GFP/ubiquitin interaction foci were not affected upon knockdown of MSL2, as already mentioned previously. These experiments were optimized by improved sample processing and method standardization, and by careful choice of the combination of antibodies (MOF/ubiquitin). Of note, it has to be considered that depletion of MSL2 directly affects stability of the MSL-DCC and the remaining MOF may therefore exclusively reside in the NSL complex (Lam, 2012) and therefore not be related to dosage compensation. Taken together, PLA demonstrated the presence of ubiquitylated MOF independent of MSL2 *in vivo*. The distribution throughout the nucleus and cytoplasm points to extensive turnover of MOF and suggests involvement of ubiquitylated MOF in several cellular processes apart from dosage compensation. For example MOF is also participating in the NSL complex acting on the transcriptional regulation of housekeeping genes (Mendjan, 2006; Lam, 2012; Raja, 2010; Feller, 2012).

Both approaches described above shared one observation: a large pool of ubiquitylated MOF was detected not only in nucleus but also in the cytoplasm of *Drosophila* cells. This observation is also supported by unpublished data from the Akhtar laboratory (MPI, Freiburg, presentation given at various conferences), showing that human MOF (hMOF) not only localizes to the nucleus but also to mitochondria, explaining the cytoplasmatic staining. Conceivably, hMOF, in the context of the KANSL2 complex, is involved in regulating mitochondrial transcription (Dias, 2014; Chatterjee, 2016).

Another approach to determine whether MOF ubiquitylation is involved in dosage compensation was the analysis of the chromosomal localization of MOF K>R mutants by immunofluorescence microscopy. X chromosome targeting and complex association was only mildly affected upon expression of N-terminal mutants and MOF-3KC. MOF-9KC is an exception to this observation and will be discussed separately. To evaluate whether mild effects observed in cells are biologically relevant also in the whole organism, flies lines were generated expressing the mutated MOF forms from transgenes. Genetic complementation is

the classical approach to assess functionality of given mutants. Here, the male-lethal *mof*<sup>2</sup> mutant was employed to assay the functionality of MOF K>R derivatives through their ability to rescue the viability phenotype. Whereas immunofluorescence microscopy suggested that N-terminal K>R mutants are mildly affected in their X territory targeting and complex assembly, in the fly the corresponding N-terminal mutants as well as MOF-3KC complemented the male lethality similar to wildtype MOF. These results indicate that the K>R mutations within the N-terminus and 3KC indeed only exhibit subtle effects of low biological relevance.

Nevertheless, these complementation experiments provided important principles that have to be considered when setting up viability assays in flies. First, the choice of suitable driver lines is an essential determinant of the outcome. For example, utilization of the constitutive *tubulin*-GAL4 driver was inappropriate as massive overexpression of the MOF transgenes resulted in lethality during pupal stage. On the other hand, employment of the heat shock inducible *hsp70*-GAL4 driver line at normal temperature was insufficient to ensure sufficient induction of transgene expression for complementation assays. Instead, employment of the *armadillo*-GAL4 driver provided constitutive transgene expression at a moderate level.

Second, it was observed that complementation assays rely on functional MOF at early stages of development. Thus, a fly line balanced for the *mof*<sup>2</sup> mutation on the X in combination with *armadillo*-GAL4 driver on the second chromosome was established with the help of Anne Classen to maternally deposit wildtype MOF in early stages of embryonic development (*mof*<sup>2</sup>/*FM7*; *armadillo*-GAL4/*armadillo*-GAL4).

Taken together, mutation of lysines that may be target for MOF ubiquitylation mostly displayed only mild effects that did not impair dosage compensation in males. This either suggests that MOF ubiquitylation is dispensable for dosage compensation and exclusively involved in proteasomal turnover or that the physiological system compensates for the relevant deficiencies under these conditions. This is even more remarkable if one considers that lysine residues are not only modified by ubiquitylation. Out of all 20 naturally occurring amino acids lysine is the residue that is targeted by posttranslational modifications both most abundantly and most diversely (Azevedo and Saiardi, 2016): alkylation (methylation, butyrylation, propionylation), deamination, succinylation, SUMOylation and acetylation amongst others influence the biological properties of a given protein. In particular acetylation of lysine residues is known to participate in dynamic regulatory programs by interfering with various PTMs and analysis of ubiquitylation sites in U2OS cells revealed that approximately 20% of ubiquitylated lysine residues are also known to be acetylated (Danielsen, 2011). This observation highlights that PTMs not only exhibit complex networks by themselves but also

act in extensive competitive crosstalks. It will be interesting to determine whether the lysines we identified as potential ubiquitylation sites are also subject to other modifications.

#### 4.1.3 MOF-9KC mutant exhibits male-specific lethality

Whereas most of the investigated MOF mutants were only mildly affected in their X territory enrichment and complex association, cell lines expressing the C-terminal MOF-9KC mutant was dramatically affected in the ability targeting of its GFP-fusion derivative to the X chromosome and for impaired complex association. In line with the observations obtained in cells, expression of 9KC in flies resulted in reduced male viability. Most likely these defects do not result from impaired ubiquitylation but rather from diminished complex association or defective HAT activity.

MOF interaction with the MSL-DCC is achieved via the scaffold protein MSL1, featuring a conserved C-terminal PEHE domain that interacts with the zinc finger residing within the HAT domain of MOF (Morales, 2004). In human MOF the highly conserved key binding residues important for interaction with MSL1 are E199, Y201, Y216, Q261 and F278, which correspond to E563, Y565, Y580, Q625 and F642 in *Drosophila* MOF, respectively (Figure 37; Kadlec, 2011). Interestingly, 9KC features three point mutations of highly conserved lysine residues (K539R, K541R, K545R), which are in steric proximity to the residues crucial for MOF/MSL1 interaction and might affect electrostatic properties of the HAT domain resulting in diminished interaction with MSL1.

In order to address functional consequences of K>R mutations and of 9KC in particular, the HAT activity of recombinant MOF on free histones and nucleosomal histones was monitored. MOF wt, MOF-9KN and  $\Delta$ N mutants share one common feature: they all exhibited similar acetylation activity on free H4 histone proteins. This observation can be attributed to the presence of a wildtype HAT domain. At the same time introduction of K>R point mutations into the N-terminus (9KN) did not change substrate specificity and enzymatic activity towards free histones.

Many members of the MYST HAT family have been described to exhibit full enzymatic activity and specificity only in the background of their native complexes. For example, TIP60 readily acetylates free histones but fails to modify histone-containing polynucleosomes unless it is incorporated into the TIP60 complex (Ikura, 2000). Similar, MOF alone is able to acetylate free H4, yet acetylation of H4 in a nucleosomal context requires association of MOF with MSL1-MSL3 (Morales, 2004). In the absence of MSL3 MOF exhibits acetylation activity primarily towards MSL1 even in the presence of a nucleosomal substrate, highlighting that interaction of MOF with the MSL-DCC directly affects substrate specificity. Interestingly, not only faithful complex assembly but also the MOF N-terminus itself was suggested to be involved in the autoregulation of HAT activity (Conrad, 2012).

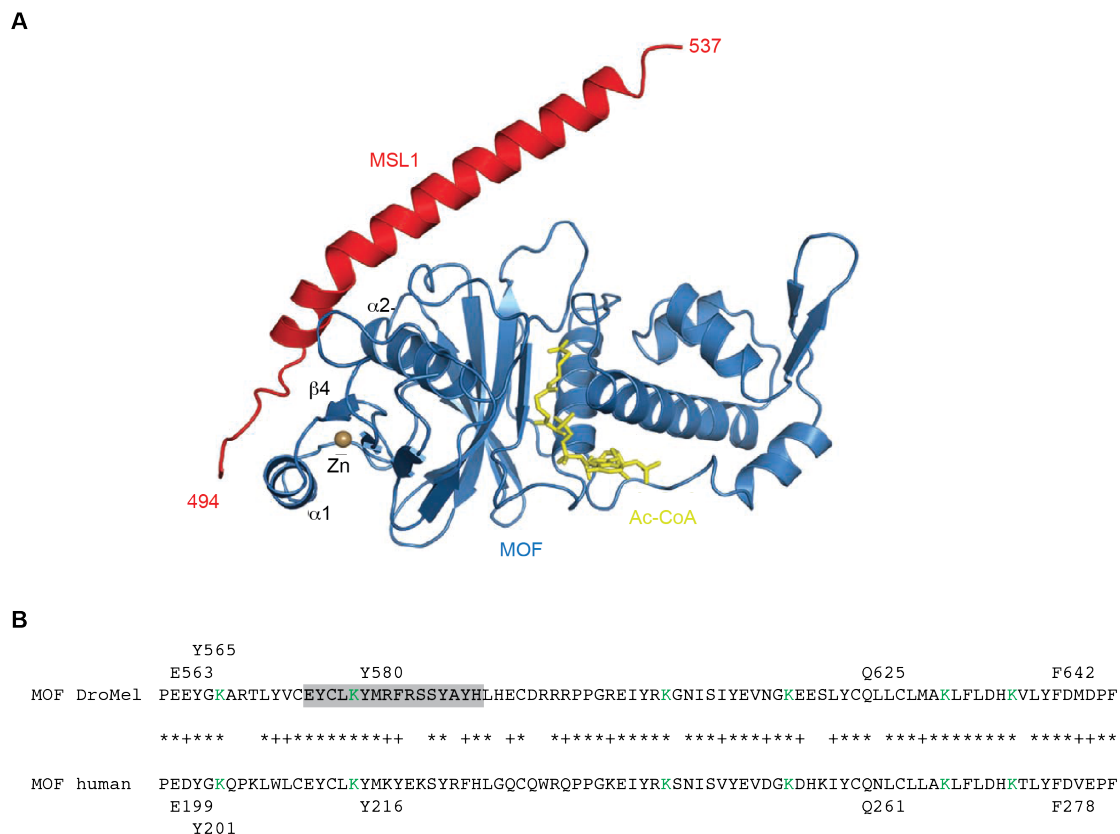


**Figure 37: The MSL1-MOF subcomplex - structure and sequence alignment.** (A). Crystal structure of the human MSL1-MOF subcomplex displayed as ribbon diagram. MOF HAT domain is shown in blue, acetyl-CoA bound to the HAT domain is shown in yellow, MSL1 fragment is shown in red. [Adapted and reprinted with permission (Kadlec, 2011; NSMB).] (B) Sequence alignment of *Drosophila* and human MOF HAT domain. Numbers indicate amino acid positions of key binding residues in MOF required for MSL1 binding. MOF zinc finger is highlighted by grey background color (aa 575-592). Conserved lysine residues between *Drosophila* and human MOF are shown in green.

Analysis of MOF mutants in the presence of the MSL1-MSL3 subcomplex on nucleosomal histones further confirmed that MOF-9KN is not impaired in HAT activity. Moreover, 9KC exhibited acetylation activity similar to MOF wt and 9KN, in contrast to 3KC, which displayed changes in substrate specificity. These results appear not intuitive: why should the mutant with more K>R mutations be less affected in enzymatic activity than the one with fewer mutations? MOF-3KC still interacts with the MSL-DCC and insertion of mutations within the HAT domain might change substrate specificity and perturb enzymatic activity as seen by increased acetylation of H4 and MSL1, but also increased autoacetylation on MOF. In turn, 9KC might still possess hyperactive enzyme activity, however might be covered by the fact that 9KC does not interact with the MSL-DCC thus cannot exhibit acetylation activity on MSL1.

Taken together these results suggest that interference with the N-terminal lysine residues does not influence HAT activity, while on the other side introduction of C-terminal mutations close to the enzymatic domain affect substrate specificity and enzymatic activity.

#### 4.1.4 Possible functions of MOF ubiquitylation

To recapitulate the functions of ubiquitylation it is not only crucial to study the functions of ubiquitylated substrates *per se* but also to identify respective writer enzymes. In *Drosophila* MOF is modified by the E3 RING ligase MSL2, however it has to be assumed that MOF is also substrate to other E3 RING ligases.

RING finger-containing E3 ligases are characterized by a reaction mechanism in which the ubiquitin ligase binds both E2 and substrate to ensure proximity for efficient and direct transfer of the activated ubiquitin from E2 to the substrate (Özkan, 2005). However, E3 ligases also interact with substrates by indirect means via an interaction partner (Buetow and Huang, 2016; Mizushima, 2007). For example, in the context of DNA damage and repair, the E3 CRL-DDB complex recognizes UV-induced pyrimidine dimer lesions on DNA where CRL-DDB ubiquitylates associated XPC and DDB2 to trigger nucleotide excision repair (Scrima, 2008; El-Mahd, 2006; Sugawara, 2005). Furthermore, some E3 ligases recognize certain domains or binding motifs that enable site-specific targeting to sites of action where E3 ligases exhibit enzymatic activity on any substrate available. So far MOF and MSL2 were never shown to directly interact with each other. Instead it is assumed that MSL1 provides a scaffold for the interaction of MSL2 and MOF (Hallacli, 2012; Morales, 2004; Scott, 2000). Even though E3 ligases are reportedly introduced as proteins with high substrate specificity some E3 ligases exhibit a rather promiscuous reaction profile not only with respect to the target residues within a particular substrate but also regarding the substrate in general. In *in vitro* ubiquitylation assays both MSL2 and Mdm2 were able to modify MOF. Considering that about 150 E3 ligases exist in *Drosophila* (Du, 2011) MOF may also be substrate to other E3 ligases, which complicates the analysis of MSL2-dependent MOF ubiquitylation *in vivo*. While it remains unclear, whether MSL-2 dependent MOF ubiquitylation exists at all, the observed ubiquitylation pattern on MOF *in vitro* clearly demonstrated that N-terminal ubiquitylation is possible. Still the question remains: why is N-terminal ubiquitylation never detected *in vivo*?

One possible explanation for this phenomenon could be a rapid turnover of N-terminally ubiquitylated MOF species *in vivo*. PEST motifs (proline, glutamic acid, serine and threonine) mediate ubiquitylation, induce subsequent degradation and point to rapid turnover of target protein (Marchal, 1998) thus might be involved in the clearance of N-terminally ubiquitylated MOF. Indeed, the MOF N-terminus exhibits several such motifs whereas for the C-terminus no such motifs were predicted (Figure 38). On the other hand, N-terminal ubiquitylation might occur at very low levels only and be dominated by C-terminal modification that represents bulk cellular MOF ubiquitylation outside of the MSL-DCC.

## 4 DISCUSSION

```

*****
1  MSEAELEQTPSAGHVQEQPIEEEHEPEQEPTDAYTIGGPPRTPVEDAAAELSASLDVSGS 60
*****
61  DQSAEQSLDLSGVQAEAAAEESEPPAKRQHRDISPISEDSTPASSTSTSSSTRSSSSRYDD 120
***** K145 K153 K170
121 VSEAEAEAPPEPEPEPQQQQQEEKEDGQDQVKSPGPVLEAQEPAQPQKQKEVVDQEIE 180
*****
181 TEDEPSSDTVICVADINPYGSGSNIDDFVMDPDAPPNAIITEVVVTIPAPLHLKGTQQLGL 240
*****
241 PLAAPPPPPPPAAEQVPETPASPTDDGEEPPAVYLSPIRSRYMQESTPGLPTRLAPRD 300
*****
301 PRQRNMPPPAVVLPDIQTVLSANVEAISDDSSSETSSSSDDDEEEEEEDEDDALTMEDHNTSRE 360
K372 K381
361 TVITTGDPMLQKIDISENPKIYFIRREDGTVHRGQVLQSRRTENAAAPDEYYVHYVGLN 420
K483 K532
421 RRLDGWVGRHRISDNADDLGGITVLPAPPLAPDQPSTPREMLAQAAAAAASSERQKRA 480
481 ANKDYLYSYCENSRYDYSRDKMTRYQKRRYDEINHVQKSHAELTATQAALKEHESITKI 540
541 KYIDKLQFGNYEIDTWYFSPFPPEEYGKARTLYVCEYCLKYMRFRSSYAYHLHECDRRRPP 600
601 GREIYRKGNISIEYVNGKEESLYCQLLCLMAKFLDHKVLVYFMDPFLFYILCETDKEGS 660
K706 K715
661 HIVGYFSKEKKSLENYNVACILVLPHPQRKGFGLLIAFSYELSRKEGVIGSPEKPLSDL 720
K776
721 GRLSYRSYWAYTLELMKTRCAPEQITIKELSEMSGITHDDIIYTLQSMKMIKYWKQONV 780
K801
K798
781 ICVTSKTIQDHLQLPQFKQPKLTIDTDYLVWSPQTAAAVVRAPGNSG 827

```

**Figure 38: Functions of MOF ubiquitylation.** MOF exhibits N-terminal PEST-motifs. Motif prediction of MOF protein sequence reveals PEST motifs, indicated by asterisks. Ubiquitylated lysine residues after MSL2 *in vitro* ubiquitylation are highlighted in yellow, modified lysines found by ubiquitylome analysis are underscored and highlighted in yellow. Numbers indicate aa positions. Unstructured MOF N-terminus (aa 1-350).

Another explanation might be attributed to a specialized role of N-terminal MOF ubiquitylation in the context of dosage compensation. MSL2-dependent modification of MOF within the N-terminus might reflect only a small proportion of total MOF ubiquitylation. One hypothesis poses that ubiquitylation of MOF serves as a checkpoint to target wrong protein assemblies for degradation. Accordingly, MOF-MSL2 interactions that occur off the X chromosome may be eliminated and not be detectable. Following this line of argument, regular MSL2-MOF complexes assembled at the X chromosomal HAS may be stable. In such a scenario, the N-terminus of MOF may be stably engaged in protein interactions in the context of the MSL-DCC, which may occlude access of any E3 ligase. *In vitro* ubiquitylation assays performed in the presence of DNA support this hypothesis as loss of MOF ubiquitylation was observed after addition of DNA to the ubiquitylation reaction. Despite many lines of evidence and different experimental setups to approach MOF ubiquitylation, it remains elusive whether ubiquitylated MOF is involved in functions apart from proteasomal targeting.

#### 4.1.5 Conclusions and future perspectives on MOF ubiquitylation

Despite multiple many efforts and various assays employed both *in vitro* and *in vivo* functions of MOF ubiquitylation remain elusive. In general, the genetic complementation analyses of mutated transgenes offers a powerful tool to study the biological functions of a given protein *in vivo*. Similar approaches have been successfully employed for the analysis of MSL2-GFP and MLE-GFP in the Becker laboratory before. In contrast to MOF, the *in vitro* ubiquitylation sites of MLE were nicely recapitulated also on MLE-GFP *in vivo* (unpublished data, R. Villa). Observed discrepancies between *in vitro* and *in vivo* data might be explained by the different molecular context of transgenic and endogenous MOF. In a theoretical scenario the two MOF species could either compete with each other or, in an extreme case, MOF-GFP will not be incorporated into the MSL-DCC at all. MOF, in contrast to the other MSL-DCC proteins, is involved in cellular processes apart from dosage compensation. Thus it is likely that a fraction of expressed MOF-GFP will associate with the NSL complex to fulfill different tasks. Moreover, the fraction of MOF-GFP observed in the cytoplasm accounts for a big proportion of neither MSL-DCC or NSL-related MOF. Accordingly, the ubiquitylated MOF-GFP species detected by mass spectrometry represent a combination of both nuclear and cytoplasmic protein of diverse physiological context and function. Hence, employment of refined experimental setups on endogenous protein might be more suitable in this context. In general, two central steps can be improved: (1) affinity purification of ubiquitylated proteins and (2) enrichment of ubiquitin remnants using suitable di-glycine antibodies followed by peptide fractionation (Porrás-Yakushi and Hess, 2014). Moreover, coupling proteome-wide ubiquitin remnant profiling to metabolic labeling of endogenous MOF in a SILAC approach allows the quantification of relative abundance of ubiquitylation sites. Such an experiment is currently being performed in male and female cells and might reveal male-specific MSL2-related MOF ubiquitylation sites *in vivo* as well as confirm the MOF ubiquitylation sites obtained from the S2 ubiquitylome. In addition, application of ubiquitin remnant profiling using di-glycine enrichment of wildtype, endogenous MOF after proteasome inhibition offers an alternative perspective for follow up experiments. The di-glycine enrichment requires less cell material, allowing MG132 treatment at smaller scales, where sufficient endogenous MOF accumulates.

An approach to specifically study the impact of MOF ubiquitylation may be provided by the SpyCatcher system, a methodology that uses the principles of peptide tagging (Zakeri, 2012; Li, 2014). Usually interactions of proteins with peptides are unstable and rapidly reversible. The SpyCatcher system in turn is characterized by a rapid and irreversible formation of an isopeptide linkage between Spy-tag and SpyCatcher. The Spy-tag consists of 13 amino acids able to form a covalent bond to its protein partner (SpyCatcher, 138 amino acids, 15 kDa). A

scenario where the Spy-tag is integrated into MOF and the SpyCatcher is linked to an ubiquitin moiety may enable the construction of a branched protein mimicking the site-specific mono-ubiquitylation of MOF with high efficiency. Such ubiquitylated MOF species might be generated with high homogeneity and thus may be subjected to HAT assays, MSL1 interaction studies and nucleosome binding assays to characterize the impact of site-specific ubiquitylation. In an attempt to follow this approach Spy-tagged MOF versions were established as well as a SpyCatcher linked to a mono-ubiquitin moiety. However, expression and purification of recombinant protein was insufficient and will need further optimizations. Finally, employment of a functional MOF mutant that cannot be incorporated into the NSL-complex and therefore exclusively resides in the MSL-DCC might be further explored to avoid analyzing the NSL-related MOF fraction.

## 4.2. SPT6, a target for MSL2-mediated ubiquitylation?

Many studies have highlighted the role of transcriptional elongation in the mechanism of dosage compensation to mediate upregulation of X-linked genes in *Drosophila* males (Ferrari, 2013; Larschan, 2011; Prabhakaran and Kelley, 2012; Regnard, 2011; Straub and Becker, 2007). The identification of SPT6 as a putative substrate for MSL2-dependent ubiquitylation raised the possibility that such modification of SPT6 is implicated in the regulation of elongation (Ardehali, 2009; Dronamraju and Strahl, 2014). To prepare future studies on SPT6 *in vitro* and *in vivo*, recombinant protein, stable cell lines and monoclonal antibodies directed against SPT6 were established. The antibodies were highly specific in Western blot and immunofluorescence microscopy. Moreover, first results indicated that *in vitro* SPT6 is ubiquitylated by MSL2.

The mechanism of twofold upregulation of X-linked genes in *Drosophila* dosage compensation is mechanistically linked to transcriptional elongation (Larschan, 2011; Prabhakaran and Kelley, 2012; Ferrari, 2013; Kuroda, 2016). Still, the implications of SPT6 in the context of dosage compensation haven't been studied so far. The observation that MSL2 is able to ubiquitylate SPT6 *in vitro* might provide a link for its involvement in the regulation of dosage compensation. The experimental approaches to address this question will rely on an elaborate study design because SPT6 is critically involved in many functions outside of dosage compensation that must be differentiated from its potential effect on X chromosomal genes.

SPT6 is a well-studied histone H3-H4 chaperone associated with elongating RNAPII in yeast, flies and humans (Andrulis, 2000; Kaplan, 2000; Yoh, 2007). It acts as a multifunctional regulator of transcription and epigenetic modification of chromatin. For example, SPT6 also associates with the H2A-H2B histone chaperone FACT to coordinate disassembly and reassembly of nucleosomes during gene transcription (Belotserkovskaya 2003; Saunders, 2003). Moreover, *Drosophila* SPT6 was implicated in the turnover of improperly processed pre-mRNAs through the exosome machinery, a complex of 3'-5' exonucleases (Andrulis, 2002). SPT6 is further involved in the Set2-dependent positioning of H3K36me<sub>3</sub>, a histone mark found in regions of active transcription (Youdell, 2008). In contrast, SPT6 negatively regulates H3K27me<sub>3</sub>, which marks polycomb-repressed gene regions (Kato, 2013). Recent studies have linked yeast SPT6 to the control of H4K16ac levels by deposition of K16-unacetylated H4 into strongly transcribed genes (Reiter, 2015).

The experience gained from difficulties of the analysis of MOF ubiquitylation highlighted the complexity and challenges in this research field and precluded addressing the more difficult question of a role for SPT6 ubiquitylation in X-chromosome-specific regulation.

### 4.3 The analysis of ubiquitylation- limitations and challenges

Since the pioneering experiments of Peng et al. proteomic ubiquitylome analyses have provided a wealth of data on the role of ubiquitylation, novel ubiquitylation targets as well as their involvement in the regulation of biological pathways (Peng, 2003; Porras-Yakushi and Hess, 2014). The rapid development of mass spectrometry-based proteomics in combination with classical molecular biology methods (site-directed mutagenesis), biochemical assays (*in vitro* ubiquitylation assays) and investigation of biological systems allows unraveling the complexity of the ubiquitin network. Yet, the field of ubiquitylation faces major challenges and limitations.

First of all, numerous types of ubiquitin modifications are present *in vivo* and it is not always clearly defined which modification exactly translates which biological role. Due to the manifold potential to create ubiquitin chains varying not only in length of attached ubiquitin moieties but also in type of linkages exhibited, ubiquitylation is a very complex modification with manifold functions and biological consequences. On a historical basis cellular functions of protein ubiquitylation were separated into proteolytic functions marked by Lys48-linked ubiquitin chains and non-proteolytic functions represented by Lys63-linked chains. Lys48-linked chains are still most abundantly found in all organisms and rapidly accumulate upon inhibition of the proteasome (Peng, 2003; Xu, 2009; Kim et al., 2011). However, today this view appears too simplistic. For example, it is now clear that Lys63-linked chains are able to transmit degradation and Lys48-linked chains also act on the regulation of transcription factors (Flick, 2006; Kaiser, 2000). Hence, the current view on deciphering the ubiquitin code suggest that chain topology rather than individual ubiquitin linkages translate the functions and consequences of ubiquitylation (Swatek and Komander, 2016). The separation of biological consequences of ubiquitin attachment into proteolytic and non-proteolytic functions in general is still valid in a way that ubiquitin might either regulate proteasomal and lysosomal degradation, respectively, or as examples for non-proteolytic function, acts on the regulation of protein interactions, protein localization and protein activity (Komander and Rape, 2012).

Importantly, ubiquitin is not only substrate for ubiquitylation itself but the interdependency and crosstalk between ubiquitin and other PTMs adds another layer of complexity to the ubiquitin signaling network (Swaney, 2013; Wu, 2011). Another challenge in studying protein ubiquitylation is the usually rapid turnover of proteins modified for degradation by the proteasomal machinery. In addition, deubiquitylating enzymes (DUBs) further contribute to low steady state levels of protein ubiquitylation.

State of the art techniques in the ubiquitylation field focus on two major approaches: biochemical methods for the analysis of ubiquitin chain architecture and mass spectrometry-

based approaches. The first approach either utilizes specific ubiquitin-binding proteins that recognize certain polyubiquitin chains with high affinity (Sims, 2012; van Wijk, 2012) or employ DUBs on endogenous proteins to visualize ubiquitin linkage type in a PAGE-based assay (UbiCRest; Hospenthal, 2015). UbiCRest is based on the linkage preference of the employed DUB, e.g. for Lys48 or Lys63-specific ubiquitin linkages. Electrophoretic mobilities of the obtained ubiquitin cleavage products after DUB treatment reveal ubiquitin linkages originating from the protein of interest. Mass spectrometry-based methods on the other hand still provide the most important tools for the detection of ubiquitylated peptides. Despite the constant improvements in data analysis, purification methods as well as technical advance in detecting ubiquitylated peptides still faces some critical limitations: LC-MS/MS is biased towards highly abundant ubiquitylated species, thus not all modified peptides resulting from trypsin digestion of the cellular proteome will be detected. Moreover, it has to be considered that analysis and quantification of ubiquitylomics using mass spectrometry is still highly affected by experimental variation. Both sample preparation as well as the mass spectrometry analysis itself might introduce errors. Whereas errors in sample preparation can be limited by co-preparation of technical replicates within a particular set of experiments, errors in mass spectrometry analysis are caused by the instrument itself (Heidelberger, 2016). The classical workflow of isolating the sample of interest, digestion into peptides, followed by chromatographic peptide separation and finally mass spectrometry can be optimized by combination of both enrichment and labeling strategies. Isolation of the protein of interest from distinct cellular organelles, enrichment by protein or protein tag-specific antibodies and well as enrichment via the PTMs already narrow down the input material for shotgun proteomics. Finally, generation of quantitative data involves the labeling of cells (SILAC) or peptides (TMT, tandem mass tags) and the utilization of labeled proteins or peptide standards (Ordureau, 2015).



## **5 ABBREVIATIONS**

## 5 ABBREVIATIONS

---

aa	Amino acid
ac	Acetylation
ADP	Adenosine diphosphate
Amp	Ampicillin
ATP	Adenosine triphosphate
BLAST	Basic Local Alignment Search Tool
bp	Base pair
BSA	Bovine serum albumin
°C	Degree Celsius
CBD	Chromobarrel domain
cDNA	complementary DNA
CES	Chromatin entry site
ctrl	Control
DAPI	4',6-diamidino-2-phenylindole
DCC	Dosage compensation complex
DGRC	<i>Drosophila</i> Genomics Resource Center
DNA	Deoxyribonucleic acid
dsRNA	Double stranded RNA
E1	Ubiquitin-activating enzyme E1
E2	Ubiquitin-conjugating enzyme E2
E3	Ubiquitin protein ligase E3
fw	forward
Gal4	Yeast transcription activator protein GAL4
GFP	Green fluorescent protein
gp	guinea pig
H2B	Histone 2B
H4	Histone 4
HAS	High affinity site
HAT	Histone acetyltransferase
HDAC	Histone deacetylase
I	Input
IF	Immunofluorescence
IP	Immunoprecipitation
K	Lysine
Kan	Kanamycin
Kc	<i>Drosophila</i> cell line, female karyotype
kDa	Kilodalton

---

LC-MS/MS	Liquid chromatography–mass spectrometry/ mass spectrometry
L2-4	<i>Drosophila</i> Schneider cells, S2 clone, male karyotype
mA	Milliampere
Mdm2	Mouse double minute 2
me	Methylation
MLE	Maleless
MOF	Males-absent-On-the-First
mRNA	Messenger RNA
MRE	MSL recognition element
ms	mouse
MSL	Male-Specific-Lethal
NDS	Normal donkey serum
NGS	Normal goat serum
NSL	Non-specific lethal
P	Pellet
PBS	Phosphate buffered saline
PCR	Polymerase chain reaction
PionX	Pioneering sites on the X
PMSF	Phenylmethanesulfonyl fluoride
PTM	Posttranslational modification
rb	rabbit
RING	Really interesting new gene
RNA	Ribonucleic acid
RNAi	RNA interference
RNAPII	RNA polymerase II
rpm	Revolutions per minute
rox	RNA-on-the-X
RT	Room temperature
S/N	Supernatant
S2	<i>Drosophila</i> Schneider cells, male karyotype
SDS-PAGE	Sodium dodecyl sulfate-polyacrylamide gel electrophoresis
Sf21	<i>Spodoptera frugiperda</i> 21
Sgs3	Salivary gland secretion 3
SILAC	Stable isotope labeling by amino acids in cell culture
siRNA	small interfering RNA
SPT6	Suppressor of Ty 6; Transcription elongation factor
SXL	Sex lethal

## 5 ABBREVIATIONS

---

PFA	<i>para</i> -Formaldehyde
PLA	Proximity ligation assay
rv	Reverse
UAS	Upstream activating sequence
Ub	Ubiquitin
UTR	Untranslated region
v/v	Volume per volume
WB	Western blot
wt	Wild type
w/v	Weight per volume

## **6 REFERENCES**

- Adkins, N.L., Watts, M. & Georgel, P.T., 2004. To the 30-nm chromatin fiber and beyond. *Biochimica et Biophysica Acta - Gene Structure and Expression*, 1677(1–3), pp.12–23.
- Akhtar, A. & Becker, P.B., 2000. Activation of transcription through histone H4 acetylation by MOF, an acetyltransferase essential for dosage compensation in *Drosophila*. *Molecular cell*, 5(2), pp.367–375.
- Akhtar, A. & Becker, P.B., 2001. The histone H4 acetyltransferase MOF uses a C2HC zinc finger for substrate recognition. *EMBO Reports*, 2(2), pp.113–118.
- Alekseyenko, A.A. et al., 2008. A Sequence Motif within Chromatin Entry Sites Directs MSL Establishment on the *Drosophila* X Chromosome. *Cell*, 134(4), pp.599–609.
- Alekseyenko, A.A. et al., 2012. Sequence-specific targeting of dosage compensation in *Drosophila* favors an active chromatin context. *PLoS Genetics*, 8(4).
- Allfrey, V.G., Faulkner, R. & Mirsky, A.E., 1964. Acetylation and Methylation of Histones and Their Possible Role in the Regulation of Rna Synthesis. *Proceedings of the National Academy of Sciences of the United States of America*, 51(1938), pp.786–94.
- Andrulis, E.D. et al., 2000. High-resolution localization of *Drosophila* Spt5 and Spt6 at heat shock genes in vivo: Roles in promoter proximal pausing and transcription elongation. *Genes and Development*, 14(20), pp.2635–2649.
- Andrulis, E.D. et al., 2002. The RNA processing exosome is linked to elongating RNA polymerase II in *Drosophila*. *Nature*, 420(6917), pp.837–41.
- Ardehali, M.B. et al., 2009. Spt6 enhances the elongation rate of RNA polymerase II in vivo. *The EMBO journal*, 28(8), pp.1067–1077.
- Avery, O.T., Macleod, C.M. & McCarty, M., 1944. Studies on the Chemical Nature of the Substance Inducing Transformation of Pneumococcal Types : Induction of Transformation By a Desoxyribonucleic Acid Fraction Isolated From Pneumococcus Type Iii. *The Journal of experimental medicine*, 79(2), pp.137–158.
- Avvakumov, N., Nourani, A. & Côté, J., 2011. Histone Chaperones: Modulators of Chromatin Marks. *Molecular Cell*, 41(5), pp.502–514.
- Azevedo, C. & Saiardi, A., 2016. Why always lysine? The ongoing tale of one of the most modified amino acids. *Advances in Biological Regulation*, 60, pp.144–150.
- Bannister, A.J. & Kouzarides, T., 2011. Regulation of chromatin by histone modifications. *Cell research*, 21(3), pp.381–395.
- Bashaw, G.J. & Baker, B.S., 1997. The Regulation of the *Drosophila* msl-2 Gene Reveals a Function for Sex-lethal in Translational Control. *Cell*, 89(5), pp.789–798.
- Belmont, A.S. & Bruce, K., 1994. Visualization of G1 chromosomes: A folded, twisted, supercoiled chromonema model of interphase chromatid structure. *Journal of Cell Biology*, 127(2), pp.287–302.
- Belote, J.M. et al., 1980. Lethal mutations of. *Public Health*, pp.165–186.
- Belotserkovskaya, R., 2003. FACT Facilitates Transcription-Dependent Nucleosome

- Alteration. *Science*, 301(5636), pp.1090–1093.
- Ben-Saadon, R. et al., 2006. The Polycomb Protein Ring1B Generates Self Atypical Mixed Ubiquitin Chains Required for Its In Vitro Histone H2A Ligase Activity. *Molecular Cell*, 24(5), pp.701–711.
- Benbow, R.M., 1992. Chromosome structures. *Science progress*, 76(301-302–4), pp.425–450.
- de Bie, P., Zaaroor-Regev, D. & Ciechanover, A., 2010. Regulation of the Polycomb protein RING1B ubiquitination by USP7. *Biochemical and Biophysical Research Communications*, 400(3), pp.389–395.
- Bischof, J. et al., 2007. An optimized transgenesis system for Drosophila using germ-line-specific phiC31 integrases. *Proceedings of the National Academy of Sciences of the United States of America*, 104(9), pp.3312–7.
- Bone, J.R. et al., 1994. compensation in Drosophila. *Genes & Development*, pp.96–104.
- Boveri, T., 1902. Über mehrpolige Mitosen als Mittes zur Analyse des Zellkerns. *Verhandlungen der Physikalisch-Medizinischen Gesellschaft zu Wurzburg*, 35, pp.67–90.
- Braun, S. & Madhani, H.D., 2012. Shaping the landscape: mechanistic consequences of ubiquitin modification of chromatin. *EMBO reports*, 13(7), pp.619–630.
- Buetow, L. & Huang, D.T., 2016. Structural insights into the catalysis and regulation of E3 ubiquitin ligases. *Nature Reviews Molecular Cell Biology*.
- Buscaino, A. et al., 2003. MOF-regulated acetylation of MSL-3 in the Drosophila dosage compensation complex. *Molecular Cell*, 11(5), pp.1265–1277.
- Chatterjee, A. et al., 2016. MOF Acetyl Transferase Regulates Transcription and Respiration in Mitochondria. *Cell*, 167(3), p.722–738.e23.
- Chen, Z.J. & Sun, L.J., 2009. Nonproteolytic Functions of Ubiquitin in Cell Signaling. *Molecular Cell*, 33(3), pp.275–286.
- Ciechanover, a et al., 1980. ATP-dependent conjugation of reticulocyte proteins with the polypeptide required for protein degradation. *Proceedings of the National Academy of Sciences of the United States of America*, 77(3), pp.1365–1368.
- Conrad, T. et al., 2012a. The MOF Chromobarrel Domain Controls Genome-wide H4K16 Acetylation and Spreading of the MSL Complex. *Developmental Cell*, 22(3), pp.610–624.
- Conrad, T. et al., 2012b. The MOF Chromobarrel Domain Controls Genome-wide H4K16 Acetylation and Spreading of the MSL Complex. *Developmental Cell*, 22(3), pp.610–624.
- Conrad, T. & Akhtar, A., 2012. Dosage compensation in Drosophila melanogaster: epigenetic fine-tuning of chromosome-wide transcription. *Science*, 13(July), pp.123–134.
- Copps, K. et al., 1998. Complex formation by the Drosophila MSL proteins: role of the MSL2 RING finger in protein complex assembly. *The EMBO journal*, 17(18), pp.5409–17.
- Corn, J.E. & Vucic, D., 2014. Ubiquitin in inflammation: the right linkage makes all the difference. *Nature Structural & Molecular Biology*, 21(4), pp.297–300.
- Dammer, E.B. et al., 2011. Polyubiquitin linkage profiles in three models of proteolytic stress suggest the etiology of alzheimer disease. *Journal of Biological Chemistry*, 286(12),

pp.10457–10465.

Danielsen, J.M.R. et al., 2011. Mass spectrometric analysis of lysine ubiquitylation reveals promiscuity at site level. *Molecular & cellular proteomics : MCP*, 10(3), p.M110.003590.

Davey, C.A. et al., 2002. Solvent mediated interactions in the structure of the nucleosome core particle at 1.9 ?? resolution. *Journal of Molecular Biology*, 319(5), pp.1097–1113.

Dekker, J. & Oudet, P., 1975. Electron Microscopic and Biochemical Evidence that Chromatin Structure Is a Repeating Unit. *Cell*, 4(April), pp.281–300.

Deshai, R.J. & Joazeiro, C.A., 2009. RING domain E3 ubiquitin ligases. *Annu Rev Biochem*, 78, pp.399–434.

Dias, J. et al., 2014. Structural analysis of the KANSL1/WDR5/ KANSL2 complex reveals that WDR5 is required for efficient assembly and chromatin targeting of the NSL complex. *Genes and Development*, 28(9), pp.929–942.

Dikic, I., Wakatsuki, S. & Walters, K.J., 2009. Ubiquitin-binding domains - from structures to functions. *Nature reviews. Molecular cell biology*, 10(10), pp.659–671.

Dion, M.F. et al., 2005. Genomic characterization reveals a simple histone H4 acetylation code. *Proceedings of the National Academy of Sciences of the United States of America*, 102(15), pp.5501–6.

Dronamraju, R. & Strahl, B.D., 2014. A feed forward circuit comprising Spt6, Ctk1 and PAF regulates Pol II CTD phosphorylation and transcription elongation. *Nucleic Acids Research*, 42(2), pp.870–881.

Du, J. et al., 2011. In vivo RNAi screen reveals neddylation genes as novel regulators of hedgehog signaling. *PLoS ONE*, 6(9).

El-Mahd, M.A. et al., 2006. Cullin 4A-mediated proteolysis of DDB2 protein at DNA damage sites regulates in vivo lesion recognition by XPC. *Journal of Biological Chemistry*, 281(19), pp.13404–13411.

Eltsov, M. et al., 2008. Analysis of cryo-electron microscopy images does not support the existence of 30-nm chromatin fibers in mitotic chromosomes in situ. *Proceedings of the National Academy of Sciences of the United States of America*, 105(50), pp.19732–7.

Fauth, T. et al., 2010. The DNA binding CXC domain of MSL2 is required for faithful targeting the dosage compensation complex to the X chromosome. *Nucleic Acids Research*, 38(10), pp.3209–3221.

Feller, C. et al., 2012. The MOF-containing NSL complex associates globally with housekeeping genes, but activates only a defined subset. *Nucleic Acids Research*, 40(4), pp.1509–1522.

Ferrari, F. et al., 2013. “Jump Start and Gain” model for dosage compensation in drosophila based on direct sequencing of nascent transcripts. *Cell Reports*, 5(3), pp.629–636.

Fiil, B.K. et al., 2013. OTULIN Restricts Met1-Linked Ubiquitination to Control Innate Immune Signaling. *Molecular Cell*, 50(6), pp.818–830.

- Finch, J.T. & Klug, A., 1976. Solenoidal model for superstructure in chromatin. *Proceedings of the National Academy of Sciences of the United States of America*, 73(6), pp.1897–901.
- Fischle, W., 2008. Talk is cheap--cross-talk in establishment, maintenance, and readout of chromatin modifications. *Genes Dev*, 22(24), pp.3375–3382.
- Flick, K. et al., 2006. A ubiquitin-interacting motif protects polyubiquitinated Met4 from degradation by the 26S proteasome. *Nature cell biology*, 8(5), pp.509–15.
- Franke, A. & Baker, B.S., 1999. The rox1 and rox2 RNAs are essential components of the compensasome, which mediates dosage compensation in *Drosophila*. *Molecular Cell*, 4(1), pp.117–122.
- Fussner, E., Ching, R.W. & Bazett-Jones, D.P., 2011. Living without 30nm chromatin fibers. *Trends in Biochemical Sciences*, 36(1), pp.1–6.
- Gelbart, M.E. & Kuroda, M.I., 2009. *Drosophila* dosage compensation: a complex voyage to the X chromosome. *Development*, 136(9), pp.1399–1410.
- Gomez, D. et al., 2013. Detection of histone modifications at specific gene loci in single cells in histological sections. *Nature methods*, 10(2), pp.171–177.
- Graindorge, A., Militti, C. & Gebauer, F., 2011. Posttranscriptional control of X-chromosome dosage compensation. *Wiley Interdisciplinary Reviews: RNA*, 2(4), pp.534–545.
- Green & Sambrook, 2012. [*Molecular Cloning A LABORATORY MANUAL*]
- Groettrup, M. et al., 2008. Activating the ubiquitin family: UBA6 challenges the field. *Trends in Biochemical Sciences*, 33(5), pp.230–237.
- Gurard-Levin, Z.A., Quivy, J.-P. & Almouzni, G., 2014. Histone chaperones: assisting histone traffic and nucleosome dynamics. *Annual review of biochemistry*, 83, pp.487–517.
- Haglund, K., Di Fiore, P.P. & Dikic, I., 2003. Distinct monoubiquitin signals in receptor endocytosis. *Trends in Biochemical Sciences*, 28(11), pp.598–604.
- Hallacli, E. et al., 2012. Msl1-Mediated Dimerization of the Dosage Compensation Complex Is Essential for Male X-Chromosome Regulation in *Drosophila*. *Molecular Cell*, 48(4), pp.587–600.
- Heidelberger, J.B., Wagner, S.A. & Beli, P., 2016. Mass Spectrometry-Based Proteomics for Investigating DNA Damage-Associated Protein Ubiquitylation. *Frontiers in Genetics*, 7(June), pp.1–7.
- Hershko, A. et al., 1980. Proposed role of ATP in protein breakdown: conjugation of protein with multiple chains of the polypeptide of ATP-dependent proteolysis. *Proceedings of the National Academy of Sciences of the United States of America*, 77(4), pp.1783–6.
- Hershko, A. & Ciechanover, A., 1998. The ubiquitin system. *Annual review of biochemistry*, 67, pp.425–479.
- Hershko, A & Ciechanover, A, 1992. The ubiquitin system for protein degradation. *Annual review of biochemistry*, 61, pp.761–807.

- Hilfiker, A. et al., 1997. mof, a putative acetyl transferase gene related to the Tip60 and MOZ human genes and to the SAS genes of yeast, is required for dosage compensation in *Drosophila*. *EMBO Journal*, 16(8), pp.2054–2060.
- Hospenthal, M.K., Mevissen, T.E.T. & Komander, D., 2015. Deubiquitinase-based analysis of ubiquitin chain architecture using Ubiquitin Chain Restriction (UbiCRest). *Nature Protocols*, 10(2), pp.349–361.
- Husnjak, K. & Dikic, I., 2012. Ubiquitin-Binding Proteins: Decoders of Ubiquitin-Mediated Cellular Functions. *Annual Review of Biochemistry*, 81(1), pp.291–322.
- Ikura, T. et al., 2000. Involvement of the TIP60 histone acetylase complex in DNA repair and apoptosis. *Cell*, 102(4), pp.463–473.
- Inoue, H., Nojima, H. & Okayama, H., 1990. High efficiency transformation of *Escherichia coli* with plasmids. *Gene*, 96(1), pp.23–28.
- Izzo, A. et al., 2008. Structure-function analysis of the RNA helicase maleless. *Nucleic Acids Research*, 36(3), pp.950–962.
- Jack, A.P.M. & Hake, S.B., 2014. Getting down to the core of histone modifications. *Chromosoma*, 123(4), pp.355–371.
- Jeronimo, C. & Robert, F., 2016. Histone chaperones FACT and Spt6 prevent histone variants from turning into histone deviants. *BioEssays*, 38(5), pp.420–426.
- Jin, J. et al., 2005. In and out: Histone variant exchange in chromatin. *Trends in Biochemical Sciences*, 30(12), pp.680–687.
- Johnson, E.S. et al., 1995. A proteolytic pathway that recognizes ubiquitin as a degradation signal. *Journal of Biological Chemistry*, 270(29), pp.17442–17456.
- Joti, Y. et al., 2012. Chromosomes without a 30-nm chromatin fiber. *Nucleus*, 3(5), pp.1–7.
- Kadlec, J. et al., 2011. Structural basis for MOF and MSL3 recruitment into the dosage compensation complex by MSL1. *Nature structural & molecular biology*, 18(2), pp.142–149.
- Kaiser, P. et al., 2000. Regulation of Transcription by Ubiquitination without Proteolysis. *Cell*, 102(3), pp.303–314.
- Kaplan, C.D. et al., 2000. Spt5 and Spt6 are associated with active transcription and have characteristics of general elongation factors in *D. melanogaster*. *Genes and Development*, 14(20), pp.2623–2634.
- Kato, H., Okazaki, K. & Urano, T., 2013. Spt6: Two fundamentally distinct functions in the regulation of histone modification. *Epigenetics*, 8(12), pp.1249–1253.
- Kelley, R.L. et al., 1995. Expression of Msl-2 causes assembly of dosage compensation regulators on the X chromosomes and female lethality in *Drosophila*. *Cell*, 81(6), pp.867–877.
- Keusekotten, K. et al., 2013. XOTULIN antagonizes LUBAC signaling by specifically hydrolyzing met1-linked polyubiquitin. *Cell*, 153(6), pp.1312–1326.

- Kim, W. et al., 2011. Systematic and quantitative assessment of the ubiquitin-modified proteome. *Molecular Cell*, 44(2), pp.325–340.
- Komander, D. & Rape, M., 2012. The Ubiquitin Code. *Annual Review of Biochemistry*, 81(1), pp.203–229.
- De Koning, L. et al., 2007. Histone chaperones: an escort network regulating histone traffic. *Nat Struct Mol Biol*, 14(11), pp.997–1007.
- Kornberg, R.D., 1974. Chromatin structure: a repeating unit of histones and DNA. *Science (New York, N.Y.)*, 184(139), pp.868–871.
- Kouzarides, T., 2007. SnapShot: Histone-Modifying Enzymes. *Cell*, 128(4), p.802.e1-802.e2.
- Kruse, J.P. & Gu, W., 2009. MSL2 promotes Mdm2-independent cytoplasmic localization of p53. *Journal of Biological Chemistry*, 284(5), pp.3250–3263.
- Kulathu, Y. & Komander, D., 2012. Atypical ubiquitylation — the unexplored world of polyubiquitin beyond Lys48 and Lys63 linkages. *Nature Reviews Molecular Cell Biology*, 13(8), pp.508–523.
- Kuroda, L. and, 2015. Dosage Compensation in Drosophila: Evidence That. *Cold Spring Harb Perspect Biol*, (1983), pp.1–20.
- Kuroda, M.I., Hilfiker, A. & Lucchesi, J.C., 2016. Dosage Compensation in Drosophila--a Model for the Coordinate Regulation of Transcription. *Genetics*, 204(2), pp.435–450.
- Lai, Z. et al., 2013. Msl2 Is a Novel Component of the Vertebrate DNA Damage Response. *PLoS ONE*, 8(7).
- Lam, K.C. et al., 2012. The NSL complex regulates housekeeping genes in Drosophila. *PLoS Genetics*, 8(6).
- Längst, G. & Manelyte, L., 2015. Chromatin remodelers: From function to dysfunction. *Genes*, 6(2), pp.299–324.
- Larschan, E. et al., 2007. MSL Complex Is Attracted to Genes Marked by H3K36 Trimethylation Using a Sequence-Independent Mechanism. *Molecular Cell*, 28(1), pp.121–133.
- Larschan, E. et al., 2011. X chromosome dosage compensation via enhanced transcriptional elongation in Drosophila. *Nature*, 471(7336), pp.115–118.
- Li, L., 2014. NIH Public Access. , 426(1002362), pp.309–317.
- Loyola, A. & Almouzni, G., 2007. Marking histone H3 variants: How, when and why? *Trends in Biochemical Sciences*, 32(9), pp.425–433.
- Lucchesi, J.C., Kelly, W.G. & Panning, B., 2005. Chromatin Remodeling in Dosage Compensation. *Annual Review of Genetics*, 39(1), pp.615–651.
- Luger, K. et al., 1997. Crystal structure of the nucleosome core particle at 2.8 Å resolution. *Nature*, 389(6648), pp.251–60.

- Luger, K., 2003. Structure and dynamic behavior of nucleosomes. *Current Opinion in Genetics and Development*, 13(2), pp.127–135.
- Luger, K., Dechassa, M.L. & Tremethick, D.J., 2012. New insights into nucleosome and chromatin structure: an ordered state or a disordered affair? *Nature reviews. Molecular cell biology*, 13(7), pp.436–47.
- Maenner, S. et al., 2013. ATP-dependent roX RNA remodeling by the Helicase maleless enables specific association of MSL proteins. *Molecular Cell*, 51(2), pp.174–184.
- Maeshima, K. et al., 2014. Chromatin as dynamic 10-nm fibers. *Chromosoma*, 123(3), pp.225–237.
- Maeshima, K. et al., 2016. Nucleosomal arrays self-assemble into supramolecular globular structures lacking 30-nm fibers. *The EMBO journal*, 35(10), p.e201592660.
- Maeshima, K., Hihara, S. & Eltsov, M., 2010. Chromatin structure: Does the 30-nm fibre exist in vivo? *Current Opinion in Cell Biology*, 22(3), pp.291–297.
- Marchal, C., Haguenuer-Tsapis, R. & Urban-Grimal, D., 1998. A PEST-like sequence mediates phosphorylation and efficient ubiquitination of yeast uracil permease. *Molecular and cellular biology*, 18(1), pp.314–321.
- Markson, G. et al., 2009. Analysis of the human E2 ubiquitin conjugating enzyme protein interaction network. *Genome research*, pp.1905–1911.
- Marmorstein, R. & Roth, S.Y., 2001. Histone acetyltransferases: Function, structure, and catalysis. *Current Opinion in Genetics and Development*, 11(2), pp.155–161.
- Marmorstein, R. & Trievel, R.C., 2009. Histone modifying enzymes: Structures, mechanisms, and specificities. *Biochimica et Biophysica Acta - Gene Regulatory Mechanisms*, 1789(1), pp.58–68.
- Marzluff, W.F. & Duronio, R.J., 2002. Histone mRNA expression: multiple levels of cell cycle regulation and important developmental consequences. *Current Opinion in Cell Biology* 2002, 14:692–699.
- Matsumoto, M.L. et al., 2010. K11-linked polyubiquitination in cell cycle control revealed by a K11 linkage-specific antibody. *Molecular Cell*, 39(3), pp.477–484.
- Meas, R. & Mao, P., 2015. Histone ubiquitylation and its roles in transcription and DNA damage response. *DNA Repair*, 36, pp.36–42.
- Meller, V.H., 2003. Initiation of dosage compensation in Drosophila embryos depends on expression of the roX RNAs. *Mechanisms of Development*, 120(7), pp.759–767.
- Mendjan, S. et al., 2006. Nuclear pore components are involved in the transcriptional regulation of dosage compensation in Drosophila. *Molecular Cell*, 21(6), pp.811–823.
- Michelle, C. et al., 2009. What was the set of ubiquitin and ubiquitin-like conjugating enzymes in the eukaryote common ancestor? *Journal of Molecular Evolution*, 68(6), pp.616–628.

- Minsky, N. et al., 2008. Monoubiquitinated H2B is associated with the transcribed region of highly expressed genes in human cells. *Nature cell biology*, 10(4), pp.483–488.
- Mizushima, T. et al., 2007. Structural basis for the selection of glycosylated substrates by SCF(Fbs1) ubiquitin ligase. *Proceedings of the National Academy of Sciences of the United States of America*, 104(14), pp.5777–5781.
- Morales, V. et al., 2004. Functional integration of the histone acetyltransferase MOF into the dosage compensation complex. *The EMBO journal*, 23(11), pp.2258–2268.
- Mosesson, Y. et al., 2009. Monoubiquitylation Regulates Endosomal Localization of Lst2, a Negative Regulator of EGF Receptor Signaling. *Developmental Cell*, 16(5), pp.687–698.
- Nielsen, P.R. et al., 2005. Structure of the chromo barrel domain from the MOF acetyltransferase. *Journal of Biological Chemistry*, 280(37), pp.32326–32331.
- Nishino, Y. et al., 2012. Human mitotic chromosomes consist predominantly of irregularly folded nucleosome fibres without a 30-nm chromatin structure. *The EMBO journal*, 31(7), pp.1644–53.
- Nusinow, D.A. & Panning, B., 2005. Recognition and modification of seX chromosomes. *Current Opinion in Genetics and Development*, 15(2), pp.206–213.
- Ordureau, A., Münch, C. & Harper, J.W., 2015. Quantifying Ubiquitin Signaling. *Molecular Cell*, 58(4), pp.660–676.
- Özkan, E., Yu, H. & Deisenhofer, J., 2005. Mechanistic insight into the allosteric activation of a ubiquitin-conjugating enzyme by RING-type ubiquitin ligases. *Proceedings of the National Academy of Sciences*, 102(52), pp.18890–18895.
- Park, Y.-J. & Luger, K., 2006. The structure of nucleosome assembly protein 1. *Proceedings of the National Academy of Sciences of the United States of America*, 103(5), pp.1248–1253.
- Pelzer, C. et al., 2007. UBE1L2, a novel E1 enzyme specific for ubiquitin. *Journal of Biological Chemistry*, 282(32), pp.23010–23014.
- Peng, J. et al., 2003. A proteomics approach to understanding protein ubiquitination. TL - 21. *Nature biotechnology*, 21 VN-r(8), pp.921–926.
- Phillips, D.M.P., 1963. The Presence of Acetyl Groups in Histones. *Biochemical Journal*, 87(1958), pp.258–263.
- Porras-Yakushi, T.R. & Hess, S., 2014. Recent advances in defining the ubiquitylome. *Expert review of proteomics*, 11(4), pp.477–90.
- Prabhakaran, M. & Kelley, R.L., 2012. Mutations in the Transcription Elongation Factor SPT5 Disrupt a Reporter for Dosage Compensation in *Drosophila*. *PLoS Genetics*, 8(11), pp.1–12.
- Praefcke, G.J.K., Hofmann, K. & Dohmen, R.J., 2012. SUMO playing tag with ubiquitin. *Trends in Biochemical Sciences*, 37(1), pp.23–31.
- Prestel, M. et al., 2010. The Activation Potential of MOF Is Constrained for Dosage Compensation. *Molecular Cell*, 38(6), pp.815–826.

- Raja, S.J. et al., 2010. The nonspecific lethal complex is a transcriptional regulator in *Drosophila*. *Molecular cell*, 38(6), pp.827–41.
- Rattner, J.B. & Lin, C.C., 1985. Radial loops and helical coils coexist in metaphase chromosomes. *Cell*, 42(1), pp.291–296.
- Regnard, C. et al., 2011. Global analysis of the relationship between JIL-1 kinase and transcription. *PLoS Genetics*, 7(3).
- Regnard, C. et al., 2000. Polyglutamylation of nucleosome assembly proteins. *Journal of Biological Chemistry*, 275(21), pp.15969–15976.
- Reiter, C. et al., 2015. A link between Sas2-mediated H4 K16 acetylation, chromatin assembly in S-phase by CAF-I and Asf1, and nucleosome assembly by Spt6 during transcription. *FEMS yeast research*, 15(7), pp.1–12.
- Richmond, T.J. & Davey, C.A., 2003. The structure of DNA in the nucleosome core. *Nature*, 423(6936), pp.145–50.
- Robinson, P.J.J. et al., 2008. 30-nm Chromatin Fibre Decompaction Requires both H4-K16 Acetylation and Linker Histone Eviction. *Journal of Molecular Biology*, 381(4), pp.816–825.
- Rohs, R. et al., 2009. Nuance in the double-helix and its role in protein – DNA recognition. , 19(2), pp.171–177.
- Saunders, A., 2003. Tracking FACT and the RNA Polymerase II Elongation Complex Through Chromatin in Vivo. *Science*, 301(5636), pp.1094–1096.
- Saunders, A., Core, L.J. & Lis, J.T., 2006. Breaking barriers to transcription elongation. *Nat Rev Mol Cell Biol*, 7(8), pp.557–567.
- Scott, M.J. et al., 2000. MSL1 plays a central role in assembly of the MSL complex, essential for dosage compensation in *Drosophila*. *The EMBO journal*, 19(1), pp.144–155.
- Scrima, A. et al., 2008. Structural Basis of UV DNA-Damage Recognition by the DDB1-DDB2 Complex. *Cell*, 135(7), pp.1213–1223.
- Shi, Y. et al., 2004. Histone demethylation mediated by the nuclear amine oxidase homolog LSD1. *Cell*, 119(7), pp.941–953.
- Shogren-Knaak, M. et al., 2006. Histone H4-K16 Acetylation. *Science*, 311(5762), pp.844–848.
- Sims, J.J. et al., 2012. Polyubiquitin-sensor proteins reveal localization and linkage-type dependence of cellular ubiquitin signaling. *Nature methods*, 9(3), pp.303–9.
- Sims, R.J., Belotserkovskaya, R. & Reinberg, D., 2004. Elongation by RNA polymerase II : the short and long of it. *Genes & Development*, 18(20), pp.2437–2468.
- Skaug, B., Jiang, X. & Chen, Z.J., 2009. The role of ubiquitin in NF-kappaB regulatory pathways. *Annual review of biochemistry*, 78, pp.769–796.
- Straub, T. et al., 2013. Different chromatin interfaces of the *Drosophila* dosage compensation complex revealed by high-shear ChIP-seq. *Genome Research*, 23(3), pp.473–485.

- Straub, T. & Becker, P.B., 2007. Dosage compensation: the beginning and end of generalization. *Nature reviews. Genetics*, 8(1), pp.47–57.
- Strieter, E.R. & Korasick, D.A., 2012. Unraveling the complexity of ubiquitin signaling. *ACS Chemical Biology*, 7(1), pp.52–63.
- Struck, A.W. et al., 2012. S-Adenosyl-Methionine-Dependent Methyltransferases: Highly Versatile Enzymes in Biocatalysis, Biosynthesis and Other Biotechnological Applications. *ChemBioChem*, 13(18), pp.2642–2655.
- Sugasawa, K. et al., 2005. UV-induced ubiquitylation of XPC protein mediated by UV-DDB-ubiquitin ligase complex. *Cell*, 121(3), pp.387–400.
- Sussman, R.T. et al., 2013. The epigenetic modifier ubiquitin-specific protease 22 (USP22) regulates embryonic stem cell differentiation via transcriptional repression of sex-determining region Y-box 2 (SOX2). *Journal of Biological Chemistry*, 288(33), pp.24234–24246.
- Swaney, D.L. et al., 2013. Global analysis of phosphorylation and ubiquitylation cross-talk in protein degradation. *Nature methods*, 10(7), pp.676–82.
- Swatek, K.N. & Komander, D., 2016. Ubiquitin modifications. *Cell research*, 26(4), pp.399–422.
- Thiriet, C. & Hayes, J.J., 2005. Chromatin in need of a fix: Phosphorylation of H2AX connects chromatin to DNA repair. *Molecular Cell*, 18(6), pp.617–622.
- Thoma, F. & Koller, T., 1977. Influence of histone H1 on chromatin structure. *Cell*, 12(1), pp.101–7.
- Torres, I.O. & Fujimori, D.G., 2015. Functional coupling between writers, erasers and readers of histone and DNA methylation. *Current Opinion in Structural Biology*, 35, pp.68–75.
- Udeshi, N.D. et al., 2012. Methods for quantification of in vivo changes in protein ubiquitination following proteasome and deubiquitinase inhibition. *Molecular & Cellular Proteomics*, 11(5), pp.148–159.
- Villa, R. et al., 2012. MSL2 Combines Sensor and Effector Functions in Homeostatic Control of the Drosophila Dosage Compensation Machinery. *Molecular Cell*, 48(4), pp.647–654.
- Villa, R. et al., 2016. PionX sites mark the X chromosome for dosage compensation. *Nature*, 537(7619), pp.244–248.
- Wagner, S. a. et al., 2011. A Proteome-wide, Quantitative Survey of In Vivo Ubiquitylation Sites Reveals Widespread Regulatory Roles. *Molecular & Cellular Proteomics*, 10(10), p.M111.013284-M111.013284.
- Wang, L. et al., 2008. Structure and chemistry of the p300/CBP and Rtt109 histone acetyltransferases: implications for histone acetyltransferase evolution and function. *Current Opinion in Structural Biology*, 18(6), pp.741–747.
- Wang, Z. et al., 2009. Genome-wide Mapping of HATs and HDACs Reveals Distinct Functions in Active and Inactive Genes. *Cell*, 138(5), pp.1019–1031.
- Watts, R.J., Hoopfer, E.D. & Luo, L., 2003. Axon pruning during Drosophila metamorphosis: Evidence for local degeneration and requirement of the ubiquitin-proteasome system. *Neuron*,

38(6), pp.871–885.

Weibrecht, I. et al., 2013. In situ detection of individual mRNA molecules and protein complexes or post-translational modifications using padlock probes combined with the in situ proximity ligation assay. *Nature Protocols*, 8(2), pp.355–372.

van Wijk, S.J.L. et al., 2012. Fluorescence-Based Sensors to Monitor Localization and Functions of Linear and K63-Linked Ubiquitin Chains in Cells. *Molecular Cell*, 47(5), pp.797–809.

Wu, L. et al., 2011. The RING Finger Protein MSL2 in the MOF Complex Is an E3 Ubiquitin Ligase for H2B K34 and Is Involved in Crosstalk with H3 K4 and K79 Methylation. *Molecular Cell*, 43(1), pp.132–144.

Xu, P. et al., 2009. Quantitative Proteomics Reveals the Function of Unconventional Ubiquitin Chains in Proteasomal Degradation. *Cell*, 137(1), pp.133–145.

Yang, X.J., 2004. The diverse superfamily of lysine acetyltransferases and their roles in leukemia and other diseases. *Nucleic Acids Research*, 32(3), pp.959–976.

Yoh, S.M. et al., 2007. The Spt6 SH2 domain binds Ser2-P RNAPII to direct Iws1-dependent mRNA splicing and export. *Genes and Development*, 21(2), pp.160–174.

Youdell, M.L. et al., 2008. Roles for Ctk1 and Spt6 in regulating the different methylation states of histone H3 lysine 36. *Molecular and cellular biology*, 28(16), pp.4915–4926.

Yuan, H. et al., 2012. MYST protein acetyltransferase activity requires active site lysine autoacetylation. *The EMBO journal*, 31(1), pp.58–70.

Zakeri, B. et al., 2012. Peptide tag forming a rapid covalent bond to a protein, through engineering a bacterial adhesin. *Proceedings of the National Academy of Sciences of the United States of America*, 109(12), pp.E690-7.

Zentner, G.E. & Henikoff, S., 2013. Regulation of nucleosome dynamics by histone modifications. *Nature structural & molecular biology*, 20(3), pp.259–66.

Zheng, S. et al., 2014. Structural basis of X chromosome DNA recognition by the MSL2 CXC domain during *Drosophila* dosage compensation. *Genes & Development*, pp.2652–2662.

## **7 APPENDIX**



## Acknowledgements

First of all, I would like to express my gratitude to Prof. Dr. Peter Becker for giving me the opportunity to join the lab and for providing an environment of outstanding scientific quality. The last years I have been deeply grateful for your support, valuable input, your confidence and a door that was always open even in busy times.

Special thanks go to Raffi for being the most critical and helpful supporter of my work. You were the mentor I feared most but at the same time you helped me to improve my scientific skills and to develop both as a scientist.

I want to thank the members of my thesis advisory committee Dr. Raffaella Villa, Dr. Anne Classen and Dr. Sigurd Braun for the interest in my work, discussions and advice.

In addition, I want to acknowledge my collaboration partner Dr. Petra Beli for providing support and advice in the analysis of ubiquitylated proteins by mass spectrometry.

I want to sincerely thank Dr. Elizabeth Schroeder-Reiter from the IRTG Graduate Program for being more than a coordinator you cared for each of your students and always had an open door whenever we felt overjoyed or devastated.

I furthermore want to thank all former and present members of the Becker lab as well as the whole Molecular Biology Unit for creating an enjoyable mixture between science and fun in the lab.

I want to thank...

... Edith Müller and Caroline Brieger, you made our PhD life in so many ways easier and always had so much patience with any of our paper work.

... Kenneth Börner - still did not overcome the separation from my desk neighbor after our move from Schillerstraße to the BMC.

... Christian Albig for support in the Isotope Lab.

... Dr. Matthias Prestel for introducing and training me in fly genetics.

... Dr. Tobias Straub for the quantification of immunofluorescence experiments.

... Dr. Andreas Thomae for support and help in the microscopy business.

... Dr. Marisa Müller and Dr. Catherine Regnard for input and support in technical questions.

... Silke Krause and Angie Zabel for your helping/magic hands and steady technical support.

... Dr. Sylvain Maenner, I miss being the target of your ever so funny "jokes".

... the former North-Lab aka newly formed Nerd-Lab (Nils Krietenstein, Corinna Lieleg, Elisa Oberbeckmann, Sebastian Pünzeler, Maria Walker, Lisa-Maria Zink) with you the lab was a place full of laughter, support, delicious food and crazy ideas.

Meiner Familie gilt besonderer Dank! Eure Liebe und fortwährende Unterstützung kennt keine Grenzen, dafür bin ich unendlich dankbar. Mamuska, Du bist und bleibst mein größter Supporter – VTS.

Micha, Du hast alle Höhen und Tiefen der letzten Jahre mit mir durchlebt und mir doch auch stets den Raum gegeben, meine diversen Spleens auszuleben (auch wenn Dich das sicher oft genug an den Rand des Wahnsinns getrieben hat). Worte können nicht beschreiben, wie dankbar ich Dir dafür bin. KBxTB

